

Contribution to Design of 120 kHz, 300 kV peak to peak RF Transformer for Industrial Accelerator

By

Suryaprakash Dewangan



NET/2003/M
D 511 C

**DEPARTMENT OF NUCLEAR ENGINEERING AND TECHNOLOGY
INDIAN INSTITUTE OF TECHNOLOGY KANPUR**

AUGUST, 2003

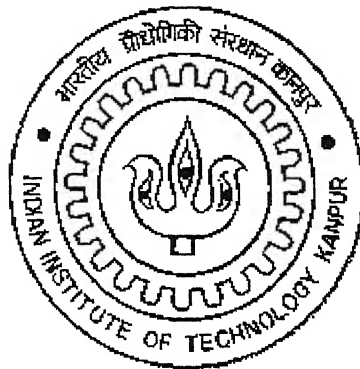
Contribution to Design of 120 kHz, 300 kV_{peak to peak} RF Transformer for Industrial Accelerator

*A thesis submitted
in partial fulfillment of the requirements
For the degree of*

Master of Technology

by

Suryaprakash Dewangan



**Department of Nuclear Engineering and Technology
INDIAN INSTITUTE OF TECHNOLOGY, KANPUR**

August 2003

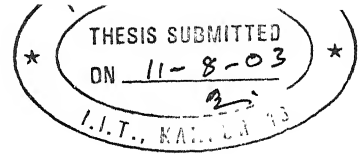
25 SEP 2003

गुरुचोत्तम काशीनाथ केलकर पुस्तकालय
भारतीय प्रौद्योगिकी संस्थान कानपुर
अवधि क्र० A.....145110




A145110

CERTIFICATE



This is certified that the work contained in this thesis entitled “**Contribution to Design of 120 kHz, 300 kV_{peak to peak} RF Transformer**”, by **Suryaprakash Dewangan**, has been carried out under my supervision and this work has not been submitted elsewhere for a degree.

August 2003


(Dr. Ravindra Arora)

Professor
Department of Electrical Engineering
Indian Institute of Technology
Kanpur - 208016

Dedicated to my
Grandfather, Maa, Babuji
&
Maa Saraswati

ACKNOWLEDGEMENTS

I express my deep sense of gratitude and sincere thanks to my supervisor Prof. Ravindra Arora for his invaluable guidance and constant encouragement throughout the course of this work. It has been a great experience to get the basic training of research under their rich experience, exemplary patience and exceptional capabilities of reducing complexity to simpler form. In spite of their busy schedule, they were available whenever I needed help. My thanks to Mr. S.V. Ghorpade and Mr. Lekhraj Singh for help in preparing the experiments setups and using the HV equipments.

I express my deep gratitude to the Department of Atomic Energy for sponsoring my M.Tech program at IIT Kanpur. I thank the Accelerator and Pulse Power Division of Bhabha Atomic Research Centre for providing me the opportunity to work on the present problem. Special thanks go to Mr. R. I. Bakhtsingh, Dr. K.V. Nagesh and others of the APPD for their invaluable suggestions and guidance during my work at BARC, which was intended to understand the problem and get required details.

I want to express my sincere thanks to my teachers Prof. P. Munshi, Prof. M.S. Kalra, Prof. A. Sengupta, Prof. S. Qureshi, Prof. A. ghosh and others. I also thank my seniors for their valuable cooperation during my stay at IIT Kanpur.

I sincerely thank my friends Vivek Shrivastav, Amar singh, Rajit Ram, Amit Kumar Pawar, Rajneesh Choudhary, Manas Ranjan Gartia, Vinay Kumar, Dayashankar Chaubey, Pankaj Kumar Meena, Tirtha Shankar Vishwakarma, Satyendra Singh and many others who made my stay at IIT memorable in my life. I am very thankful to my wife Chandraprabha , son Hansraj, younger brother Rajendra kumar and othetr family members for their constant support and encouragement.

Finally I would like to express my thanks to all those who helped me directly or indirectly in the progress and completion of this work.

CONTENTS

	Abstract	
	List of figures	
	List of tables	
	List of symbols	
Chapter 1	Introduction	1
Chapter 2	Selection of core material	7
	2.1 Core material	7
	2.2 Shape of the core	8
	2.3 Advantages of toroidal shaped transformer	8
Chapter 3	High voltage high frequency transformer	11
	3.1 Introduction	11
	3.2 Working principle of air-core transformer	11
	3.3 A design procedure of RF transformer	15
Chapter 4	Design of secondary winding	19
	4.1 Introduction	19
	4.2 4.2.1 The inductance of an air-cored coil	19
	4.2.2 Inductance calculations	21
	4.3 Q-factor	23
	4.3.1 General	23
	4.3.2 Loss due to dc resistance of winding	23
	4.3.3 Loss due to eddy current in winding conductor	24
	4.3.4 Loss due to stray capacitance	25
	4.3.4.1 Dielectric loss	25
	4.3.4.2 Loss due to circulating current in self capacitance	27
	4.3.5 The combined loss tangents	29
Chapter 5	Properties of Litz wire	31
	5.1 Introduction	31
	5.2 Power loss due to eddy currents in the winding	32
	5.2.1 General	32

	5.2.2	Skin effect	32
	5.2.3	Proximity effect	40
	5.3	When to use Litz wire	44
	5.4	DC resistance of a Litz conductor	45
Chapter 6		Insulation and dielectric circuit	46
	6.1	Electric fields	46
	6.2	Electric field Intensity	46
	6.3	Classification of electric fields	47
	6.3.1	Uniform fields	47
	6.3.2	Weakly nonuniform fields	47
	6.3.3	Extremely nonuniform fields	48
	6.4	Schwaiger factor	48
	6.5	Analysis of electric field intensity in homogeneous isotropic single dielectric	49
	I	Needle-needle electrode geometry	49
	II	Asymmetrical electrodes	49
	III	Corona and Partial Breakdown	50
	6.6	Field Enhancement factor	51
	6.7	6.7.1 Properties of composite dielectric	51
		6.7.2 Resultant permittivity for composite dielectrics	53
	6.8	Polarization under alternating voltage in insulating materials	54
	6.9	Insulating materials used in RF transformer	58
	6.9.1	Application of insulating materials	58
Chapter 7		Optimal design of single-layer air-core toroidal inductor for high frequency applications	61
	7.1	7.1.1 Introduction	61
		7.1.2 Basic assumptions	61
	7.2	Formulation of the problem	63
	7.2.1	Calculation of distributed capacitances	66
	7.2.2	Calculation of the overall parasitic or stray capacitance	67

7.3	Results and discussion	68
7.3.1	Stray capacitance for different edge factor k	70
7.3.2	Value of stray capacitance with and without insulation coating over wire	72
7.3.3	Values of stray capacitance for different values of the winding pitch	74
7.3.4	Values of stray capacitance for different values of the shield distance	77
Chapter 8	Experimental investigations	80
8.1	Introduction	80
8.2	High frequency response of toroidal shaped inductor	80
8.3	High frequency response of 2464/AWG 40 Litz Wire of one meter length	86
8.3.1	Determination of loss tangent of Litz wire conductor with increasing frequency	86
8.3.2	Determination of dielectric loss tangent for Litz wire insulation with increasing frequency	88
8.4	Breakdown test on square Litz polyester yarn insulated wire	91
Chapter 9	Finite Element Analysis of electric field intensity	93
9.1	Introduction	93
9.2	Finite Element Method (FEM)	93
9.3	Boundary conditions	100
9.4	FEMLAB Simulation results	101
Chapter 10	Conclusion and scope for future work	114
Appendix A	Comparison of Litz wire with solid wire	117
Appendix B	The high-frequency resistance of toroidal coils	120
Appendix C	Number of turns in primary winding of air-core toroidal transformer	122
References		124

ABSTRACT

A 3 MeV, 10 mA, 30 kW Dynamitron type electron beam accelerator for processing plastics is being commissioned at Khargur, Navi-Mumbai. The voltage of 3 MV is generated by 68-stage Parallel coupled Voltage Multiplier Circuit. The multiplier needs a stage voltage of $300 \text{ kV}_{\text{peak to peak}}$ at 120 kHz to feed the RF electrodes. This requirement is achieved by using 10 kV, 120 kHz vacuum triode power oscillator and then stepped up by the air-core RF transformer. The secondary winding of the air-core RF transformer acts as a tuned inductor for the power oscillator. For better attenuation, high Quality factor (about 1000) is required. It is achieved by providing special winding scheme; single layer, single wire spaced winding. The 120 kHz RF transformer has to handle a circulating current of $50 \text{ A}_{\text{rms}}$ in the secondary. The transformer is insulated and cooled by SF_6 gas at 6-atm. pressure. The air-core transformer is given shape by former of nonmagnetic material, epoxy laminates glass-fiber, which is compatible with SF_6 .

In this work the parameter affecting the Quality factor, 'Q' of inductor are investigated. Traditionally, transformer design has been based on sinusoidal voltage and current waveforms at low frequencies. At high frequency, skin and proximity effects, as well as dielectric losses contribute differently to transformer losses. Quality factor is the reciprocal of the sum of all loss tangents dc and ac (Loss tangent due to dc resistance of winding, loss tangent due to skin effect, loss tangent due to proximity effect, loss tangent due to residual core loss, dielectric loss tangent etc). Therefore, to achieve high Quality factor, loss tangents should be minimum. The Litz wire has been selected for this purpose. The choice of insulating material has been made knowing that dielectric loss tangent of any dielectric is maximum at its "eigen frequency".

The highest operating frequency affects the overall stray capacitance of the coil and it is determined by the first self-resonant frequency. In this work, a method for predicting stray or parasitic capacitances of high frequency toroidal inductors has been made which comprises of single wire, single layer of turns with circular cross section uniformly wound around a toroidal nonmagnetic core. The method is based on an analytical approach to obtain the turn-to-turn and turn-to-shield capacitances of the coil. The influence of wire insulation on the stray capacitances is taken into account. An

estimation of overall equivalent stray capacitance is made using typical high frequency equivalent lumped parameter circuit of inductors.

Electric field analysis for circular and square conductor configurations was made by FEMLAB. It is evident from this analysis that electric field enhancement is more at sharp edges of the conductor. Hence square conductor without sharp edges is recommended to achieve more uniform electric stress in the solid dielectric.

LIST OF FIGURES

Fig 1.1	Block diagram of 3 MeV, 30 kW accelerator	3
Fig 1.2	A schematic diagram showing Impedance scheme of 3 MeV, 30 kW EB accelerator	3
Fig 2.1	Schematic diagram of former of RF transformer	9
Fig 2.2	Magnetic flux line in Toroidal coil and Stick Coil	10
Fig. 3.1	General case of inductive coupling	12
Fig 3.2	Tuned air-core transformer	12
Fig 3.3	Toroidal coil equivalent circuit	12
Fig 3.4	Response curve for circuit tuned secondary of fig 3.2	14
Fig.3.5	Schematic diagram showing tank capacitance	15
Fig.3.6	Litz wire details	17
Fig. 4.1	Toroidal winding with opening at ends	20
Fig.4.2	Conductive mechanism in insulating materials for alternating voltage with equivalent circuit and vector diagrams.	26
Fig.4.3	Equivalent circuit to illustrate the loss due to circulating currents in the self-capacitance.	28
Fig 4.4	Typical variation of contributory loss tangents with frequency	30
Fig 5.1	Schematic diagram of Litz wire.	31
Fig.5.2 (a)	Skin effect in round conductors.	33
Fig 5.2 (b)	Proximity effect in round conductors	34
Fig 5.3	Frequency behavior of normalized ac current density for a copper wire of radius $a = 1\text{mm}$	37
Fig 5.4	Skin effect in metallic conductors	38
Fig 5.5	Skin effect factor F and proximity effect factor G_r , as a function of $2a/\Delta$ for round conductors, based on figures given by Butterworth ¹⁴ .	39
Fig 5.6	Calculation of eddy currents in a thin strip.	41
Fig 5.7	The cancellation of eddy-current emfs induced in twisted strands of bunched conductors determined by transverse flux.	44

Fig. 6.1	Extremely nonuniform field between needle-needle electrodes	49
Fig. 6.2	Asymmetrical electrode: point-plane geometry.	50
Fig. 6.3	Potential and field intensity distribution in uniform field with a perpendicular dielectric interface.	52
Fig. 6.4	Field intensity with varying dielectric layer thickness in a twin dielectric parallel plate condenser.	53
Fig. 6.5	Polarization under alternating voltage showing effect of frequency and temperature on relative permittivity and polarization losses.	55
Fig. 6.6	Plot of complex relative permittivity variation with frequency of applied voltage.	57
Fig. 7.1	Simplified HF model of inductors	61
Fig. 7.2	HF distributed equivalent circuit for a single layer air-core inductor with shield.	62
Fig. 7.3	Simplified HF distributed equivalent circuit	62
Fig. 7.4	VHF equivalent circuit for a single layer air-core inductor with shield.	63
Fig. 7.5	Air core inductor cross section with its essential dimensions.	64
Fig. 7.6	Cross-sectional view of coils and shields.	66
Fig. 7.7	Dimensions of toroidal shaped air-core.	69
Fig 7.8	Calculated stray capacitances for different values of the winding edge factor k .	71
Fig. 7.9	Comparison of Stray capacitance at different winding edge factor.	71
Fig. 7.10	Measured capacitances with and without insulation coating.	73
Fig. 7.11	Comparison of stray capacitances with and without insulation coating.	73
Fig. 7.12	Calculated Stray capacitance for different values of the winding pitch.	75
Fig. 7.13	Calculated Stray capacitance for different values of the winding pitch.	76
Fig. 7.14	Comparison of stray capacitances for different value of the winding pitch.	76
Fig. 7.15	Calculated stray capacitances for different values of the shield distance.	78
Fig. 7.16	Calculated stray capacitances for different values of the shield distance.	78

Fig. 7.17	Comparison of stray capacitances for different values of the shield distance.	79
Fig.8.1	(a) Q-curve and (b) Inductance curve, for prototype air-core toroidal inductor (rectangular cross section) of following specifications: Number of turns, $N=220$, Outer diameter of toroid (OD)=1515 mm, Inner diameter of toroid (ID)=455 mm, Axial height of toroid =510 mm, Winding: SWG 17 single wire single layer spaced. Original data measured using “HP 4284A precision LCR meter.	83
Fig.8.2	(a) Q-curve and (b) Inductance curve, for ferrite core toroidal inductor (circular cross section) of following specifications: Number of turns, $N=136$, Outer diameter of toroid (OD)=145 mm Inner diameter of toroid (ID)=83 mm Winding: SWG 17 single wire single layer spaced. Original data measured using “HP 4284A precision LCR meter.	84
Fig. 8.3	Q (magnitude) curves for (a) prototype air-core toroidal inductor, (b) Ferrite core toroidal inductor.	84
Fig. 8.5	Litz wire dc resistance and eddy current loss tangents as a function of frequency for one-meter length Litz wire. Litz wire details are: Number of strands=2464, dimension of each strands=40 American Wire Gauge (AWG),Dimensions of Litz wire: 5mm×5mm square Cross-section with no sharp edge.	88
Fig. 8.6	(a) Dielectric loss factor and (b) capacitance as a function of frequency for one meter length Litz wire having following specifications: Number of strands=2464 of AWG40 ,each are insulated with each other by enamel. Litz wire outer insulation is polyester fiber (Tergel). Size of Litz wire: 5mm×5mm square cross section with no sharp edge.	90
Fig. 8.7	Breakdown characteristics for one meter length Litz wire having following specifications: Nunmer of strands=2464 of AWG40, insulated with each other by enamel coating. Litz wire outer insulation is polyester fiber (Tergel). Size of Litz wire: 5mm×5mm square Cross-section with no sharp edge. Thickness of polyester fiber	

	over Litz wire conductor, $t=0.1$ mm, relative permittivity of polyester fiber, $\varepsilon_r=3.0$.	92
Fig. 9.1	Finite Element Mesh using Triangles.	94
Fig.9.2	A Tetrahedron and a triangular finite element.	94
Fig. 9.3	Part of two-dimensional field subdivided into irregular triangular elements on x- y plane.	96
Fig. 9.4	Node k of element (e), shown as node No. 5 connected to four triangular elements (1) to (4).	99
Fig. 9.5	Finite element mesh using triangles for (a) circular conductor configuration, (b) square conductor configuration and (c) square conductor configuration with no sharp edge.	101
Fig. 9.6	An electric potential distribution in dielectric for (a) circular conductor configuration, (b) square conductor configuration and (c) square conductor configuration with no sharp edge.	103
Fig.9.7	An electric field distribution in dielectric for (a) circular conductor configuration, (b) square conductor configuration and (c) square conductor configuration with no sharp edge.	105
Fig. 9.8	Comparison of maximum electric field intensity at the conductor surface for circular, square and square with no sharp edge conductor configurations.	106
Fig. 9.9	Electric potential and electric field intensity distribution for (a) circular conductor configuration, (b) square conductor (b) configuration and (c) square conductor configuration with no sharp edge.	108
Fig. 9.10	Electric field lines through dielectric for (a) circular conductor configuration, (b) square conductor configuration, and (c) square conductor with no sharp edge configuration.	110
Fig. 9.11	Surface charge distribution for (a) circular conductor configuration, (c) square conductor configuration, and (c) square conductor with no sharp edge configuration.	112
Fig. 9.12	Electric potential and electric field lines for square conductor with no sharp edge configuration.	113

LIST OF TABLES

Table 4.1	Correction term H in formula (4.3)	22
Table 4.2	Summary of loss expressions for inductors	29
Table 6.1	Dielectric properties of insulating materials used in RF transformer	58
Table 7.1	Geometrical Parameters of Inductor for different edge factor (k)	70
Table 7.2	Stray capacitance for different values of edge factor (k)	70
Table 7.3	Geometrical parameters for inductor with and without insulation Coating	72
Table 7.4	Stray capacitance with and without insulation coating	72
Table 7.5	Geometrical parameters of inductor for different winding pitch	74
Table 7.6	Values of stray capacitance for different values of winding pitch	75
Table 7.7	Geometrical parameters of inductor for different shield distance	77
Table 7.8	Values of stray capacitances for different values of winding pitch	77
Table 8.1	Measured data for prototype air-core toroidal inductor (rectangular cross section), N = 220 turns, SWG = 17, single wire, single layer spaced, Outer diameter of toroid = 1515 mm, Inner diameter of toroid = 455 mm, Axial height = 510 mm.	81
Table 8.2	Measured data for ferrite core toroidal inductor (circular cross section), N = 136 turns, SWG = 17, single layer single wire spaced, Outer diameter of toroid = 145 mm, Inner diameter of toroid = 83 mm	82
Table 8.3	Measured values of loss tangent for 1 m length Litz wire conductor of 2464/AWG 40	87
Table 8.4	Measured data for Insulation characteristics for 1 m length Litz wire of 2464/AWG 40	89
Table 8.5	Measured results for breakdown characteristics for one meter length Litz wire insulation	91
Table 9.1	Simulated values of electric field intensity at the conductor for Circular, square and square with no sharp edge, conductor Configurations	106

LIST OF SYMBOLS

RF	Radio frequency
HVDC	High Voltage Direct Current
Q-factor	Quality Factor
PB	Partial Breakdown
Δ	Skin Depth
2464/AWG 40	2464 number of strands each 40 American Wire Gauge
SWG	Standard Wire Gauge
P_c	Core loss per unit volume
B_p	Peak Flux Density
$\tan \delta$	Loss Tangent
E	Electric field intensity
H	Magnetic field intensity
η	Schwaiger Factor, Degree of uniformity
U_b	Breakdown Voltage
U_i	Partial Breakdown Inception Voltage
E_b	Breakdown Strength of dielectric
E_{\max}	Maximum electric field intensity
E_{mean}	Average electric field intensity
f	Field enhancement Factor
τ	Time constant
C_t	Turn-to-turn capacitance
C_s	Turn-to-shield capacitance
C_o	Overall stray capacitance
h	Average distance from turn-to-shield
pF	Pico Farad, 10^{-12} Farad
FEM	Finite Element Method

CHAPTER 1

INTRODUCTION

In recent times, continuous wave electron beam with beam voltage in the range 0.2-10 MV has found a large number of industrial applications such as modification of bulk polymers, cross linking of plastic film, foam & cables, degradation of scrap Teflon & cellulose materials, treatment of stack gases, disinfection of sewage sludge & waste water, sterilization of medical product and food irradiation. While beams of less than 1 MV are suitable for treatment of unit density materials of a few millimeter thickness, the higher energy beam can be used for thickness of a few centimeters. Further the higher energy beams can be efficiently converted into X-rays and then used to treat materials of tens of centimeter thickness. As compared to Co and other radiation sources, electron beam sources have the advantages of producing radiation when needed by switching on to the electron beam. The high power electron accelerators can provide high throughput rates at low unit costs compared to Gamma ray sources and X-ray generators. Of course depending upon the application, each energy source has some advantages over the others.

The 3 MeV, 30 kW industrial electron accelerator is similar to “Dynamitron” made by Radiation Dynamics, U.S.A.. Dynamitron type accelerators are highly versatile high voltage generators, where RF energy is capacitively coupled to the corona guard shields and HV rectifier column. Unlike Cockcroft Walton series multiplier, this is a parallel fed high voltage generator. This type of accelerator is developed because it has several advantages over others viz. (a) its ripple is independent of number of stages (N), (b) regulation is a function of N , unlike Cockcroft Walton where regulation is a function of N^2 , (c) there are no discrete capacitors, feedback and filter capacitors are all geometrically configured and (d) its operation at 100-120 kHz results in use of low value capacitors, hence energy stored is low and low loss to the components in case of dielectric failure.

The various subsystems of the 3 MeV, 30 kW industrial electron beam accelerators are:

- 1) HVDC power supply.
- 2) 120 kHz high power Oscillator.

- 3) High frequency (120 kHz), High voltage (300 kV_{peak}) Air core Transformer.
- 4) Parallel coupled voltage multiplier circuit.
- 5) Electron beam generation, Transport Focusing, Scanning & Extraction.
- 6) X-ray production.
- 7) Pumping system.
- 8) Accelerator tank.
- 9) SF₆ Gas handling system.
- 10) Ozone Extraction system.
- 11) Radiation shielding.
- 12) Control system.

OBJECTIVE OF THESIS WORK

This work is totally concentrated on the development of “High frequency (120 kHz), High voltage (300 kV_{peak}) Air core Transformer”. This transformer is to be used between the high frequency oscillator and voltage multiplier circuit to step up the voltage and to match the impedance for maximum power transfer. 120 kHz sinewave is generated by a class-c push-pull vacuum triode power oscillator. A toroidal inductor acts as the tuning inductor and step-up transformer to obtain a stage voltage of 150 kV_{peak} – 0 – 150 kV_{peak}. A schematic diagram representing impedance scheme and various subsystems are shown in Fig 1.1 and Fig 1.2.

The design of high frequency, high voltage air core transformer differs widely from the standard transformer design methodologies used for power frequency voltage applications [1]. One must analyse several related issues:

- 1) Insulation requirements.
- 2) Parasitic elements.
- 3) Core loss and Heat dissipation.
- 4) Corona effects.
- 5) High frequency skin and proximity effects.
- 6) Voltage and current waveforms.

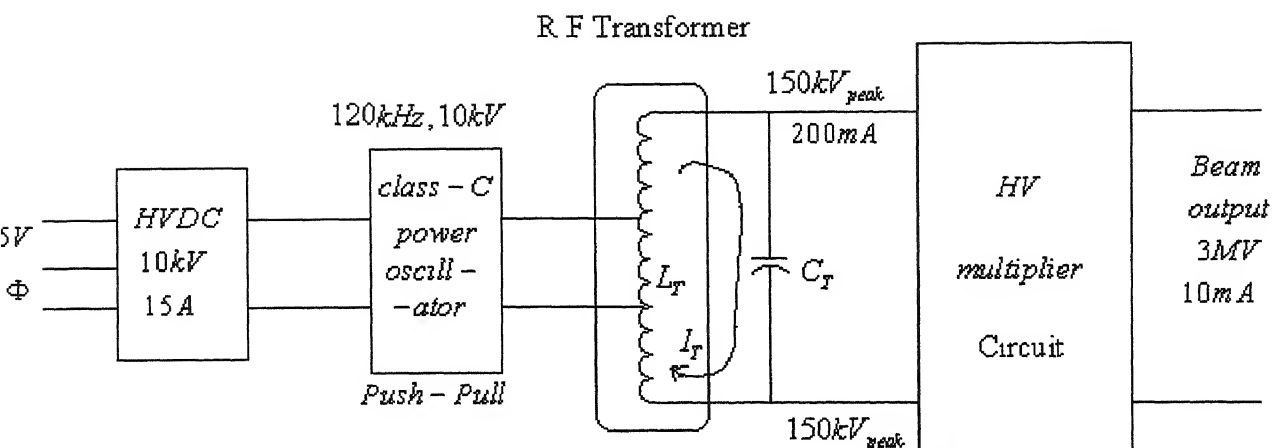


Fig 1.1 Block diagram of 3 MeV, 30 kW accelerator.

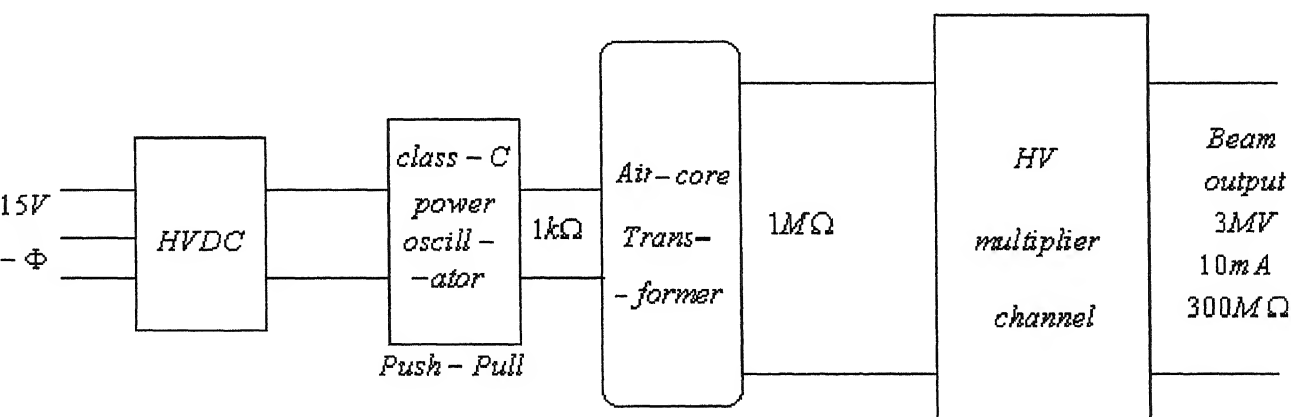


Fig 1.2 A schematic diagram showing Impedance scheme of 3 MeV, 30 kW EB accelerator.

Traditionally, transformer design has been based on sinusoidal voltage and current waveform operating at low frequency. Physical and electrical properties of a transformer form the basis of the new design methodology while taking full account of the current and voltage waveforms and high-frequency effects into consideration. It is well known that at high frequencies, eddy current induced skin and proximity effects cause additional losses within conductor windings. These effects alter the field and current distribution within the windings, which results in an increase in ac resistance. Due to high operating frequency, special attention must be paid to limit winding and core losses. These may lead to conflicting winding designs, especially with the use of litz wire. While litz wire can reduce high- frequency ac losses, its benefits are limited to a narrow frequency band and relatively low-current densities.

High voltage transformers generally have a high turns ratio. Sufficient insulation thickness between the primary and secondary is required to avoid electrical breakdown. Therefore, the electromagnetic coupling of the primary and secondary windings will not be as close as in conventional low voltage transformer [3]. These results in parasitic leakage inductance referred to the primary side, which can affect the maximum power transfer of the transformer. Hence, there is a trade off between insulation required and leakage inductance.

Furthermore, the high number of turns required for the secondary winding cause a high distributed capacitance. This parasitic capacitance induces an ineffective current through the secondary winding which results in a loss of transformer efficiency. To eliminate the parasitic capacitance effect, resonant transformer with high quality factor is a better choice, in which the secondary side of transformer is tuned at resonance frequency 120 kHz.

Partial Breakdown (PB) can seriously affect the operation and life expectancy of a high voltage transformer. Any sharp corner or protrusion may lead to an enhanced electric field and hence Partial Breakdown (PB) in the vicinity. With time it may degrade the insulation leading to electrical breakdown.

DESIGN SPECIFICATIONS

Bearing these factors in mind a high voltage, high frequency transformer is designed with the following electrical specification:

Primary voltage	: $5kV_{peak} - 0 - 5kV_{peak}$
Secondary voltage	: $150kV_{peak} - 0 - 150kV_{peak}$
Power rating	: 42 kW
Frequency	: 120 kHz
Temperature rise	: $< 30^{\circ}C$
Loaded Q-factor of coil	: 200

DESIGN BASIS AND ITS FEATURES

The transformer winding inductance is part of a parallel tuned circuit, at 120 kHz. The impedance reflected to the primary should not load the oscillator. The following parameters were chosen for the design:

- 1) Skin depth at 120 kHz, Δ : $190 \mu m$ (for copper)
- 2) Maximum flux density, B_{max} : 0.5 Tesla
- 3) Maximum current density, J_{max} : $4 A/mm^2$
- 4) Inductance of secondary : 5 mH
- 5) Secondary circulating current : $50 A_{rms}$
- 6) Insulation : SF_6 gas at 6 atm. Pressure
- 7) Litz wire for 120 kHz : 2464/AWG-40

Impedance matching at the primary side (vacuum Triode oscillator output) and secondary side (Voltage multiplier circuit input) are taken into consideration. To minimize the distributed capacitance between layers and windings, single layer spaced winding scheme is adopted.

For efficient heat transfer and cooling and to achieve a good electric insulation level, the entire transformer is placed in SF_6 gas at 6 atm. and the secondary cooling is done by forced cooling using low sound level blower.

Solid Insulating materials used are selected taking with consideration the following factors:

- (1) The coil former, support and winding materials should be compatible with SF_6 gas.

- (2) Eigen frequency of insulating material should not lie within working frequency.
- (3) Good dielectric and mechanical strength.
- (4) High radiation resistance.
- (5) Good thermal conductivity.

CHAPTER 2

SELECTION OF CORE MATERIAL

2.1 CORE MATERIAL

The characteristics of a good core material include low specific core losses (defined as losses per unit volume or per unit mass) at high operating frequencies, high saturation flux density, high power/weight ratio, and good thermal and mechanical properties. The use of high frequency in excess of 100 kHz enables the power-supply designer to reduce the size and weight of the power supply significantly. This reduction occurs because filter component values and transformer size decrease with increasing frequency. One problem with using transformers at frequencies above 100 kHz, however, is that core loss is much more significant than at lower frequencies such as 20 kHz. Core loss in ferrites is related to frequency by

$$P_c = Kf^{1.3}B_p^{2.6} \quad (2.1)$$

Where P_c is the core loss per unit volume (mW/cm³), f is the frequency (Hz), B_p is the peak flux density (G) so the core loss at 100 kHz is approximately eight times the core loss at 20 kHz assuming the same flux density [3].

Transformer design at low frequency (20 kHz) uses the saturation flux density of the core material as a primary design constraint [4]. Core loss is of secondary importance and is usually checked after the transformer design is finished. In most cases the core loss turns out to be acceptably low so that temperature rise due to core loss is not a problem.

At 100 kHz or above, however, operation at saturation flux-density level will result in an overheated transformer due to excessive core loss. Transformer design therefore, becomes more complicated at frequencies near or above 100kHz because peak flux density cannot be considered to be constant due to excessive temperature rise. So temperature rise and temperature dependence of permeability of magnetic material is the main constraint for the selection of core material. Since permeability of air is very stable with respect to the ambient conditions, all air-core, therefore, should make an ideal inductor [5]. So an air core has been selected for our RF transformer.

2.2 SHAPE OF THE CORE

The basic problem with air core is high leakage flux, which is minimised by using core in the form of toroidal shape (fig 2.1). The main reason for choosing a toroidal core is very small external magnetic field. Leakage flux can be a problem with solenoids, especially in power electronics circuits where it can cause interference to nearby equipment. It is shown more clear in fig 2.2. Whereas the external field of solenoid drops approximately as inverse cube of distance, that of a toroid falls much more steeply, and can be made virtually negligible if a reverse loop is used to counter the one-turn of the winding progression. Although, for economic use of wire air-cored toroids need not be considered further [6]. Also, a well-designed toroidal coil has more than twice the higher-frequency resistance of a well-designed solenoidal coil. Toroidal coils should only be employed when one cannot afford the slightest trace of electromagnetic interference, for example, when it is desired to construct an oscillating set to inject a very small measurable electromotive force into another circuit. For this reason it is considered worth to obtain conditions for minimum resistance [7].

2.3 ADVANTAGES OF TOROIDAL SHAPED TRANSFORMER

- (a) **Smaller size and Weight:** Higher efficiency of toroidal shaped winding over laminated type transformers can save up to 50% in weight and size. This helps simply the design of cabinets, mechanical geometry, and mounting configuration. It suits the trend for smaller, more compact electrical and electronic equipments. The diameter-to-height ratio of a toroid can easily be varied (as long as the cross sectional is held constant) to suit the mechanical design.
- (b) **Low Stray Magnetic Fields:** Toroid emits very low stray magnetic fields. For most applications no special shielding is needed.
- (c) **Low Mechanical Noise (Hum):** The uniformity in windings enveloping the core greatly reduce magnetostriction – the main source of the familiar “hum” found in conventional laminated transformers. Hence compared to conventional transformers, toroidal transformers are silent. This makes toroidal transformers ideal for hospital and office environments where an annoying hum would be unacceptable.

- (d) **Electrical Efficiency:** Toroidal design requires less copper wire as compared to conventional laminated transformers, resulting in low copper losses and hence more efficiency.
- (e) **Easy to Mount:** A single center screw quickly and easily mounts a toroidal transformer.

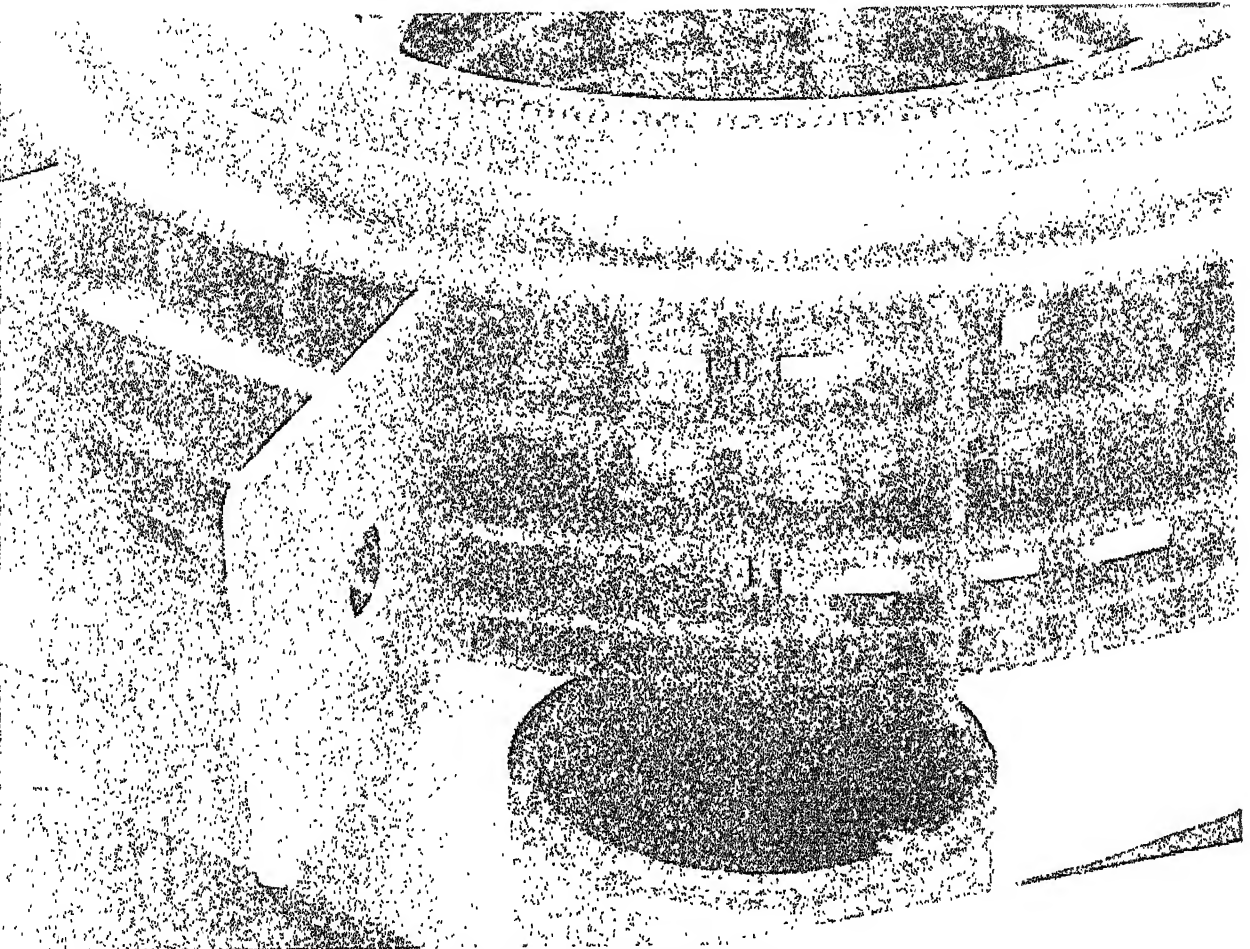


Fig 2.1 Schematic diagram of former of RF transformer.

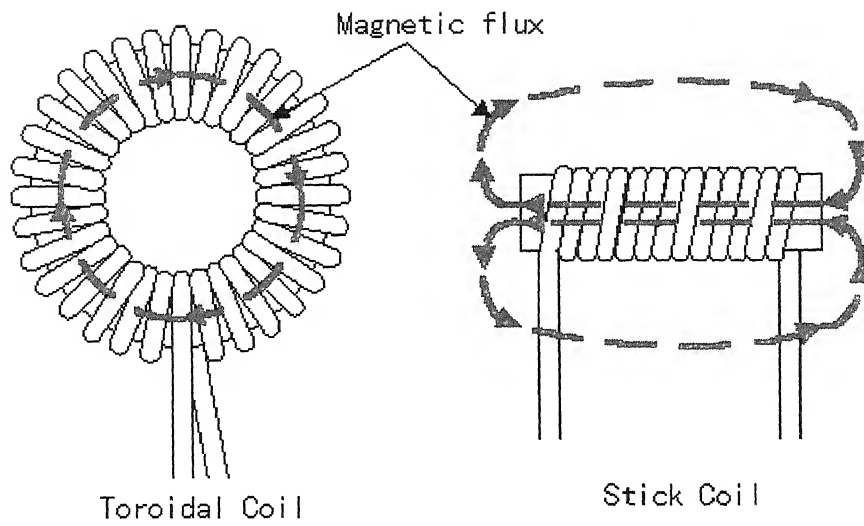


Fig 2.2 Magnetic flux line in Toroidal coil and Stick Coil.

CHAPTER 3

HIGH VOLTAGE, HIGH FREQUENCY TRANSFORMER

3.1 INTRODUCTION

High frequency high voltages are required for rectifier dc power supplies when a ripple of very small magnitude is required without the use of costly filters to smoothen the ripple [8]. The advantages of high frequency transformers are:

- (I) the absence of iron core in transformers and hence saving in cost and weight,
- (II) Pure sine wave output.

In a transformer with an iron core, the excitation current is required for producing the magnetic field in the core. This is a small percentage of the load component of the current in iron core transformers. In air-core transformers all the current is excitation current and the secondary voltage is induced proportional to the mutual inductance.

The commonly used high frequency, high voltage resonant and impedance matching transformers are the toroidal coil, which is single side tuned resonant circuit shown schematically in Fig. 3.2 and Fig.3.3. The primary voltage rating is 10 kV and the secondary is rated to 300 kV_{peak}. The secondary winding is wound on an insulated material body known as former. Hence, it is in real sense an air-cored transformer. Like in any autotransformer for primary winding suitable tapping is taken from the secondary, which is decided by the value of L_m , k and currents in both windings. The secondary windings are tuned to a frequency of 120 kHz by means of condenser C_T .

3.2 WORKING PRINCIPLE OF AIR-CORE TRANSFORMER

Consider the circuit of Fig. 3.1 in which Z_1 is complex and includes the self-inductance of the primary coil. Likewise, secondary impedance Z_2 is complex and includes the self-inductance of the secondary coil. With a sinusoidal voltage applied, Kirchhoff's laws give the following,

$$V_1 = Z_1 I_1 + j \omega L_m I_2 \quad (3.1)$$

$$0 = Z_2 I_2 + j \omega L_m I_1 \quad (3.2)$$

where $\omega = 2\pi$ times operating frequency, and L_m is the mutual inductance between the primary and secondary coils. From equation 3.2 we see that the voltage in the secondary coil is numerically equal to $\omega L_m I_1$, the product of primary current and mutual reactance at the frequency of applied voltage E_1 . The equivalent impedance of the circuit of fig 3.1 when referred to the primary side is given by

$$Z' = Z_1 + (X_m^2 / Z_2) \quad (3.3)$$

Where $X_m = \omega L_m$

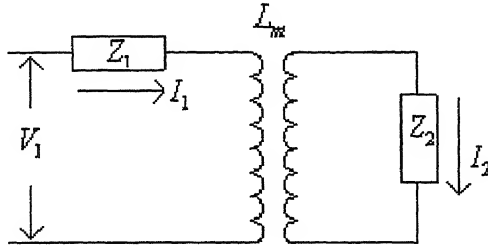


Fig. 3.1 General case of inductive coupling

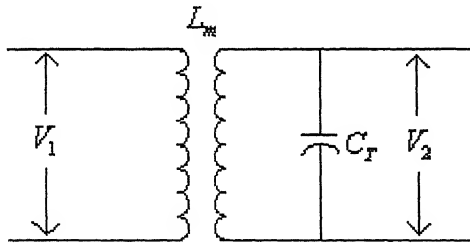


Fig 3.2 Tuned air-core transformer

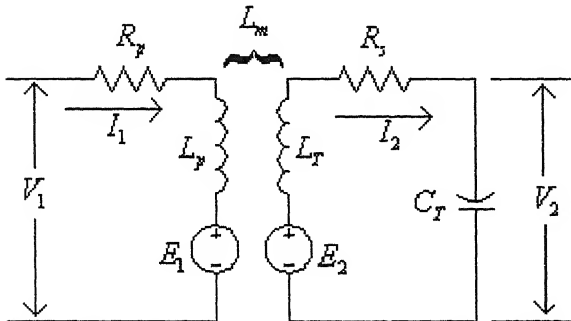


Fig 3.3 Toroidal coil equivalent circuit

When primary resistance is zero, or virtually zero, and the secondary coil is tuned to resonance so that Z_2 is a pure resistance R_2 . Under these conditions, equation 3.3 reduces to

$$R' = X_m^2 / R_2 \quad (3.4)$$

Where R' is the equivalent resistance in the primary.

Equation 3.4 gives the value of mutual inductance required for coupling a resistance R_2 so that it will appear like resistance R' with a maximum power transfer between the two coils, and states that the mutual reactance X_m is the geometric mean between the two value of the resistance.

The ratio of mutual inductance to the geometric mean of the primary and secondary self-inductances is the coupling coefficient:

$$k = L_m / \sqrt{L_p L_T} \quad (3.5)$$

The value of k is never greater than unity, even when coils are compacted to the maximum possible extent. Values of k down to 0.01 or lower are common at high frequencies. In present case feasible value of k is 0.2-0.3.

A single side (secondary) tuned air-core transformer is shown in fig 3.2 in which secondary coil is tuned at operating frequency 120 kHz. Its equivalent circuit is as shown in fig 3.3. A sinusoidal 120 kHz voltage V_1 may be impressed upon the primary circuit from vacuum triode oscillator. The value of voltage V_2 obtained from this circuit depends upon the Q factor of the tuned circuit. Fig 3.4 shows the admittance curve for tuned secondary of fig 3.2.

Voltages induced in primary and secondary coils are given by equations 3.6 and 3.7 respectively.

$$E_1 = j\omega L_m I_2 \quad (3.6)$$

$$E_2 = j\omega L_m I_1 \quad (3.7)$$

$$\Rightarrow \frac{E_1}{E_2} = \frac{I_2}{I_1} \quad (3.8)$$

$$\text{At resonance, } X_{L_T} = X_{C_T} \quad (3.9)$$

$$\omega L_T = \frac{1}{\omega C_T} \quad (3.10)$$

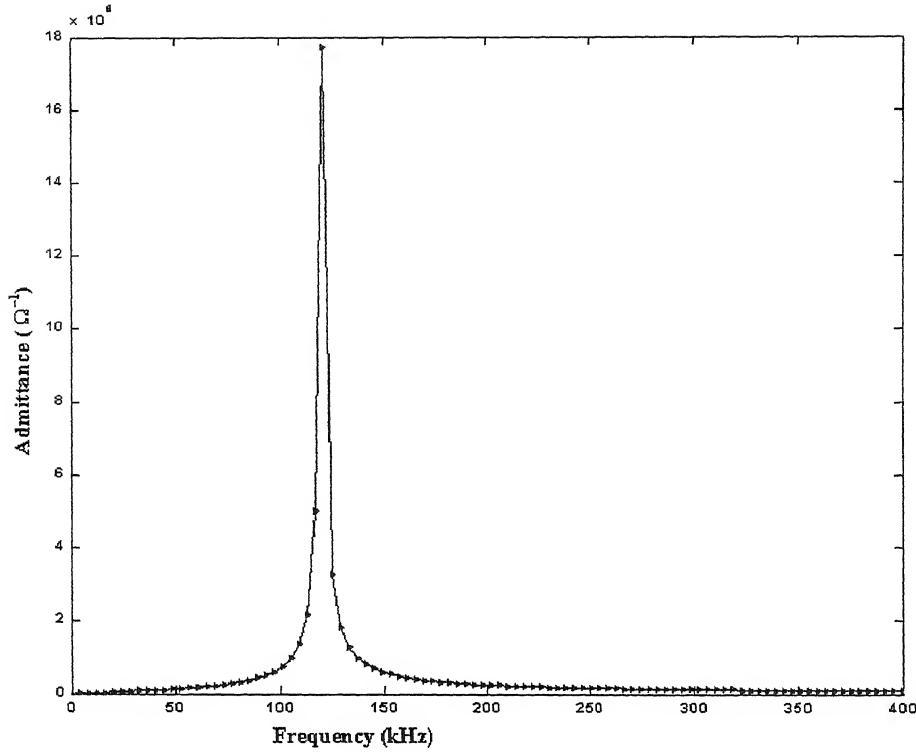


Fig 3.4 Response curve for circuit tuned secondary of fig 3.2

$$f = \frac{1}{2\pi\sqrt{L_T C_T}} \quad (3.11)$$

Under this condition, magnitudes of voltages across capacitor (C_T) and inductor (L_T) are equal. These are given by

$$V_2 = V_{L_T} = V_{C_T} = QE_2 \quad (3.12)$$

Where Q is the quality factor of the circuit, given by

$$Q = \frac{\omega L_T}{R_s} = \frac{1}{\omega C_T R_s} \quad (3.13)$$

The circulating current in secondary winding under resonance condition is given by

$$I_2 = \frac{V_{L_T}}{X_{L_T}} = \frac{V_{C_T}}{X_{C_T}} = \frac{E_2}{R_s} \quad (3.14)$$

Because of air-core, no load current cannot be neglected as in case of iron core transformer. In our case even at no load secondary circulating current is 50 A_{rms} at 300 kV_{peak} and primary current is 5 A_{rms} and when it is in operation it deliver only 200 mA. Hence primary mmf is not equal to secondary mmf in air-core transformer.

$$N_1 I_1 \neq N_2 I_2 \quad (3.15)$$

$$\frac{E_2}{E_1} \neq \frac{N_2}{N_1} \quad (3.16)$$

so induced voltage in secondary is based on L_1 , L_2 , L_m .

3.3 A DESIGN PROCEDURE OF RF TRANSFORMER

The design procedure depends upon the requirements and the specifications. The procedure outlined below includes the steps in the design of a high voltage, RF transformer.

- (1) Fixing operating frequency (f) and its tolerance: $110 \text{ kHz} \pm 10 \text{ kHz}$, which is determined by high frequency rectifier of voltage multiplier circuit, time required for reverse bias recovery, ripple etc.
- (2) Inductance and Capacitance of tank circuit (secondary of RF transformer): Tank capacitor (C_T) is the equivalent capacitance across RF electrode as shown in fig 3.5. It is of known quantity. Based on this value of inductance required can be calculated by the following equation;

$$L_T = \frac{1}{(2\pi f)^2 C_T};$$

For $f = 120 \text{ kHz}$ and $C_T = 350 \text{ pF}$,

$$L_T = 5 \text{ mH}$$

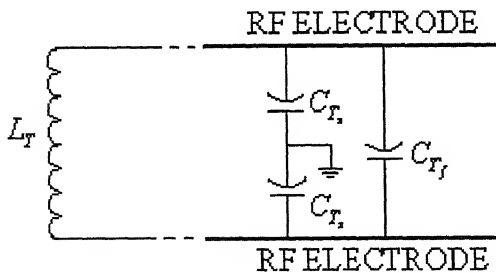


Fig.3.5 Schematic diagram showing tank capacitance

C_{T_r} - Capacitance between RF electrode and shield

C_{T_f} - Capacitance between RF electrode

C_T - Tank capacitor which is the equivalent capacitance across RF electrode

- (3) Fixing impedance criteria to match the input impedance of multiplier circuit and output impedance of oscillator (Fig. 1.2).
- (4) Fixing secondary voltage (V_2): V_2 required is $150 \text{ kV}_{\text{peak}} - 0 - 150 \text{ kV}_{\text{peak}}$. This voltage is given to the RF electrode of parallel coupled voltage multiplier circuit. By this multiplier circuit the voltage is stepped-to 3 MV.
- (5) Circulating current in tank ($L_T C_T$) circuit: Circulating current in tank circuit (secondary winding) under resonance condition can be calculated with given specification using equation (3.14) as following

$$I_2 = \frac{V_{2_{\text{rms}}}}{X_{L_T}} = \frac{300 \times 10^3 / \sqrt{2}}{2\pi \times 120 \times 10^3 \times 10^{-3}}$$

$$= 56 \text{ A}_{\text{rms}}$$

- (6) Losses (P_0) depend upon heat dissipation in transformer winding as well as Q factor: Q factor can be calculated using equation (3.13). Losses in the tank circuit are given by

$$\text{losses}(P_0) = I_2^2 R_{ac}$$

$$P_0 = \frac{V_{2_{\text{rms}}}^2}{X_{L_T}^2} R_{ac} = \frac{V_{2_{\text{rms}}}^2}{Q X_{L_T}}$$

- (7) Components of R_{ac} : More detail are in chapter 4.

$$R_{ac} = R_{dc} + R_{\text{skin-effect}} + R_{\text{proximity-effect}} + R_{\text{dielectric}}$$

- (8) (a) Selection of wire to minimize skin and proximity effect: 2464 strands/AWG-40 litz wire were chosen for this purpose. All strands are twisted in a regular pattern. More detail are in chapter 5. Litz wire details are

- (i) Copper Area = 12.4 mm^2
- (ii) Insulation: 180°C grade single polyurethane based enamel on individual strands and double layer 130°C grade Tergal (polyester fiber) over the entire bunch of 2464 strands.
- (iii) $R_{dc} = 1.7 \text{ m}\Omega/\text{meter}$

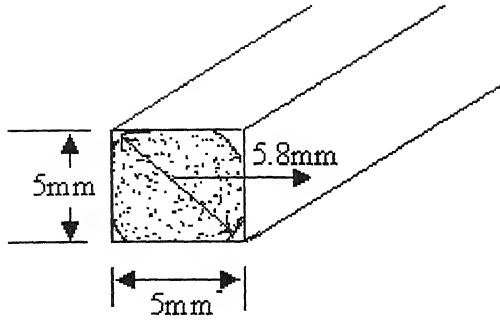


Fig.3.6 Litz wire details

(b) Selection of winding scheme and its dimensions to minimise self capacitance and dielectric losses. The self capacitance is fixed such that self resonance frequency should be greater than and equal to three times the working frequency. More details are in chapter 7.

(9) Effective removal of heat: It is made effective by using blowers, heat exchanger inside RF Transformer vessel.

(10) Determination of current density as per (8 and 9) .

$$J = \frac{50}{12.5} = 4A/mm^2, \text{ for single layer spaced winding and forced}$$

cooling in SF₆ gas at 6 atm pressure.

(11) Design of primary winding: It is based on the source voltage (10 kV), vacuum triode oscillator output.

$$\frac{E_1}{E_2} = \frac{N_1}{N_2} \text{ is valid if and only if coupling coefficient (k) between primary}$$

and secondary winding is equal to 1. But in present case feasible value of k is given as 0.2-0.3, so primary induced voltage is based on the primary winding inductance, secondary winding inductance, mutual inductance between primary winding and secondary winding and coupling coefficient. In present case we know the value of secondary winding inductance and coupling coefficient. By knowing Q factor we can obtain secondary induced voltage using equation (3.12) and then using equation (3.7) and (3.5) we can obtain mutual inductance and value of primary inductance. With the help of inductance formula we find number of turns required in primary winding (appendix C).

(12) Design of stress control rings across 300 kV_{peak} terminal.

(13) Design of bushing across $300 \text{ kV}_{\text{peak}}$ opening for mechanical strength..

(14) Insulation scheme for entire RF transformer

- (i) turn to turn insulation
- (ii) winding to winding insulation
- (iii) Winding Former: Structure made of insulating material to provide desired shape of winding.
- (iv) Insulation between RF transformer and pressure vessel at ground potential.

CHAPTER 4

DESIGN OF SECONDARY WINDING

4.1 INTRODUCTION

An Inductor is an element that stores energy in the magnetic field. It is comprises of a coil wound in a several turns on a core with a closed magnetic path. The magnetic path may comprise of material of homogeneous or heterogeneous permeability. The homogeneous path may comprise of all ferrous alloys or ferrites or air alone. A heterogeneous permeability path is a combination of magnetic core path with air gaps.

Inductance has been one of the principle passive elements of frequency-selective networks. Before considering the theory and practice of inductor (secondary winding of RF transformer) design in detail it may be useful to survey the requirements of a high-quality inductor. A high Q-factor for a given volume is nearly always desirable because this enables a better network to be made from a given number of inductors or alternatively a given attenuation/frequency characteristic to be obtained. A high Q-factor implies a low magnetic loss. It is true that the core that can contain a winding giving the lowest ratio of d.c.resistance to inductance has the best overall performance [9].

4.2.1 THE INDUCTANCE OF AN AIR-CORED COIL

Consider an inductor wound on non-magnetic toroidal core as shown in Fig. 4.1. The inductance of equivalent cylindrical air-cored solenoid having N turns is given by Nagaoka's formula [10].

$$L = \frac{\mu_0 N^2 A}{l_c} \text{ H} \quad (4.1)$$

Where $A = \frac{\pi D^2}{4}$, D is the mean diameter of the coil in m = $\frac{(OD - ID)}{2}$

l_c is the axial length of the coil in m = $\frac{\pi(OD + ID)}{2}$ - length of opening at ends

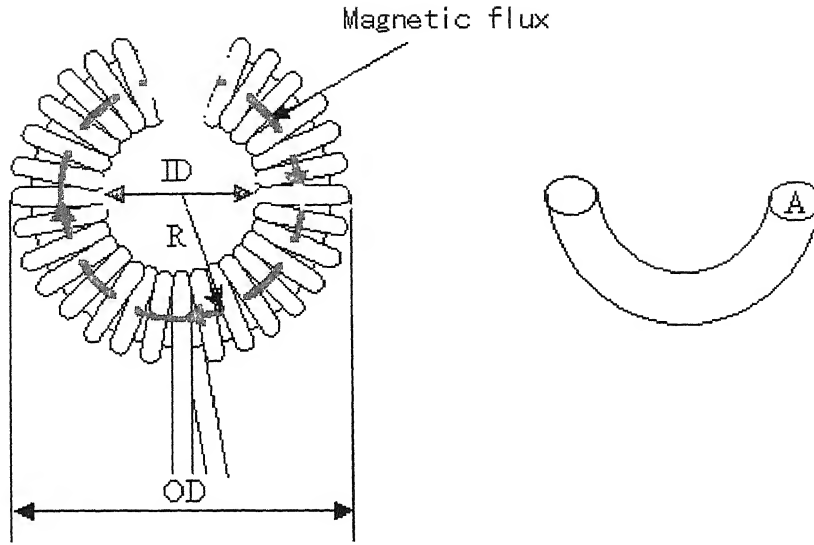


Fig. 4.1 Toroidal winding with opening at ends

Formulas for the ideal case of a current sheet, such as would be attained by a winding of very thin tape with negligible insulating space between the turns that are wound in a single layer on a toroidal-shaped form is given by Grover [11] are

$$L = 1.257 N^2 \left(R - \sqrt{R^2 - (D/2)^2} \right) \mu H \quad (4.2)$$

where R = the mean radius of winding form in meter and D = the diameter of the circle enclosed by each turn in meter.

The correction for insulating space ΔL , which is to be subtracted from L , is given by Rosa's method [11].

$$\Delta L = 0.2 N \pi D (G + H) \mu H \quad (4.3)$$

in which H is to be taken from table 4.1 for a given number of turns and G is to be obtained from the following defining equation:

$$G = \frac{5}{4} - \log_e 2 \frac{p}{d} \quad (4.4)$$

where p is the mean of the inner and outer pitches of the winding.

d is the bare diameter of the wire.

4.2.2 INDUCTANCE CALCULATIONS

The designed toroidal air-cored winding specifications are given below:

Outer Diameter (OD) of toroid = 1500 mm,

Inner Diameter (ID) of toroid = 600 mm,

Number of turns, $N = 280$,

opening at ends = 200 mm

$$\text{Mean axial length of winding } l_c = \frac{\pi(OD + ID)}{2} - 0.2 = 3.098m$$

$$\text{The core area } A = \frac{\pi(OD - ID)^2}{16} = 0.159m^2$$

$$\text{The mean radius of the winding form } R = \frac{OD - D}{2} = \frac{1500 - 450}{2} = 525mm = 0.525m$$

The diameter of the circle enclosed by each turn

$$D = \frac{OD - ID}{2} = \frac{1500 - 600}{2} = 450mm = 0.450m$$

The inductance is calculated from equation (4.1) as follows:

$$L = \frac{\mu_0 N^2 A}{l_c} = \frac{4 \times \pi \times 10^{-7} \times 280^2 \times 0.159}{3.098} \approx 5mH$$

The value of inductance calculated from equation (4.2) is as follows:

$$L = 1.257N^2 \left(R - \sqrt{R^2 - (D/2)^2} \right) = 1.257 \times 280^2 \left(0.525 - \sqrt{(0.525)^2 - (.450/2)^2} \right) \\ \approx 5mH$$

These calculation shows that value of inductance is same for both toroidal coil formula (equ. 4.1) and equivalent solenoidal coil formula (equ. 4.2).

Table 4.1 CORRECTION TERM H IN FORMULA (4.3)

N	H	N	H
1	0	45	0.3164
2	0.1137	46	.3168
3	.1163	47	.3172
4	.1973	48	.3175
5	0.2180	49	.3179
6	.2329	50	0.3182
7	.2443	55	.3197
8	.2532	60	.3210
9	.2604	65	.3221
10	0.2664	70	.3230
11	.2715	75	0.3238
12	.2758	80	.3246
13	.2795	85	.3253
14	.2828	90	.3259
15	0.2857	95	.3246
16	.2883	100	0.3269
17	.2906	110	0.3278
18	.2927	120	.3285
19	.2946	130	.3291
20	0.2964	140	.3296
21	.2980	150	0.3301
22	.2994	160	.3305
23	.3008	170	.3309
24	.3020	180	.3312
25	0.3032	190	.3315
26	.3043	200	0.3318
27	.3053	220	.3323
28	.3062	240	.3327
29	.3071	260	.3330
30	0.3079	280	.3333
31	0.3087	300	0.3336
32	.3095	450	.3341
33	.3102	400	.3346
34	.3109	450	.3349
35	0.3115	500	0.3351
36	.3121	550	.3354
37	.3127	600	.3356
38	.3132	650	.3357
40	0.3142	700	.3358
41	.3147	750	0.3360
42	.3152	800	.3361
43	.3156	850	.3362
44	.3160	∞	0.3379

4.3 Q-FACTOR

4.3.1 GENERAL

The Q-factor of a resonant circuit is the reciprocal of the sum of all the contributory loss tangents, $\tan \delta_{tot}$ corresponding to the various origins of loss. For this reason it is convenient to work in terms of loss tangents

$$\frac{1}{Q} = \tan \delta_{tot} \quad (4.5)$$

The design problem therefore is to calculate the contributory loss tangents and to minimize the total. The following sections first consider these loss factors separately and then in combination. Finally the overall Q-factor is considered in relation to frequency, inductance, type of winding conductor, and the effective permeability of the core.

4.3.2 LOSS DUE TO THE DC RESISTANCE OF WINDING

If R_{dc} is the dc resistance of a winding and L is the inductance then the corresponding loss tangent is

$$\tan \delta_{dc} = R_{dc} / \omega L \quad (4.6)$$

At a given frequency this factor depends primarily on the geometry of the core. The reciprocal of $\tan \delta_{dc}$ is the Q-factor due to the dc winding resistance. It is usually impracticable to obtain high Q-factors at low frequencies because (1) in this region $\tan \delta_{dc}$ ($= R_{dc} / \omega L$) is almost the only loss contribution so the Q-factor is proportional to f , and (2) R_{dc}/L can only be decreased significantly by using larger cores or larger effective permeabilities. Economics limit core size, and the need for inductance constancy or adequate adjustment range limits the value of effective permeability.

If winding wire is chosen in such a way that there dc resistance is very small, and then it is possible to obtain very high Q-factors at high frequency. Litz wire is chosen for this purpose.

4.3.3 LOSS DUE TO EDDY CURRENTS IN THE WINDING CONDUCTOR

As the frequency increases additional losses occur in the windings due to eddy currents induced in the conductors by the magnetic fields within the winding. The eddy current phenomenon is considered in detail in chapter 5.

In the design of inductors, both skin effect and proximity effect need to be considered. Both effects depend upon the ratio of conductor diameter, $2a$, to penetration depth (skin depth), Δ .

Skin effect is the tendency for the alternating currents to flow near the surface of the conductor. It is due to eddy currents in conductor, which arise from the magnetic field associated with the currents in the conductor itself (Fig 5.1). It causes the resistance to increase by an amount, R_{se} , above the dc value. Therefore the ac resistance due to the skin effect may be expressed by

$$R_{ac} = R_{dc} + R_{se} = R_{dc}(1 + F) \Omega \quad (4.7)$$

Where F is the skin effect factor. It is given as a function of $2a/\Delta$ in Fig 5.5. The skin effect loss tangent, $\tan \delta_{se}$, may be calculated from

$$\tan \delta_{se} = \frac{R_{se}}{\omega L} = \frac{R_{dc} F}{\omega L} \quad (4.8)$$

In most inductor designs the skin effect loss is small compared with other losses. If solid conductors are used, then at low frequencies $\tan \delta_{se}$ is very small while at frequencies for which $\tan \delta_{se}$ is near maximum, proximity effect will usually be very much larger than the skin effect. With bunched conductor, i.e. conductor formed as a rope of insulated strands, the skin effect is usually very much reduced. However, measurements have shown that most bunched conductors behave as though the strands weave between the outer surface and the center thus preventing skin effect by ensuring a uniform current distribution. This arises because bunched conductors are usually made by twisting together groups of strands which have, in turn, been twisted together. Thus most bunched conductors behave as though the strands are almost perfectly transposed, so the skin effect is negligible. More details are in chapter 5.

The major cause of eddy current loss in inductor windings is proximity effect. This is the effect of the magnetic field of the winding as a whole. In most cases this field is substantially perpendicular to the axis of the conductor at any point. Eddy

currents flow and return along the length of each conductor in such a way as to oppose the field. This effect is examined in more detail in chapter 5. Proximity effect loss tangent, $\tan \delta_{pe}$, is given by

$$\tan \delta_{pe} = \frac{\pi^2 k l_c}{32 \rho_c \mu_0 A} \times \frac{f l_w N n (2a)^2 G_r}{\mu_e} \quad (4.9)$$

Where k is constant for a given core and winding geometry.

l_w is the mean turn length

l_c is the axial length of winding

N is the number of turns,

n is the number of strands in the conductor if bunched conductor is used,

$2a$ is the diameter of the solid conductor or strand,

μ_e is the effective permeability of core

G_r is a factor that arises from the tendency of the eddy currents to prevent the field from penetrating the conductor; it is a function of $2a / \Delta$

4.3.4 LOSSES DUE TO STRAY CAPACITANCE

It is assumed that the stray capacitances may be regarded as a single self-capacitance, C_s , connected in parallel with winding. This self-capacitance may contribute to the total loss tangent in two ways. The first arises simply from the loss angle associated with C_s and is referred to as dielectric loss and the second is called shunt capacitance loss and arises in certain circumstances due to circulating currents in the LC_s circuit. Each loss will now briefly be considered.

4.3.4.1 DIELECTRIC LOSS

Besides the capacitive charging currents, real or active currents are also present in the dielectrics. These currents are caused due to different types of conductivities and polarizations present in the materials. These currents not only depend upon the frequency, magnitude of the applied voltage but also upon the thermal conditions of the dielectric [12]. The conductive currents present in an insulating material

determine its dielectric power loss property. Each conductive current mechanism causes currents in different characteristics. The currents contribute to the total dielectric current ' i_{ins} ', as depicted schematically for alternating voltage is in Fig. 4.2

The dielectric loss tangent ' $\tan \delta$ ' is defined as the quotient of active to reactive power loss in a capacitor. It is derived from Fig. 4.2 as follows:

$$\tan \delta = \text{Active Power} / \text{Reactive Power}$$

$$= \frac{u \cdot i_{ins} \cos \varphi}{u \cdot i_{ins} \sin \varphi} = \frac{i_{R(\text{total})}}{i_{C(\text{total})}} \quad (4.10)$$

The dielectric loss tangent ($\tan \delta$) represents the complete power loss in a dielectric; hence it is a parameter with which the power losses in a capacitor can be estimated.

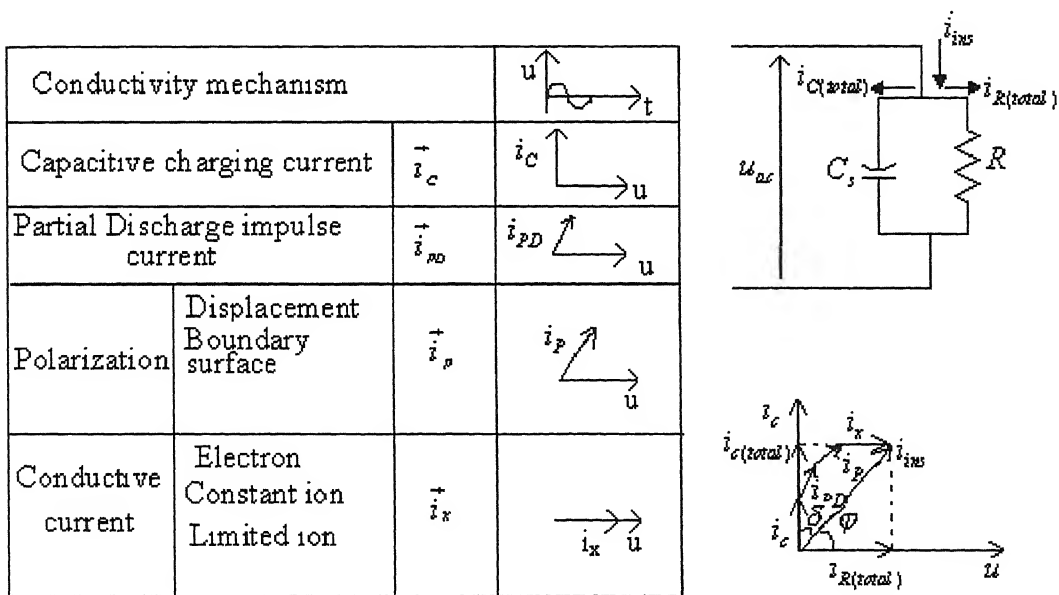


Fig.4.2 Conductive mechanism in insulating materials for alternating voltage with equivalent circuit and vector diagrams.

However, $\tan \delta$ is a function of frequency and magnitude of the applied voltage as well as the temperature of the dielectric, because these affect the conductivity and polarization process in the dielectrics.

When alternating voltage of rms magnitude U and frequency ω is applied to a condenser having total effective capacitance C_s , the total capacitive conductive current $I_{C(\text{total})}$ is given by

$$I_{C(\text{total})} = \frac{U}{1/\omega C_s} = \omega C_s U \quad (4.11)$$

The active part of the total insulation current ($I_{R(\text{total})}$) is ($\omega C_s U \cdot \tan \delta$), hence the active power loss ' P_{ac} ' is given by,

$$P_{ac} = \omega C_s U^2 \cdot \tan \delta \quad (4.12)$$

Where $\omega = 2\pi f$ and f is in Hz, C_s is in F and U is in volts, P is in watts.

Loss conductance appearing in parallel with the inductance is

$$G_s = \omega C_s \tan \delta \quad (4.13)$$

This loss contributes to a loss tangent, $\tan \delta_{cp}$, to the overall loss tangent of inductor:

$$\tan \delta_{cp} = \omega L G_s = \omega^2 L C_s \tan \delta \quad (4.14)$$

$$= \frac{C_s}{C_{res}} \tan \delta \quad (4.15)$$

where C_{res} is the total capacitance required to resonate the inductor L at the frequency $\omega/2\pi$, i.e. $C_{res} = 1/\omega^2 L$.

Normally $\omega^2 L C_s \ll 1$, i.e. the inductor will not be near self-resonance at its design frequency. If, however, a specifications calls for a high inductance at a high frequency then self-resonance may be approached and the degradation of Q-factor due to the dielectric loss would become appreciable. In the limit $\tan \delta_{cp}$ would equal $\tan \delta$.

4.3.4.2 LOSS DUE TO CIRCULATING CURRENT IN SELF CAPACITANCE

This occurs in a series resonant circuit when the inductor is shunted by a self-capacitance. The equivalent circuit is shown in Fig.4.3; R_L represents the loss associated with the inductor and C_s is at this stage considered loss-free. The impedance in series with the resonating capacitance, C_s , is

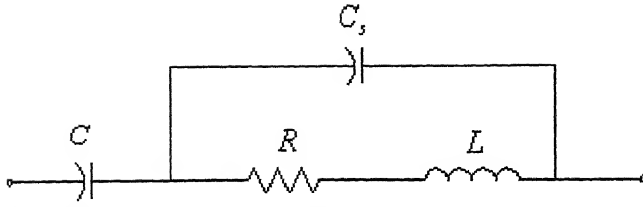


Fig.4.3 Equivalent circuit to illustrate the loss due to circulating currents in the self-capacitance.

$$\frac{R + j\omega L}{j\omega C_s \{R + j(\omega L - 1/\omega C_s)\}} \approx R(1 + 2\omega^2 LC_s) + j\omega L(1 + \omega^2 LC_s) \quad (4.16)$$

This assumes that $R/\omega L$ and $(\omega^2 LC_s)$ are negligible compared with unity, i.e. that the inductor Q-factor is reasonably high and that the inductance is far from self-resonance. Both of these conditions are normally satisfied in practice. The real part of this expression represents the series loss resistance and this is greater than R by an amount $2R\omega^2 LC_s$. Since the Q-factor of the inductor is more readily estimated than the value of R, this increase in loss resistance is more conveniently expressed as $2\omega^3 L^2 C_s / Q$, i.e. the loss tangent of the inductor is increased by $2\omega^2 LC_s / Q$ or $2C_s / C_{res} Q$.

If dielectric loss of self-capacitance, $\tan \delta$, is also taken into account, by including a resistance in series with the capacitance, an expression corresponding to equation (4.16) may be obtained in which the real part is

$$R + ((2/Q) + \tan \delta) \omega^3 L^2 C_s \quad (4.17)$$

assuming $\tan \delta \ll 1$

Thus the total loss factor, $\tan \delta_{cs}$, due to the self capacitance in a series circuit is given by

$$\tan \delta_{cs} = ((2/Q) + \tan \delta) \omega^2 LC_s \quad (4.18.1)$$

$$= (2 \tan \delta_L + \tan \delta) C_s / C_{res} \quad (4.18.2)$$

where Q and $\tan \delta_L$ refer to the inductor. From equation (4.18.1) and (4.18.2), it is clear that degradation of Q-factor due to dielectric loss would become appreciable.

4.3.5 THE COMBINED LOSS TANGENTS

Since we are using air core, eddy current and hysteresis losses in core can be neglected. The total loss tangent is the sum of all the contributory loss tangents. The loss tangent due to the dc winding resistance is inversely proportional to f while other loss tangents are approximately proportional to f or f^2 . It follows that, other parameters being constant, there will be a frequency at which the total loss tangents is a minimum. Table 4.2 shows the summary of loss expressions for inductors.

Table 4.2
Summary of loss expressions for inductors

Loss tangent due to:	Symbol	Expression	Eqn No.
DC Resistance	$\tan \delta_{dc}$	$R_{dc} / \omega L$	4.6
Skin effect	$\tan \delta_{se}$	$\frac{R_{dc} F}{\omega L}$	4.8
Proximity effect	$\tan \delta_{pe}$	$\tan \delta_{pe} = \frac{\pi^2 k l_c}{32 \rho_c \mu_0 A} \times \frac{f l_w N n (2a)^2 G_r}{\mu_e}$	4.9
Dielectric loss in self capacitance (parallel resonant circuit only)	$\tan \delta_{cp}$	$\omega^2 L C_s \tan \delta$ $= \frac{C_s}{C_{res}} \tan \delta$	4.15
Circulating current in self capacitance (series resonant circuit only)	$\tan \delta_{cs}$	$((2/Q) + \tan \delta) \omega^2 L C_s$ $(2 \tan \delta_L + \tan \delta) \frac{C_s}{C_{res}}$	4.18

Fig 4.4 shows a typical variation of all the contributory loss tangents with frequency for an arbitrary inductor design. The upper most curve is the total loss tangent. At low frequencies the total loss tangent is due almost entirely to the dc resistance of the winding. As the frequency rises this contribution first falls, and achieve a minimum. As the frequency increases further, it rises again. The relative magnitude of the contributory loss tangents at any frequency depends upon the inductor design. At higher frequencies

the total loss tangent may be dominated by the loss due to the proximity effect, the self-capacitance or the core.

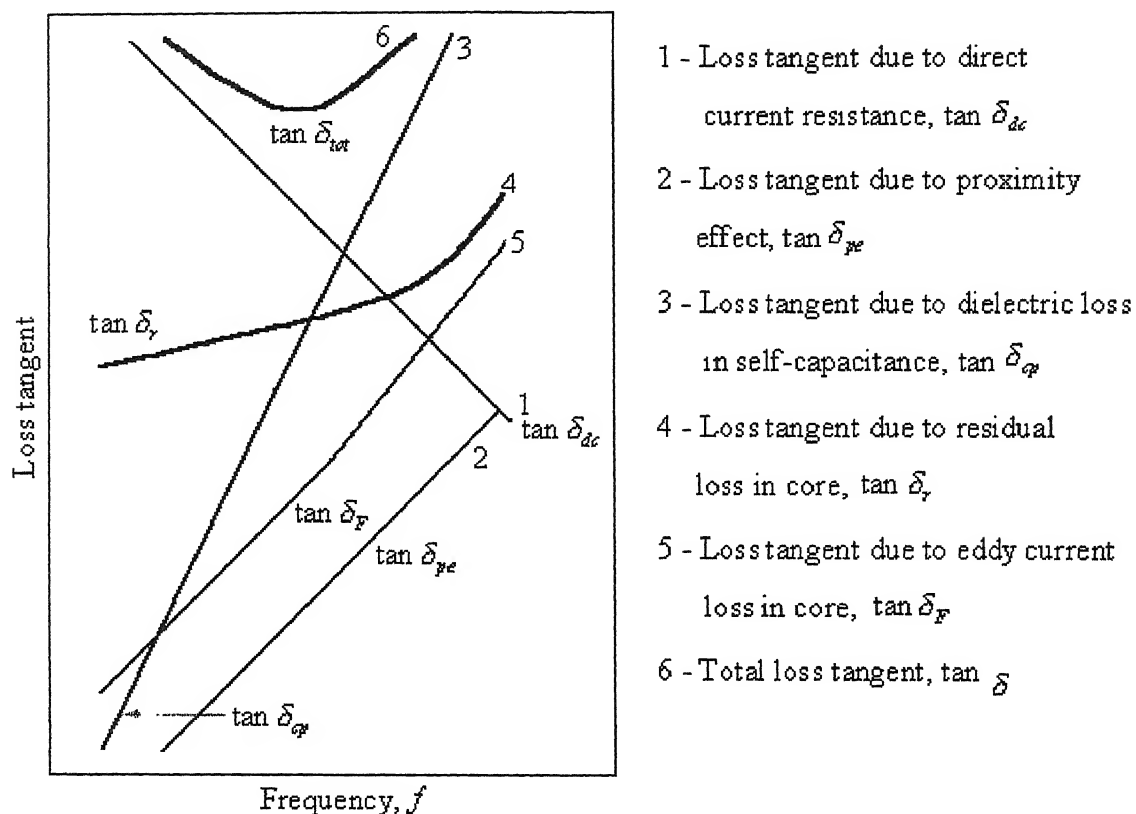


Fig 4.4 Typical variation of contributory loss tangents with frequency

CHAPTER 5

PROPERTIES OF LITZ WIRE

5.1 INTRODUCTION

The term Litz wire is derived from the German word 'litzendraht', meaning woven wire. Generally defined, it is a wire constructed of thin film insulated individual wires bunched or braided together in a uniform pattern of twist and lay length.

The multistrand configuration minimizes the power losses otherwise encountered in a solid conductor due to the "skin effect". It is a tendency of radio frequency current to be concentrated at the surface of the conductor.

In order to counteract this effect, it is necessary to increase the surface area without appreciably increasing the size of the conductor. It is also essential to position each individual strand in the litz construction in a uniform pattern moving from the center to outside and back in a given length of conductor.

Even the best constructed litz wires may exhibit some skin effect at higher frequencies due to the limitations of stranding. Enamel thin film is used for insulating individual strands. Litz wires are generally provided more insulation with a single or double wrap or serving, of polyester fiber. Fig 5.1 shows a schematic diagram of litz wire.

1. Insulated wire
2. Several groups of twisted wires
3. Core with several groups twisted together.
4. Outer Serving

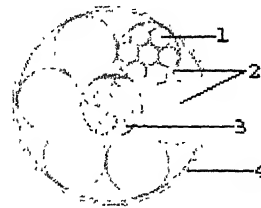


Fig 5.1 Schematic diagram of litz wire.

Before considering the theory of litz wire in detail it may be useful to discuss power loss due to eddy currents in the winding.

5.2 POWER LOSS DUE TO EDDY CURRENTS IN THE WINDING

5.2.1 GENERAL

A conductor in an alternating magnetic field develops emfs induced in it and these will give rise to eddy currents and associated power loss [13]. The magnetic fields may be due to currents flowing in other conductors or due to current flowing in the conductor in question or both. The losses may be represented as an increase in resistance of the current-carrying conductors above the value measured with direct current; this increase of resistance becomes larger as the frequency increases.

A conductor, which forms part of current-carrying winding, in general experience the magnetic field due to its own alternating current and also the field due to all the other current-carrying conductors in the vicinity.

5.2.2 SKIN EFFECT

A single, straight, isolated conductor carrying an alternating current as shown in Fig.5.2 (a), will be surrounded by a concentric magnetic field. This field will induce an electric field (according to Faraday's law) whose associated eddy currents tend to oppose the main current in the vicinity of the axis of the conductor and enhance it at the surface. Thus the current distribution tends to become non-uniform across the section, the current being least at the center and greatest at the surface of the conductor. As the frequency increases, the induced emfs increase and the non-uniformity becomes more pronounced until the current is virtually confined to a thin skin at the surface, and the inner region plays insignificant or no role in the conduction.

Applying Maxwell's equation expressed by the laws of Ampere and Faraday in differential form:

$$\nabla \times H = J = \sigma E \quad (5.1)$$

$$\nabla \times E = -\mu \left(\frac{\partial E}{\partial t} \right) \quad (5.2)$$

where displacement current density $\varepsilon \left(\frac{\partial E}{\partial t} \right)$ (from 5.1) is neglected inside a conductor.

This is permissible since the electric field in conjunction with the dielectric constant is very small, even for rapidly changing fields when compared with the conduction current.

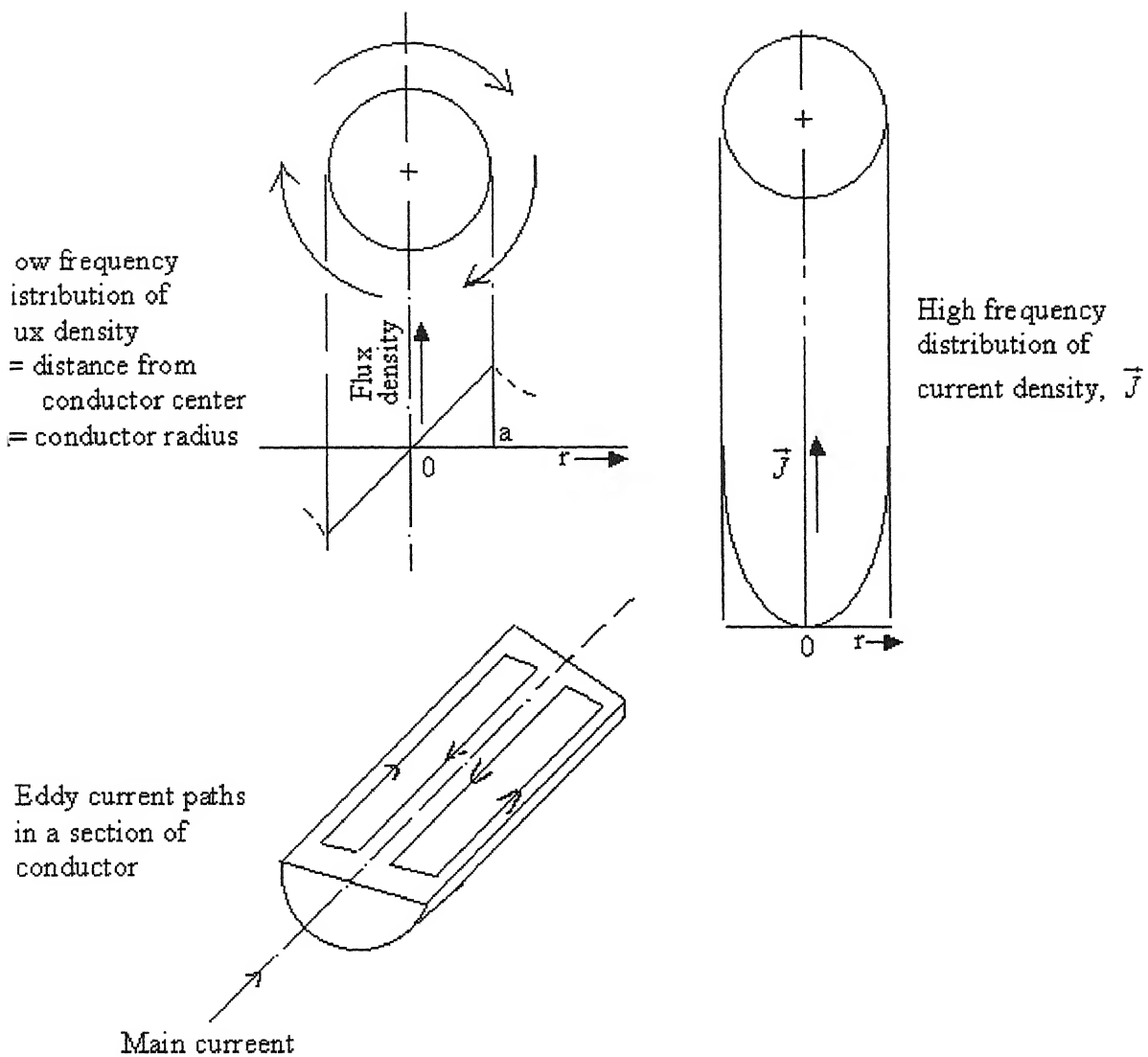


Fig.5.2 (a) Skin effect in round conductors.

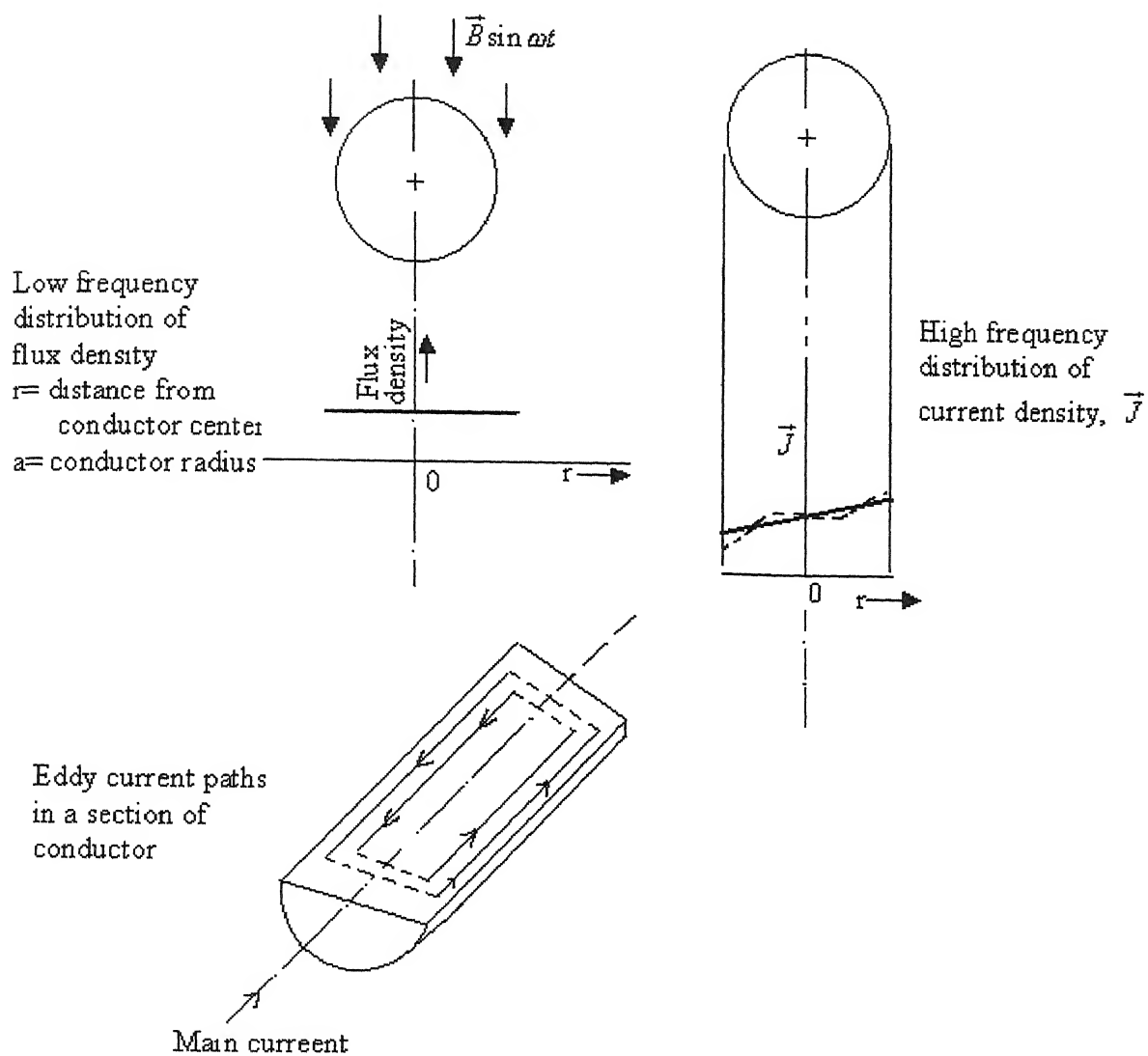


Fig 5.2 (b) Proximity effect in round conductors

We evaluate these equations (equation 5.1 and 5.2) in cylindrical coordinate system where E_z , E_r , and H_ϕ are the only nonzero components. Carrying out the curl in cylindrical co-ordinates

$$\nabla \times H = \begin{pmatrix} a_r & a_\phi & a_z \\ \frac{\partial}{\partial r} & \frac{1}{r} \frac{\partial}{\partial \Phi} & \frac{\partial}{\partial z} \\ 0 & H_\phi & 0 \end{pmatrix} = \sigma E_z$$

$$\therefore \frac{1}{r} \frac{\partial}{\partial r} (r H_\phi) = \sigma E_z \quad (5.3)$$

$$\nabla \times E = \begin{pmatrix} a_r & a_\phi & a_z \\ \frac{\partial}{\partial r} & \frac{1}{r} \frac{\partial}{\partial \Phi} & \frac{\partial}{\partial z} \\ E_r & 0 & E_z \end{pmatrix} = -\mu \frac{\partial H_\phi}{\partial t}$$

$$\Rightarrow \frac{\partial E_z}{\partial r} = \mu \frac{\partial H_\phi}{\partial t} \quad (5.4)$$

differentiating with respect to r , we get

$$\frac{\partial^2 E_z}{\partial r^2} + \frac{1}{r} \frac{\partial E_z}{\partial r} - \mu \frac{\partial}{\partial t} \frac{\partial H_\phi}{\partial r} = 0 \quad (5.5)$$

From equation (5.3) and (5.5), we have

$$\Rightarrow \frac{\partial^2 E_z}{\partial r^2} + \frac{1}{r} \frac{\partial E_z}{\partial r} - \mu \sigma \frac{\partial E_z}{\partial t} = 0 \quad (5.6)$$

For the time varying fields, $\frac{\partial}{\partial t} = j\omega$, so equation (5.6) becomes

$$\begin{aligned} & \frac{\partial^2 E_z}{\partial r^2} + \frac{1}{r} \frac{\partial E_z}{\partial r} - j\omega \mu \sigma E_z = 0 \\ \Rightarrow & \frac{\partial^2 E_z}{\partial r^2} + \frac{1}{r} \frac{\partial E_z}{\partial r} + p^2 E_z = 0 \end{aligned} \quad (5.7)$$

Equation (5.7) is the standard Bessel equation, where $p^2 = -j\omega \mu \sigma$. Its solution is given by

$$E_z = A J_0(pr) \quad (5.8)$$

where A is constant and J_0 is the Bessel function of zeroth order.

Differentiating equation (5.8) with respect to r , we have

$$\frac{\partial E_z}{\partial r} = ApJ'_0(pr) \quad (5.9)$$

From equation (5.4) and (5.9) in time harmonic form

$$ApJ'_0(pr) = j\omega\mu H_\phi \quad (5.10)$$

According to Amperer's circuital law, which states that the line integral of H about any closed path is exactly equal to the direct current enclosed by that path,

$$\begin{aligned} \oint H \cdot dL &= I \\ \Rightarrow \int_0^{2\pi} H_\phi r d\Phi &= I, \text{ where } r = a, \text{ radius of the conductor} \\ \Rightarrow H_\phi 2\pi a &= I \end{aligned} \quad (5.11)$$

From equation (5.10) and (5.11), we have

$$A = \frac{j\omega\mu I}{2\pi apJ'_0(pa)}$$

Putting value of A into equation (5.8), we get

$$\begin{aligned} E_z &= \frac{j\omega\mu}{2\pi ap} I \left(\frac{J_0(pr)}{J'_0(pa)} \right) \\ \Rightarrow E_z &= -\frac{p^2}{2\pi ap\sigma} I \left(\frac{J_0(pr)}{J'_0(pa)} \right) \\ \Rightarrow \sigma E_z &= \frac{p}{2\pi a} I \left(\frac{J_0(pr)}{J_1(pa)} \right) \quad (\text{Since } J'_0(x) = -J_1(x)) \\ \Rightarrow J_z &= \frac{p}{2\pi a} I \left(\frac{J_0(pr)}{J_1(pa)} \right) \end{aligned} \quad (5.12)$$

Equation (5.12) is the equation for ac current density. Similarly equation for dc current density is given by

$$J_{z_0} = \frac{I}{\pi a^2}$$

Normalized current density with respect to the dc current density

$$\left(\frac{J_z}{J_{z_0}} \right) = \frac{pa}{2} \frac{J_0(pr)}{J_1(pa)}$$

It shows that for a fixed frequency and fixed radius ‘ a ’, normalized current density is a function of ‘ r ’, where $r \leq a$ (Fig 5.3) [19].

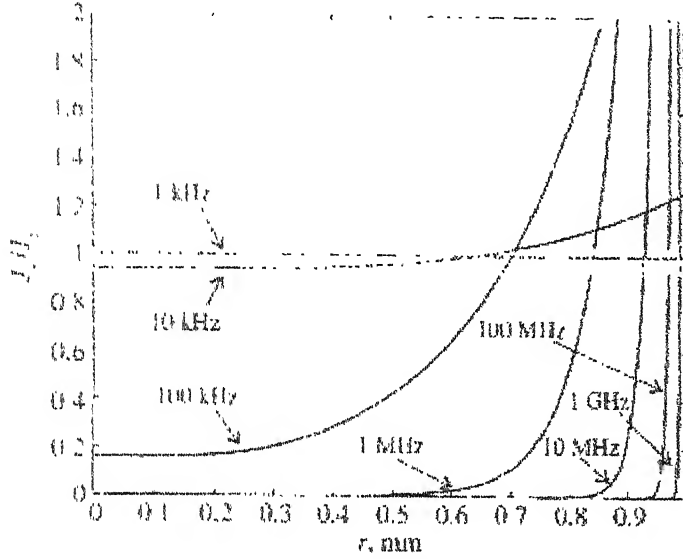


Fig 5.3 Frequency behavior of normalized ac current density for a copper wire of radius $a=1\text{mm}$

It can be noticed that there is significant increase in current flow towards the outer perimeter of the wire even for moderate frequencies of less than 1MHz . At frequencies around 1GHz , the current flow is almost completely confined to the surface of the wire with negligible radial penetration. An often-used high-frequency approximation for the ac current density in z-direction is given by:

$$J_z \cong \frac{P}{j2\pi a \sqrt{r}} e^{-(a-r)\sqrt{\pi f \mu \sigma}} e^{-j(a-r)\sqrt{\pi f \mu \sigma}} \quad (5.13)$$

Considering first the negative exponential term, there is an exponential decrease in the conduction current density with penetration into the conductor (away from the surface). The exponential factor is unity at $a-r=0$ and decreases to $e^{-1} = 0.368$ when

$$a-r = \frac{1}{\sqrt{\pi f \mu \sigma}}$$

This distance is denoted by Δ and is termed the *depth of penetration*, or the *skin depth*,

$$\Delta = \frac{1}{\sqrt{\pi f \mu \sigma}} \quad (5.14)$$

To find the ratio of ac resistance verses the dc resistance, consider a round solid conductor of radius ‘ a ’ and the skin depth Δ . The dc and ac resistances per unit conductor length are

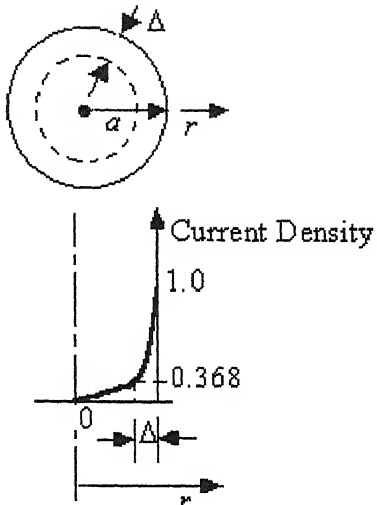
$$\begin{aligned}
 R_{dc} &= \frac{\rho}{\pi r^2} \\
 R_{ac} &= \frac{\rho}{\pi \left[a^2 - (a - \Delta)^2 \right]} \\
 &= \frac{\rho}{\pi a^2 \left[\frac{2\Delta}{a} - \left(\frac{\Delta}{a} \right)^2 \right]} \\
 &= \frac{\rho}{\pi \left[2a\Delta - \Delta^2 \right]} \\
 \frac{R_{ac}}{R_{dc}} &= \frac{1}{\left[\frac{2\Delta}{a} - \left(\frac{\Delta}{a} \right)^2 \right]}
 \end{aligned}$$


Fig 5.4 Skin effect in metallic conductors

For a conductor with $\Delta = a$, the ratio equals unity; the skin effect can be ignored if the diameter of a circular conductor is less than 2Δ . The above is a crude approximation. Even a conductor with radius smaller than Δ has an ac resistance larger than the dc resistance. In general ac resistance of a straight, isolated, conductor of circular cross-section is given by

$$R_{ac} = R_{dc} + R_{se} = R_{dc} (1 + F) \quad \Omega \quad (5.15)$$

where R_{se} is the increase in resistance due to skin effect, and F is the skin effect factor. The skin effect factor is a function of $2a/\Delta$. Referring to Fig 5.5 it is seen that when $2a/\Delta$ for a round conductor is less than 2 the skin effect is negligible. It increases rapidly as $2a/\Delta$ increases. This diagram is based on figures given by Butterworth¹⁴. When $2a/\Delta$ is greater than 5:

$$1 + F \cong \frac{1}{4} \left(\frac{2a}{\Delta} + 1 \right) \quad (5.16)$$

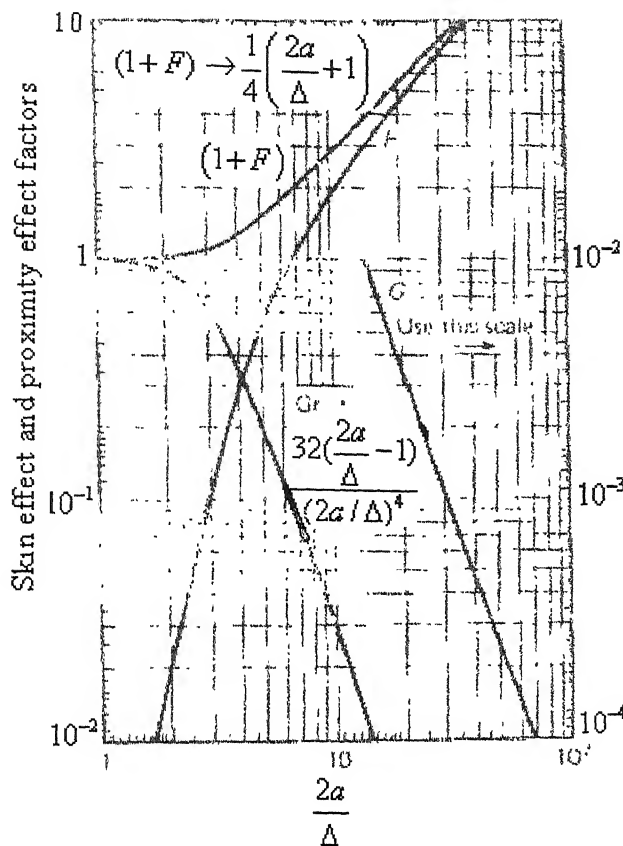


Fig 5.5 Skin effect factor F and proximity effect factor G_r , as a function of $\frac{2a}{\Delta}$ for round conductors, based on figures given by Butterworth¹⁴.

Skin effect may be virtually eliminated by using conductors consisting of thin insulated strands. These are formed so that individual strands weave cyclically from the center of the conductor to outside and back as they run along the length of the conductor. Such a conductor is referred to as Litz wire as described in section 5.1; the stranding and disposition makes the current density uniform. However, since skin effect is not usually the most important form of eddy current loss in winding conductors, it is not usual to use special stranding. To combat the proximity effect loss, described in the section 5.2.3, bunched conductors are often used. This consists of a number of thin insulated strands closely twisted into the form of a rope. If the strands formed perfect helical paths, keeping a constant distance from the axis, the skin effect would be the same as for a solid conductor having the same copper cross-section (very high), assuming that all the strands are connected together at each end of the conductor. In practice, however, such bunched conductors are usually made up of groups of strands and appreciable transposition of the strands occurs. Careful measurements have shown that most bunched conductors behave

as though the strands are transposed almost perfectly and the skin effect can be ignored being very low [9].

In isolation, a perfectly transposed bunched conductor will be subjected to further eddy current loss due to its own field of lay lengths traversing the strands, each of which carries the same current. This may be called internal proximity effect. It may be comparable to, and at high frequencies may be larger than, the skin effect in an equivalent conductor consisting of perfectly untransposed strands. However, when a perfectly transposed bunched conductor is in a winding, the field due to the bunch, as such, largely disappears due to the proximity effect of other turns. The winding behaves as if it consists only of strands, carrying all equal current. Under these conditions, only the normal proximity effect described in the section 5.2.3 is important.

Returning to the consideration of skin effect loss in general, the loss tangent due to skin effect in an inductor of L henries follows from equation (5.15)

$$\tan \delta_{se} = \frac{R_{dc} F}{\omega L} \quad (5.17)$$

At low value of $2a/\Delta$, F is proportional to $(2a/\Delta)^4$ and it is therefore proportional to f^2 . Thus at low frequencies $\tan \delta_{se}$ is proportional to f . It may easily be shown that it reaches a peak value when $(2a/\Delta) \approx 6$. Thereafter it falls; as F becomes approximately proportional to $f^{1/2}$, $\tan \delta_{se}$ approaches proportionality to $f^{-1/2}$.

5.2.3 PROXIMITY EFFECT

This is the eddy current effect in a conductor due to the alternating magnetic field of another conductor in the vicinity. In practice this may usually be interpreted as the eddy current effect in the conductor of a winding due to the magnetic field of the winding as a whole. The field will, in general, depend upon the geometry of the core, if any. It must be remembered that any additional windings or conductors in the same field will have eddy currents induced in them whether or not they are carrying the main current. The resultant energy loss simply add to the corresponding loss in the current-carrying windings and these are apparent as an additional resistance in that winding.

The magnetic field of a current-carrying winding normally cuts the conductors of that winding, or associated windings, perpendicular to the conductor axis. The resultant eddy current path and current distribution are shown in Figure 5.2(b) for a round wire for which $2a/\Delta$ is not large.

When $2a/\Delta$ is less than unity the effect of the magnetic fields of the eddy currents themselves may be ignored and the calculations of the eddy current losses are quite simple. Following derivation of proximity effect in a thin strip illustrates the principles.

Figure 5.6 shows the cross-section of a tape having width b and thickness d . An alternating magnetic flux density, $\vec{B} \sin \omega t$, is everywhere parallel to the plane of the tape. The emf induced in a loop consisting of the two elementary laminates is given by

$$E = \omega \vec{B} 2xl / \sqrt{2} \quad \text{V}$$

where l is the length of tape being considered.

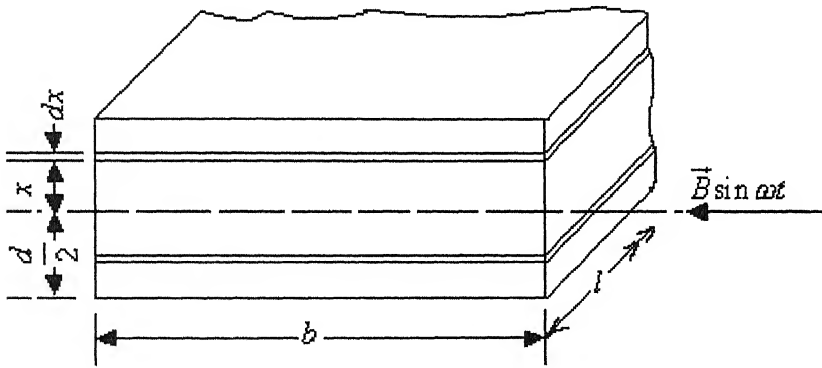


Fig 5.6 Calculation of eddy currents in a thin strip.

An eddy currents flow along the laminate parallel to the length of the strip, in one direction on one side of the axis and in the opposite direction on the other side. Neglecting the short paths connecting the laminates at the ends of the strip, the resistance offered to the elementary eddy current is given by

$$R = \frac{2\rho_c l}{bdx} \quad \Omega$$

Therefore, the power loss due to proximity effect is

$$dP_{pe} = E^2 / R = \omega^2 \widehat{B}^2 x^2 l b dx / \rho_c$$

$$P_{pe} = \frac{\omega^2 \widehat{B}^2 l b}{\rho_c} \int_0^{d/2} x^2 dx$$

$$= \frac{\omega^2 \widehat{B}^2 l b d^3}{24 \rho_c} \quad \text{W}$$

It must be remembered that this result applies only when the flux density is parallel to the plane of the strip; a small inclination may result in much greater losses. Analogous expression may be obtained for a round conductor of diameter $2a$, namely

$$P_{pe} = \frac{\pi \omega^2 \widehat{B}^2 l (2a)^4}{128 \rho_c} \quad (5.18)$$

Since the latter case is more common, the following discussions are for round conductors. If the transverse magnetic field is associated with the main current in the conductor, the eddy currents cause a distortion in the current density, enhancing it on one side of the axis and diminishing it on the other, as shown by the full line in Figure 5.2(b).

At higher frequencies and with larger conductors, such that ratio $2a/\Delta$ greater than unity, field due to these eddy currents significantly reduces the flux density inside the conductor and the associated current distribution becomes non-linear as shown by the dotted line.

The effect of eddy current field and the associated non-linear current distribution is to reduce the proximity effect loss that would otherwise be present. Butterworth¹⁴ calculated the eddy current loss in round conductors taking this eddy current screening into account. These results are most conveniently expressed by introducing a proximity effect factor, G_r , into equation (5.18):

$$P_{pe} = \frac{\pi \omega^2 \widehat{B}^2 l (2a)^4 G_r}{128 \rho_c} \quad \text{W} \quad (5.19)$$

This factor, which is dimensionless, function of $2a/\Delta$ is plotted in Fig.5.5. It is valid only for round conductors. When $2a/\Delta$ decreases to unity, $G_r \rightarrow 1$; and when $2a/\Delta$ is increasing beyond 4,

$$G_r \rightarrow \frac{32}{(2a/\Delta)^4} \left(\frac{2a}{\Delta} - 1 \right)$$

It is often necessary to express this loss as the tangent of the proximity effect loss angle, δ_{pe} , referred to the current-carrying winding. For simplicity it is assumed that here is only one winding under consideration and that it is embraced by a magnetic core. The magnetic flux density in the winding space, although non-uniform, is everywhere assumed proportional to the amperes-turns in the winding. Equation (5.19) may be combined with the following relations:

$$P_{pe} = I^2 R_{pe}$$

$$\tan \delta_{pe} = \frac{R_{pe}}{\omega L}$$

and

$$L = \frac{\mu_0 \mu_e N^2 A}{l_c}$$

It follows that

$$\begin{aligned} \tan \delta_{pe} &= \frac{P_{pe}}{\omega L I^2} \\ \tan \delta_{pe} &= \frac{P_{pe}}{\omega L I^2} = \frac{P_{pe} l_c}{\omega \mu_0 \mu_e A N^2 I^2} \\ &= \frac{\pi \omega^2 N^2 I^2 l (2a)^4 G_r}{64 \rho_c} \times \frac{l_c}{\mu_0 \mu_e A N^2 I^2} \end{aligned}$$

where $\overline{B^2} = B^2 (= \widehat{B^2} / 2)$ averaged over the winding space and $\overline{B^2} = k N^2 I^2$, where k is a constant.

$$\tan \delta_{pe} = \frac{\pi^2 k l_c}{32 \rho_c \mu_0 A} \times \frac{f l (2a)^4 G_r}{\mu_e} \quad (5.20)$$

When $2a/\Delta$ is less than unity, e.g. at low frequencies, $G_r \approx 1$ and $\tan \delta_{pe}$ is proportional to the frequency. At higher frequencies the proximity effect usually makes an appreciable contribution to the total loss of a wound component. For $2a/\Delta \approx 3.5$ the value of $\tan \delta_{pe}$ reaches a maximum. At higher frequencies G_r approaches to $(2a/\Delta)^{-3}$ or $f^{-3/2}$, so $\tan \delta_{pe}$ approaches proportionality of $f^{-1/2}$, i.e. it falls with increasing frequency.

A reduction of conductor diameter, $2a$, will be very effective in reducing proximity effect but, by itself, this reduction will rapidly increase the value of R_{dc} and

may result in a greater overall loss. The usual method of overcoming proximity effect is to use bunched conductors consisting of n insulated strands for the diameter $2a$. At each end of the winding the strands are soldered together. At low frequencies, the conductor has an effective area of $n\pi d^2/4$. The conductor is twisted such that, in its simplest form, each strand follows a helical path. Fig 5.7 shows a side view of two strands in such a bunched conductor. The emfs induced in each half-twist are cancelled by those in the next. If the bunch has more complicated composition, e.g. seven twisted bunches each of seven twisted strands, indeed emf cancellation will still occur. If the number of twists in a winding is greater than about ten, the eddy current circulating between the strands may be ignored and only those circulating within the strands need be considered. Thus equation (5.20) may be applied to the strands of the conductor; $2a$ then refers to the bare diameter of the strand and l refers to the total length of strands, i.e. Nnl_w , where l_w is the mean turn length. The above equation may now be written in more general form

$$\tan \delta_{pe} = \frac{\pi^2 k l_c}{32 \rho_c \mu_0 A} \times \frac{f l_w N n (2a)^2 G_r}{\mu_e} \quad (5.21)$$

If solid conductors are being considered the same equations may be used but then $n = 1$.

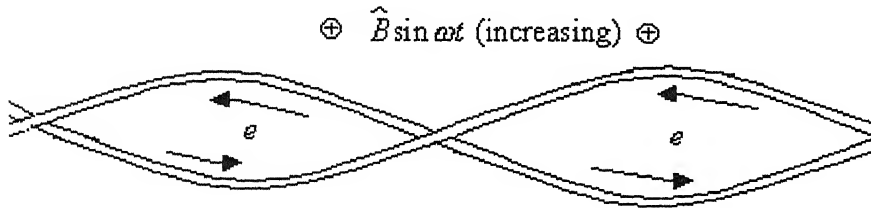


Fig 5.7 The cancellation of eddy-current emfs induced in twisted strands of bunched conductors determined by transverse flux.

5.3 WHEN TO USE LITZ WIRE

High-frequency power transformers require application of Litz wire. High currents in the winding force the use of large cross-section conductors. The combination of larger cross-section conductors and high frequencies, for the reason discussed in section 5.2, is the theoretical requirement of high-frequency Litz conductor. While using Litz wire, the following points should be considered:

1. Calculate the ratio $2a/\Delta$. If this is higher than unity, consider use of Litz wire.

2. For a magnetic design, where there is an appreciable amount of flux fringing, e.g. a large air gap in the magnetic circuit or for loosely coupled transformer design, Litz should be thought of as a means for eliminating the eddy currents due to the stray magnetic field.
3. The input power of a transformer will be increased by use of Litz wire if the same allowable temperature rise is considered as for a solid-wire design.
4. At frequencies $> 5MHz$, Litz wire becomes less practical. The effect of capacitance between the strands is the reasons for this high-frequency limit.

5.4 DC RESISTANCE OF A LITZ CONDUCTOR

The dc resistance of a Litz conductor is related to the following parameters:

1. American Wire Gauge (AWG) of the individual strands.
2. Number of strands in the conductor.
3. Factors relating to the increased length of the individual strand per unit length of the wire. For normal Litz wire construction a 1.5% increase in dc resistance for every bunch formation and 2.5% increase in dc resistance for every cabling operation is considered approximately correct.

So, dc resistance of any Litz wire is given by

$$R_{dc} = \frac{R_s (1.015)^{n_b} (1.025)^{n_c}}{n} \quad (5.22)$$

Where: R_{dc} = Resistance in ohms per unit length

R_s = Maximum resistance of the individual strands

n_b = Number of bunching formation

n_c = Number of cabling operations

n = Number of individual strand

The dc resistance of Litz wire consisting of 2464 strands of 40 AWG single polyurethane based enamel on individual strands, operating at 120 kHz and designed with seven bunching formations and one cabling operation is given by

$$R_{dc} = \frac{3.78 \times (1.015)^7 \times (1.025)^1}{2464} = 1.74 \text{ m}\Omega/\text{m}$$

CHAPTER 6

INSULATION AND DIELECTRIC CIRCUIT

In transformer dielectrics problems arise by the presence of moisture, vibration, partial breakdown (PB), and heat. This chapter is devoted to discussions and analysis of one of the most important causes of failures of the high voltage transformer insulation.

6.1 ELECTRIC FIELDS

Electric field in dielectric, produced due to the potential on an electrode stresses the dielectric (electrical insulation) in contact with 'electric stress'. The parameter, which determines the magnitude to electric stress on the dielectric, is known as the 'electric field intensity'. The knowledge of electric field intensity is essential for studying the insulation characteristics of a dielectric and to get familiar with the behavior of dielectrics.

The behavior and utilization of a dielectric mainly depends upon the magnitude and type of electric field, it is stressed with. The phenomenon of breakdown of insulating properties of a dielectric also depends upon the existing configuration of electric field.

6.2 ELECTRIC FIELD INTENSITY

Faraday described the space around a magnet to be filled with 'lines of magnetic force'. Similarly, the region around an electrified object may be considered to be filled with 'lines of electric force'. To Faraday, these lines existed as mechanical structures in the surrounding medium (the dielectric) and could exert force on an object placed therein.

The 'electric field intensity', also known as the 'electric field strength', is defined as the electrostatic force F per unit positive test charge q , placed at a particular point p , in a dielectric. It is denoted by E , and expressed in unit 'Newtons per Coulomb', that is, the force per unit charge. The electric field intensity is measured in its practical units of 'Volts per meter' (V/m or kV/cm).

The electric field intensity is numerically equal to the 'potential gradient', which may be written as,

$$\vec{E} = - \text{grad } \Phi = - \nabla \Phi \quad (6.1)$$

Where Φ is the scalar potential.

The qualitative definition of ‘electric strength’ of a dielectric is ‘the maximum electric stress a dielectric can withstand’. A quantitative definition is however complicated, because a large number of factors affect the electric breakdown of a dielectric. These factors include pressure, humidity, temperature, electric field configuration (electrode shape and size), electrode material, voltage waveform, presence of impurities and imperfections in the dielectrics, the composition of the dielectric material, and the duration and magnitude of the applied voltage[12].

6.3 CLASSIFICATION OF ELECTRIC FIELDS

Electric field can be classified as under :–

- Uniform fields
- Weakly nonuniform fields
- Extremely nonuniform fields.

6.3.1 UNIFORM FIELDS

A uniform field is one in which the potential distribution across the electrode gap is uniform. The electric field intensity is the same at any point in the electrode gap. The breakdown strength of a dielectric is maximum for this type of field. An important characteristic of this type of field is that insulation breakdown takes place without any partial breakdown preceding the global breakdown.

In other words,

$$U_i = U_b \quad (6.2)$$

Where U_i is the partial breakdown inception voltage and U_b is the breakdown voltage.

An example of a uniform field is a field existing between two parallel plates.

6.3.2 WEAKLY NONUNIFORM FIELDS

In this type of field, the potential distribution across the electrode gap is not uniform and hence the field is not the same all over the gap. However this type of field is normally

clubbed with the uniform field because of an important identical behavior, that is, here also no stable partial breakdown precede the breakdown.

Therefore,

$$U_i = U_b \quad (6.3)$$

Where U_i is the partial discharge inception voltage and U_b is the breakdown voltage.

Electrode like sphere gaps, concentric spheres and coaxial cylinders generate a weakly nonuniform field provided the electrode separation is small.

6.3.3 EXTREMELY NONUNIFORM FIELDS

An extremely nonuniform field is one in which the potential distribution across the electrodes is extremely nonuniform. An example of such a field is that between two points /needle electrodes.

Unlike in uniform and weakly nonuniform fields, in this case, breakdown of the dielectric is preceded by a stable PB. The PB is unstable only just before breakdown. Therefore,

$$U_i \ll U_b \quad (6.4)$$

In the case of solid dielectrics, the partial discharges preceding breakdown cause permanent damage to the insulation. However, for enclosed gaseous dielectrics, the effect is to reduce the breakdown strength of the gas. Every successive PB causes further reduction in the breakdown strength. These partial discharges also give rise to byproducts, depending upon the type of gaseous dielectric used, some of which are toxic and corrosive in nature. The breakdown strength of a dielectric is minimum for an extremely nonuniform field.

6.4 SCHWAIGER FACTOR

Schwaiger factor introduced by Schwaiger in year 1922 describes the degree of uniformity of an dielectric. It is defined as the ratio of the average electric field intensity across an electrode gap to the maximum electric field in the gap. Mathematically stated as

$$\eta = \frac{E_{mean}}{E_{max}} \quad (6.5)$$

Where E_{max} = Maximum electric field intensity in the gap and

E_{mean} = Average field intensity across the gap.

This factor is a geometrical quantity related to electrostatic field analysis only. Since both E_{mean} and E_{max} depend upon the geometry of the electrode system, the value of the Schwaiger factor depends upon the geometry of the electrode system^[12].

6.5 ANALYSIS OF ELECTRIC FIELD INTENSITY IN HOMOGENEOUS ISOTROPIC SINGLE DIELECTRIC

I Needle-Needle electrode geometry

In Fig. 6.1(a), which depicts much smaller spheres, there is an even smaller region in which the field is uniform. Here, $E_{max} \gg E_{mean}$. For practical purpose, the tiny sphere must be replaced by thin needles whose points have small radii of curvature. The behavior of small spheres is therefore simulated by the use of needle-shaped electrodes, described as *needle geometry* as shown in fig. 6.1(b).

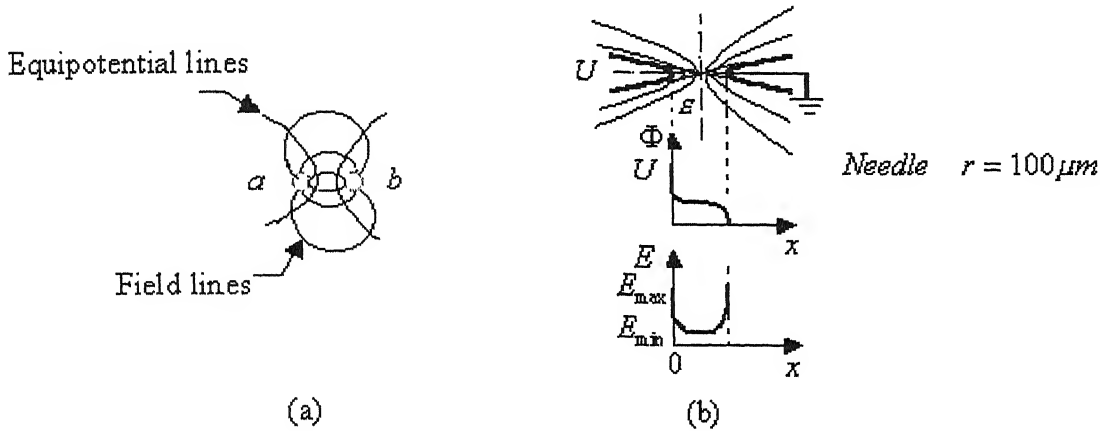


Fig. 6.1 Extremely nonuniform field between needle-needle electrodes.

II Asymmetrical Electrodes

The field may be asymmetrical as well as nonuniform. If the surface areas of each electrode are unequal, and if their separation is comparable, then the intensity of the local field in the immediate vicinity of the smaller area electrode will be greater than in the vicinity of the larger area electrode. Suppose that one electrode is a flat plane and that the other is shrunk in size to a sphere of very small radius r . We thus obtain the *point-plane electrode geometry* of Fig. 6.2, in which, because of divergent field:

$$E_a \gg E_b > E_{ab} = V_{ab} / d$$

There is less field enhancement in the vicinity of electrode ‘a’, if d is substantially increased ($d \gg r$). E_a may then be only slightly greater than E_b .

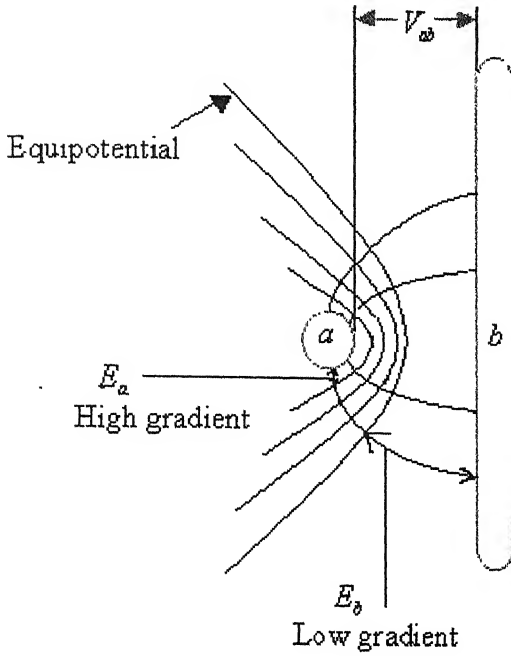


Fig. 6.2 Asymmetrical electrode: point-plane geometry.

III Corona and Partial Breakdown

Electrode configurations with extremely nonuniform fields are more common in practice than with the uniform and weakly nonuniform fields. The reasons are, firstly to achieve a uniform field, considerable efforts are needed. Secondly, the presence of undesirable foreign particles in dielectrics and electrode projections also lead to field distortions, hence nonuniform fields. As the difference between the maximum and the mean field intensity increases (smaller η), the field characteristics become more nonuniform. Consequently, a poor utilization of the insulating properties of dielectric takes place. In extremely nonuniform fields at voltage much below the breakdown, a stable ionization process in the gas confined locally to the region of extreme field intensity can be maintained. This is known as ‘Partial Breakdown’ (PB) and when it occurs at free electrodes in a gas, it is called ‘corona’.

6.6 FIELD ENHANCEMENT FACTOR

The value of η also represents the degree of utilisation of the dielectric in between any two electrodes. The reciprocal of η is denoted by 'f', which represents the 'degree of nonuniformity' of an electric field and is termed as '*field-enhancement factor*',^[20]. So

$$\text{Field-enhancement factor} = f = \frac{1}{\eta} = \frac{E_{\max}}{E_{\text{mean}}}$$

Field enhancement can occur in symmetrical fields in which there is no corona. Thus, if both electrodes are small spheres or needle points, field enhancement factor exceeds unity and breakdown occurs at lower voltages than in a geometry of large spheres or flat plane electrodes.

In the transformer, the physical manifestation of small spheres is those contours, which have a small radius of curvature. Examples are the sharp edges of a terminal or can, the ball of solder on a terminal, and even the tiny globules of solder in the vicinity of a splice. The needle point is physically represented by loose strands from a lead wire or the sharp point on a poor solder joint.

6.7.1 PROPERTIES OF COMPOSITE DIELECTRIC

In practice suitable combinations of different dielectrics, solid-solid or solid-gaseous, are frequently used in high voltage apparatus. Such a dielectric combination is known as '*composite dielectric*'. These different dielectrics or phases may be in parallel (perpendicular interface) with one another-such as SF₆ in parallel with solid insulation – or less commonly unless purposely designed, in series (longitudinal interface) with one another.

Fig. 6.3 shows a parallel plate condenser with two dielectrics ϵ_1 and ϵ_2 , forming a perpendicular interface in an uniform field. The potential difference U , between the two plates, is given by,

$$U = E_1 d_1 + E_2 d_2 = U_1 + U_2 \quad (6.6)$$

The magnitude of E_1 and E_2 for an applied voltage U between the plates can be obtained as follows:

$$E_1 = \frac{U}{\varepsilon_1 \left(\frac{d_1}{\varepsilon_1} + \frac{d_2}{\varepsilon_2} \right)} = \frac{U}{d} \cdot \frac{\varepsilon_2 / \varepsilon_1}{\left[\frac{d_1}{d} \left(\frac{\varepsilon_2}{\varepsilon_1} - 1 \right) + 1 \right]} \quad (6.7)$$

and,

$$E_2 = \frac{U}{\varepsilon_2 \left(\frac{d_1}{\varepsilon_1} + \frac{d_2}{\varepsilon_2} \right)} = \frac{U}{d} \cdot \frac{1}{\left[\frac{d_1}{d} \left(\frac{\varepsilon_2}{\varepsilon_1} - 1 \right) + 1 \right]} \quad (6.8)$$

For a similar electrode arrangement as in Fig. 6.3, equation 6.7 is plotted in Fig. 6.4 for various thickness of dielectric d_1 and for different values of the ratio $(\varepsilon_2 / \varepsilon_1)$. Fig. 6.4 reveals that the rise in field intensity E_1 in the dielectric with lower ε_1 (air) compared with the field intensity in a single system U/d , is much steeper for smaller thickness of its layers d_1 and for higher permittivities ε_2 of the other dielectric.

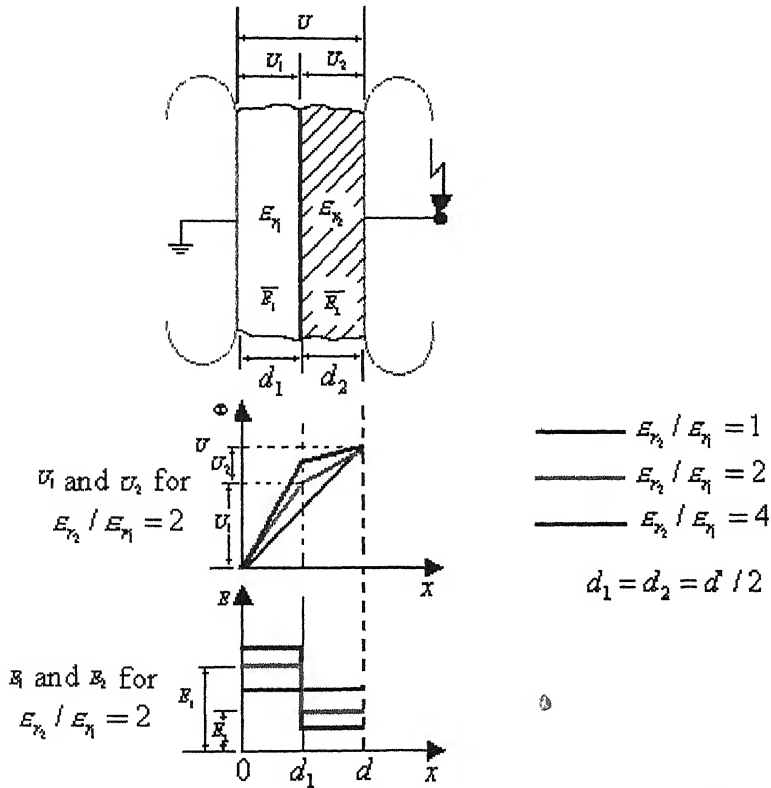


Fig. 6.3 Potential and field intensity distribution in uniform field with a perpendicular dielectric interface.

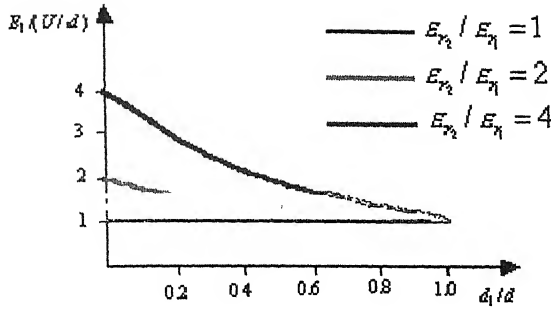


Fig. 6.4 Field intensity with varying dielectric layer thickness in a twin dielectric parallel plate condenser.

6.7.2 RESULTANT PERMITTIVITY FOR COMPOSITE DIELECTRICS

Consider Equations 6.7 and 6.8 for a homogeneous combination of two dielectrics, subdivided into infinite number of layers with materials having permittivities ϵ_1 and ϵ_2 in uniform field. Let the resultant permittivity be ϵ_{res} . Then,

$$D = \epsilon_{res} E$$

where D and E are the macroscopic mean values. Since the field intensities E_1 and E_2 in microscopic multiple layers in uniform field remain unchanged, then

$$D = \epsilon_{res} E = \epsilon_1 E_1 = \epsilon_2 E_2$$

by introducing this in equation 6.7 or 6.8 and rearranging, we obtain,

$$\epsilon_{res} E = \frac{U}{d} \cdot \frac{1}{\left(\frac{d_1/d}{\epsilon_1} + \frac{d_2/d}{\epsilon_2} \right)}$$

In this expression U/d represents the mean value of field intensity E within the composite dielectric. The relation d_1/d and d_2/d represents the volumes of respective dielectrics, hence these can be replaced by v_1 and v_2 . Therefore;

$$\epsilon_{res} = \frac{1}{(v_1/\epsilon_1) + (v_2/\epsilon_2)} \quad (6.9)$$

for a combination of n dielectrics,

$$\epsilon_{res} = \frac{1}{(v_1/\epsilon_1) + (v_2/\epsilon_2) + \dots (v_n/\epsilon_n)} \quad (6.10)$$

Thus the resultant permittivity of a homogeneously formed composite dielectric would depend the volume proportions and permittivities of individual dielectrics.

Though the above example has been explained for uniform field configuration, the phenomenon is true for nonuniform fields also. Such as air pockets of arbitrary shapes in solid dielectrics, known as voids, are very common in high voltage apparatus like power cables, bushings, insulators, capacitors, current and voltage measuring transformers, etc. It is essential to avoid such voids in solid insulation system because a sharp rise in field intensity there leads to the problems of partial discharges.

6.8 POLARIZATION UNDER ALTERNATING VOLTAGE IN INSULATING MATERIALS

On applying alternating field to a dielectric, the dipoles or the charges must change their direction every cycle. If the frequency of alternating field is very low, in other words, if the duration of half cycle is very long compared to the required relaxation time (time required for the formation of dipoles as well as their displacement) of the dipoles, then the polarization caused by orientation of dipoles would have its maximum effect. Let this be represented by ϵ_{r1} in Fig.6.5. In the equivalent circuit diagram shown in this figure for the region of the frequency ($\omega \ll \omega_e$), C_p represents the increase in capacitance caused by polarization, whereas R_p represents the pure resistance required to interpret the time dependance of polarization. The time constant is given by,

$$\tau_p = C_p R_p$$

At very high frequencies, where the duration of a half cycle is very short compared to the relaxation time, the dipoles are not in position to follow the change in the field intensity. This reduces the polarization caused by orientation of dipoles, which ultimately diminishes to zero at very high frequencies as illustrated by the right hand side of the curve in Fig.6.5. It is represented by a lower constant value of relative permittivity ϵ_{r2} . The total effective capacitance in this region of very high frequency is C , as shown in the equivalent diagram.

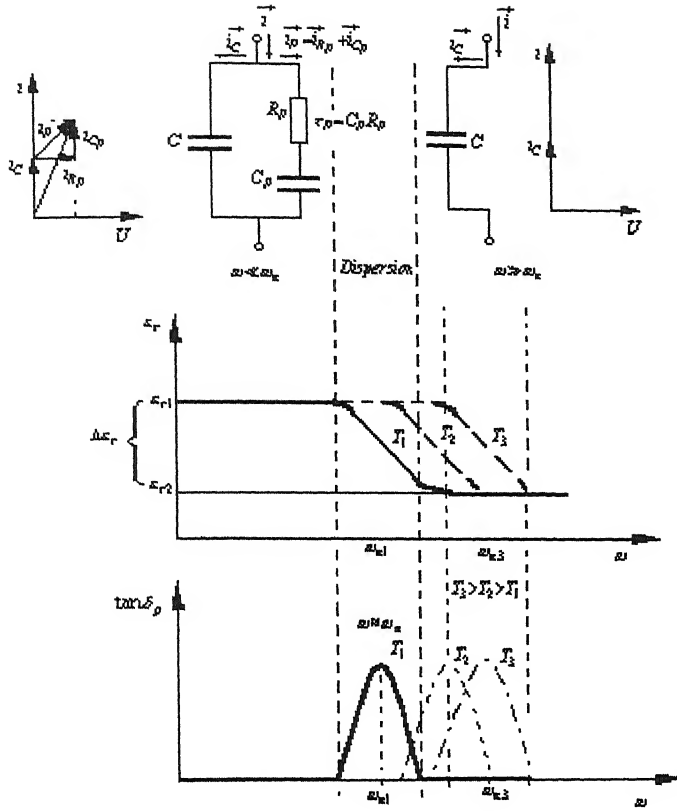


Fig. 6.5 Polarization under alternating voltage showing effect of frequency and temperature on relative permittivity and polarization losses.

In the transition domain of frequency, also known as the ‘dispersion domain’, the relative permittivity ϵ_r depends strongly upon the frequency. Corresponding to the relaxation time τ_p , the eigen frequency ‘ ω_e ’ of the dipoles is defined as:

$$\omega_e = 1/\tau_p \quad (6.11)$$

The eigen frequency ω_e of a dielectric is its characteristics property and may vary considerably for different dielectrics. For example, it is 10 kHz for hard pressed boards, whereas for highly purified water, it is of the order of 100 MHz. Eigen frequency of dielectrics is also a function of temperature. It is influenced by the binding energy of material, which in turn is affected by temperature. Consequently, at higher temperatures the eigen frequency of a dielectric increases, as shown in Fig. 6.5.

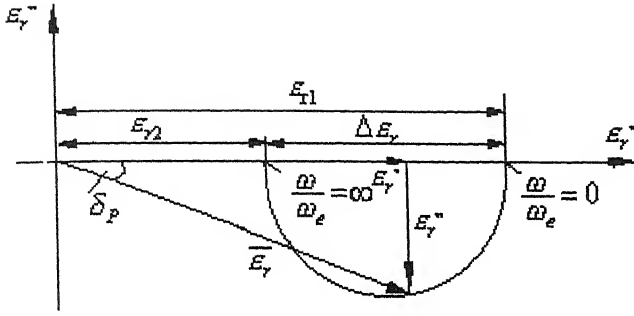


Fig. 6.6 Plot of complex relative permittivity variation with frequency of applied voltage.

From The equivalent circuit diagram given in Fig. 6.5 for the region $\omega \ll \omega_e$ (for example power frequency region), the total vector current \vec{i} is given by,

$$\vec{i} = \vec{i}_C + \vec{i}_P$$

where the polarization current \vec{i}_P constitutes of real \vec{i}_{R_p} and reactive \vec{i}_{C_p} parts. The total reactive current is then given by,

$$\vec{i}_{Total(reactive)} = \vec{i}_C + \vec{i}_{C_p}$$

and the total active current is \vec{i}_{R_p} .

The angle between total vector current and the total reactive current in the dielectric is known as angle δ_p , which is a measure of the active power loss in the dielectric due to polarization. The tangent of angle δ_p is equal to the ratio of total active to reactive currents, that is, the ratio between the real and imaginary parts of the current in the dielectric due to polarization, as shown by the vector diagram for the currents,

$$\tan \delta_p = \frac{i_{R_p}}{i_C + i_{C_p}}$$

From Fig.6.6 and equation 6.13,

$$\tan \delta_p = \frac{\epsilon_r''}{\epsilon_r'}$$

or

$$\tan \delta_p = \frac{\Delta \epsilon_r (\omega/\omega_e)}{\epsilon_{r2} \left[1 + (\omega/\omega_e)^2 \right] + \Delta \epsilon_r} \quad (6.23)$$

From Fig. 6.6, it is clear that $\tan \delta_p$ has a maximum value in the dispersion domain of the frequency, and for $(\omega/\omega_c) \ll 1$ and $(\omega/\omega_c) \gg 1$, $\tan \delta_p$ tends to be equal to zero. Accordingly a schematic plot of $\tan \delta_p$ with respect to the frequency is shown in Fig.6.5.

6.9 INSULATING MATERIALS USED IN RF TRANSFORMER

Optimum utilization of all insulating materials employed for building up a RF transformer in consonance with their mechanical, physical, chemical and thermal characteristics is necessary for obtaining a compact size transformer. Table 6.1 gives the dielectric properties of materials used in a RF transformer.

Table 6.1

Dielectric properties of insulating materials used in RF transformer

Properties	Enamel (polyurethane based)	Polyester Fibre (Tergel) ^[23]	Epoxy Resin bonded glassfibre ^[24] (G-11 grade)	Nomex Paper (10 mil)	SF ₆ at 1 atm. ^[8]	Kapton Tape(1.00mil thick) ^[25]
Relative permittivity ϵ_r at 100 Hz	3.2	3.0-3.2	4.5-5.2	2.8	1.002	3.4
Dielectric Strength in uniform field)	> 31kV/mm	157 kV/mm (for 2 mil thick)	27 kV/mm (perp. to laminations, 1/16")	39 kV/mm	8.9 kV/mm	303kV/mm
$\tan \delta$ 60 Hz 1 MHz	-----	0.0021 0.012	 0.015-0.017	.006- 0.14	$<5 \times 10^{-6}$	0.0018 (1kHz)
Hot-spot Max, °C	180	125	150	180	-----	200

6.9.1 APPLICATION OF INSULATING MATERIALS

1. **Enamel:** A very thin Polyurethane based enamel film is coated around individual strands of Litz wire because of its low losses and its solderability.
2. **Polyester Fibre:** Major component of polyester fibre is polyethylene terephthalate named as Dacron manufactured by Du Pont. Litz wires are insulated with a double yarn polyester fiber and hence function as serving.

3. **Epoxy resin bonded glassfibre:** NEMA Grade G-11 material is fine weave, continuous filament, fibreglass sheets bonded with epoxy resin. This material have the ability to maintain excellent mechanical, electrical, and physical properties at temperatures in excess of 250 ° F. RF transformer core is made of this material in toroidal shaped High machining has been done as per tolerance required for the high voltage winding. The entire toroidal structure (Fig 2.2) has been polished with epoxy material to get the compatibility with SF₆ gas.
4. **Nomex Paper:** Nomex paper have characteristics which make them ideally suited for electrical insulation application. Nomex paper is used as insulation between turn-turn where two adjacent turns touches i.e. inner side of Toroidal core.
5. **SF₆ Gas**

5.1 General: Adopting high frequency minimize the size of the transformer. A factor influencing this size is the maximum electric stress which can be tolerated by the insulating media within the transformer. Oil insulated transformers are heavy and prone to leaking. The oil needs to be regularly cleaned the impurities build up at high stress points which can lead to electrical breakdown. SF₆ gas at 6 atm. is used as insulation and cooling media in this RF transformer because of its superior dielectric properties, its chemically inert and nontoxic characteristics, and good heat transfer properties. SF₆ gas has a dielectric strength 3 times higher than that of air. A method of reducing the required insulation gap between turn-turn is to encapsulate the transformer in a sealed unit containing SF₆ gas at a pressure above atmospheric. Another advantage of adopting this technique is that SF₆ gas can have heat transfer coefficient^[27] upto 3 times that of air, which assists heat dissipation from the windings. Thermal dissociation in highly purified SF₆ gas begins at extremely high temperatures (above 1000 K). Even at continuous temperature upto about 500 K, neither thermal decomposition of SF₆ nor its chemical reaction with other materials has been reported. Further, SF₆ is a nontoxic, colorless and odorless gas.

The density of gases increases with relative molecular mass. As the molecular mass of SF₆ is quite high (146), it has a high density. Because of high density the charge carriers have a short mean free path. This properties, along with the properties of electron attachment, i.e., electronegativity and high ionization energy, results in high dielectric strength of SF₆.

At atmospheric pressure, i.e., 0.1 Mpa and 20°C the field intensity E_{bi} , for SF₆ gas in uniform fields is given by the relation;

$$E_{bi} = \left(\frac{E_b}{p}\right)_i \cdot p = 890 \cdot p \quad \text{kV/cm}$$

where $\left(\frac{E_b}{p}\right)_i$ represents the inherent relative strength of the SF₆ gas.

5.2 External factors affecting Breakdown Characteristics in SF₆ Gas

(a) Effect of electrode materials and their surface roughness on Breakdown:

The experimental measurements have shown that it is not the electrode material but its surface roughness factor, which affects the breakdown strength. For an electrode configuration in weakly nonuniform field, the practical breakdown voltage of SF₆ can be estimated from the following relation:

$$U_{bi} = E_{bi} \cdot e_R \cdot e_{\max} \cdot \eta \cdot d$$

where e_R is the pressure dependent roughness factor. At a certain value of mean roughness $\overline{R_u}$ affects the roughness factor e_R more adversely at higher pressures, bringing, down the breakdown strength/voltage of the gas for a given electrode configuration. Extra effort and care must be taken while preparing electrodes for use in high voltage insulated systems where SF₆ gas pressure of the order of 0.4 Mpa is practiced.

(b)Effect of foreign particle contaminants: Compressed gas filled systems are highly sensitive to a free or a fixed particle contaminant, which may be conducting or nonconducting. The particles may either be free to move under the influence of the applied field or be fixed on electrodes in the form of protrusions. Such particles constitute a serious threat to the safe and reliable operation of gas insulated systems. The extent of their effect on the electric strength of the gas largely depends upon the pressure and the designed electric field intensity in the system. On the top of these, the extent of damage also depends upon the type of the voltage applied and its polarity.

6. **Kapton Tape:** 1 mil thick Kapton tape is warped over polyester fiber.

CHAPTER 7

OPTIMAL DESIGN OF SINGLE-LAYER AIR-CORE TOROIDAL INDUCTORS FOR HIGH FREQUENCY APPLICATIONS

7.1.1 INTRODUCTION

The behavior of air-core inductors at high frequencies is very different from that at low frequencies. Skin and proximity effects cause the winding resistance to increase proportional to approximately \sqrt{f} and the inductance to decrease slightly with increasing operating frequency f . Furthermore, the parasitic or stray capacitances of the winding cannot be neglected at high frequencies. Parasitic capacitances significantly affect the inductor behavior and are responsible for resonant frequencies. An inductor behaves like a capacitor above its first (parallel) self-resonant frequency. Since the desired inductors must operate at high frequency (120 kHz), their first (parallel) self-resonance must be at a reasonably higher frequency.

In this chapter, a procedure for the optimum design of single-layer toroidal shaped air-core inductors is discussed using an analytical approach based on few simplifying assumptions. The presence of a shield is taken into account.

7.1.2 BASIC ASSUMPTIONS

In order to minimize the effects of parasitic capacitances, inductors are usually made of a single wire, wound as a single-layer toroid without any ferromagnetic core. Furthermore, an air core does not introduce hysteresis and eddy current losses. The distance between turns is usually increased enough to reduce turn-to-turn capacitances.

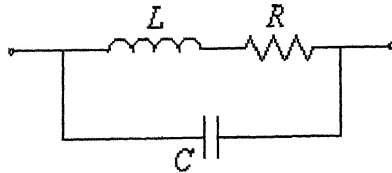


Fig. 7.1 Simplified HF model of inductors

Since the parasitic capacitances are distributed parameters, so in order to obtain the lumped parameter of the circuit shown in Fig. 7.1 the following assumptions are made:

1. For the winding of interest, capacitances between non-adjacent turns are small compared to capacitances between adjacent turns. As a consequence, the capacitances between non-adjacent turns can be neglected. Moreover, the distance between the coil and the shield is usually large enough so that we can neglect the turn-to-shield capacitances also.
2. The same current flows through all the turns. This means that edge effects are neglected and each turn has the same series equivalent inductances L_i .

Under these assumptions, the equivalent circuit of Fig 7.2 can be simplified as shown in Fig. 7.3.

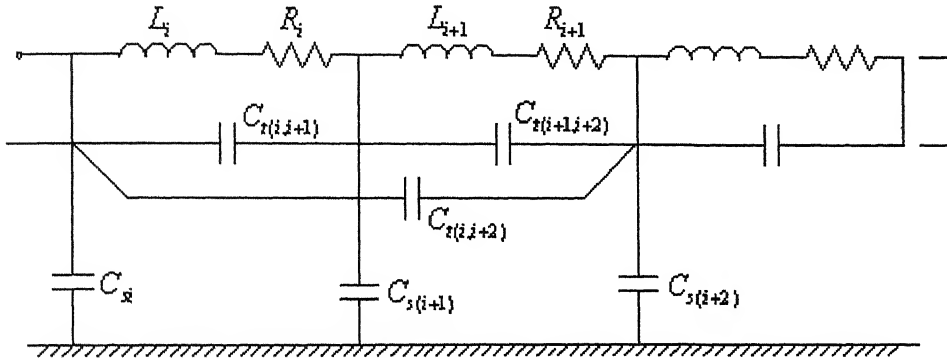


Fig. 7.2 HF distributed equivalent circuit for a single-layer air core inductor with a shield.

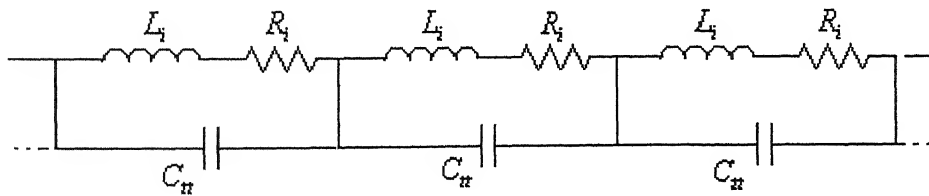


Fig. 7.3 Simplified HF distributed equivalent circuit.

In this circuit, the values of parameters of the model of Fig. 7.1 satisfy the following conditions

$$L = NL_i, \quad R = NR_i, \quad C = C_t/(N-1) \quad (7.1)$$

VHF equivalent circuit for a single-layer air-core inductor with shield is shown in Fig. 7.4. In this condition, impedances of RL branches of the equivalent circuit

of Fig. 7.2 are much higher than the impedances of the shunt capacitances C_t . As a consequence, the equivalent circuit becomes a capacitive network. In this case, turn-to-shield capacitances are also taken into account.

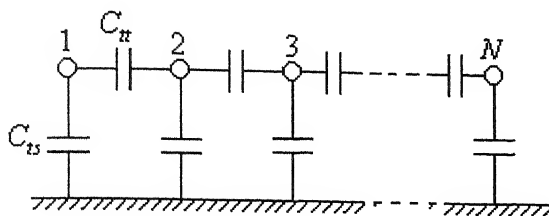


Fig. 7.4 VHF equivalent circuit for a single-layer air-core inductor with shield.

7.2. FORMULATION OF THE PROBLEM

The design of optimized inductors can be formulated as a general nonlinear programming problem [30-31] as follows:

$$\text{find } x = (x_1, x_2, \dots, x_n)$$

such that

$$F(c, x) \text{ is minimum (maximum)} \quad (7.2)$$

subject to:

$$g_i(c, x) = 0, \quad i = 1, 2, \dots, r, \quad (7.3)$$

$$h_j(c, x) \leq 0, \quad j = 1, 2, \dots, s \quad (7.4)$$

$$x_l \leq x \leq x_u \quad (7.5)$$

where $F(c, x)$, $g_i(c, x) = 0$ and $h_j(c, x) \leq 0$ are real-valued scalar functions; c is a set of constant parameters; x is a vector of n variables for which the optimization is to be accomplished. The distinction between the variables and the constants depends upon the design philosophy and the manufacturing constraints. x_l and x_u are vectors whose entries are the lower bounds, and upper bounds of x variables, respectively. The function $F(c, x)$ is called the “objective function”, for which the optimal values of x result in the minimum (maximum) of $F(c, x)$. Usually, the objective function may be identified with the cost, weight, losses, quality factor, etc. of the inductor. Additional requirements and/or dimensional limits of the inductors are referred to as “constraints”, and can be of

two types: equality (7.3), and inequality (7.4). Any design x that satisfies (7.3) and (7.4) is called a “feasible design”, and the region generated by these constraints is called a “feasible design region”. The values of x in this region comply with the design requirements, and among these points is the optimal solution. For the considered problem, both the objective function and the constraints are nonlinear multivariable functions. The input data for the HF inductor design are:

1. The rated inductance I_r ,
2. The maximum operating frequency f_{\max} ,
3. The rated current.

The maximum operating frequency can be expressed as a fraction of the first self-resonant frequency f_o of the inductor, $f_{\max} = k_f f_o$, with $k_f \leq 1$. The self-resonant frequency f_o can be calculated as a function of the overall stray capacitance C_o of the inductor:

$$f_o \cong \frac{1}{2\pi\sqrt{L_r C_o}} \tag{7.5}$$

This means the overall stray or parasitic capacitance C_o can be assumed as an input parameter instead of f_{\max} . With reference to Fig. 7.5, the geometric parameters for which the optimization must be achieved are

1. The diameter of the coil D .
2. The number of turns N .
3. The winding pitch p .
4. The wire diameter d .

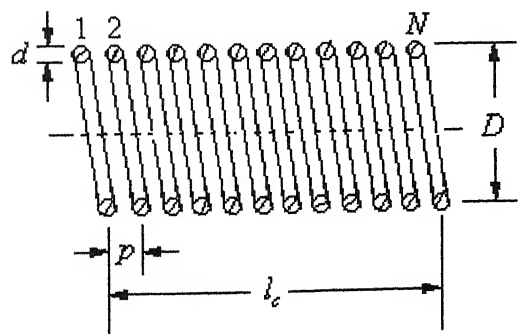


Fig.7.5 Air core inductor cross section with its essential dimensions

A single-layer solenoid air-core inductor having N turn is assumed for simplicity. Each turn consists of a single Litz-wire with a square cross section having corner in round shape. The wire diameter d is normally chosen among the standardized ones on the basis of the rated current of the inductor. Thus, if we want to optimize the inductor with respect to the weight and cost of the winding, we choose the wire diameter equal to the smallest possible diameter compatible with the expected values of the current density. Obviously, this condition does not imply minimum coil resistance and losses. Hence, at the beginning of the optimization procedure, the wire diameter d can be considered an already fixed quantity and treated as a constant parameter. We have to give a fixed Coil diameter and fixed number of turn. Therefore, we have $c = d$ and $x = (D, N, p)$.

We can adopt as an objective function the total length l_w of the copper wire. Therefore, we have

$$F(x) = l_w(D, N, p) = N\sqrt{(\pi D)^2 + p^2}$$

For a fixed diameter d , the minimization of the proposed objective function l_w reduces the copper weight (cost) to a minimum value. Neglecting the influence of the design variables on skin and proximity effects, also the winding resistance and losses are minimized.

On the basis of previous considerations, the constraints of the problem under consideration can be written as

$$g(x) = L(d, D, N, p) - L_r = 0 \quad (7.7)$$

$$h(x) = C'(d, D, N, p) - C_o \leq 0 \quad (7.8)$$

Where L and C' are the inductance and the overall stray capacitance of the coil, respectively. When shield effects are taken into account, then equation (7.8) becomes

$$h(x) = C'(d, D, N, p, h) - C_o \leq 0 \quad (7.9)$$

where h is the average distance between turns and shield.

The ranges of variation of variables D, N and p are normally limited. In particular, the lower bounds are assigned by geometrical limits as follows:

$$D \geq d, \quad N \geq 1 \text{ with integer } N, \quad p \geq d$$

The upper bounds could be limited by other technical constraints. These could be input data for the design. For example, in this case, upper limits are

$$D = 450 \text{ mm} \quad N = 280 \quad \text{and} \quad p \leq 15 \text{ mm}$$

7.2.1 CALCULATION OF DISTRIBUTED CAPACITANCES

The cross-sectional view of uniformly wound wire of square cross sections, and shields is shown in Fig. 7.6.

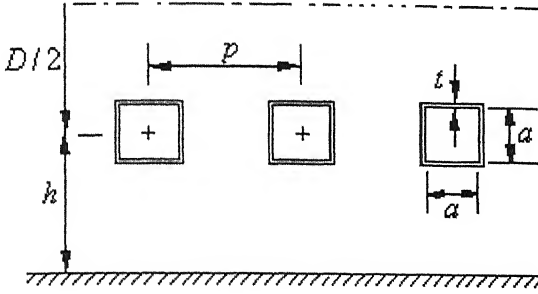


Fig. 7.6. Cross-sectional view of coils and shields.

In order to carry out the analysis of such inductor, we assume that turn-to-turn capacitances can be calculated by the capacitance per unit length of two infinitely long straight parallel conductors placed in homogeneous medium, thus neglecting the turn curvature. Under the previous assumption and if the thickness t of the insulating coating is small compared with the air-gap $(p - 2r)$, an analytical expression for the turn-to-turn capacitance C_t' can be obtained for wires of square cross-section [33] as

$$C_t' = k\epsilon_0 \frac{\pi D a}{p - a} \quad (7.10)$$

where k is a factor accounting for edge effects which is a function of the winding geometry. Equation 7.10 is obtained neglecting the contribution of the insulation coating thickness. If the thickness of the insulating coating is significant, it is possible to modify equation 7.10 obtaining the following result [34]:

$$C_t' = k\epsilon_0 \frac{\pi D a}{p - a - 2t(1 - 1/\epsilon_r)} \quad (7.11)$$

We can evaluate the turn-to-shield capacitances of the structure by neglecting the curvature of both the turns and shield. Under this assumption and neglecting the

contribution from the insulation coating, we can calculate the turn-to-shield capacitance, C_s , through the capacitance per unit length between an infinitely long straight conductor and parallel-conducting plane given by [33]

$$C_s = \frac{2\pi^2 D \epsilon_0}{\ln \left((2h/a) + \sqrt{(2h/a)^2 - 1} \right)} \quad (7.12)$$

7.2.2 CALCULATION OF THE OVERALL PARASITIC OR STRAY CAPACITANCE

For the equivalent circuit shown in Fig. 7.3, the overall stray capacitance C is given by equation 7.1. In order to evaluate the overall stray capacitance C of the equivalent circuit depicted in Fig. 7.4, the conducting shield can be regarded as a single node where all the turn-to-shield capacitances C_s are connected and the symmetries of the circuit can be exploited. In fact, for a coil with an even number of turns, we firstly can consider the two turns in the middle of the winding. For these two turns, the capacitor network consists of the capacitance between the two turns, in parallel with the series combinations of the turn-to-shield capacitances. The equivalent capacitance of this network is

$$C(2) = C_t + C_s / 2 \quad (7.13)$$

For coils consisting of an odd number of turns, we first consider the three turns placed in the middle of the winding. The equivalent capacitance of the network associated with these three turns is given by

$$C(3) = C_t / 2 + C_s / 2 \quad (7.14)$$

In order to get the overall capacitance for coils consisting of any number of turns, we observe that adding one more turn at each side of the above mentioned turns, the overall capacitance of the previous arrangement is in series with two more turn-to-turn capacitances and then in parallel with the series combination of two more turn-to-shield capacitances. Thus, for N turns we have

$$C(N) = \frac{C(N-2) \cdot C_t / 2}{C(N-2) + C_t / 2} + C_s / 2 \quad (7.15)$$

7.3 RESULTS AND DISCUSSION

In order to test the proposed method for stray or parasitic capacitance calculation, dimensions of a toroidal shaped air-core inductor with a single-wire single-layer wound having N turns is shown in Fig. 7.7. Stray capacitance for different winding pitches (p), different edge factor (k), different shield distance (h) was estimated using MATLAB. Applied technique for stray capacitance calculation matches with results of the model given in [31]. With a given values of inductance (5 mH) and working frequency (120 kHz), we required overall capacitance C_o such that self-resonant frequency (f_o) should be three times greater than working frequency f , i.e. $f_o > 3f$. So from equation 7.5,

$$\frac{1}{2\pi\sqrt{L_i C_o}} > 3f$$

Putting values of inductance and working frequency in above equation, we have

$$\frac{1}{2\pi\sqrt{5 \times 10^{-3} \times C_o}} > 3 \times 120 \times 10^3$$

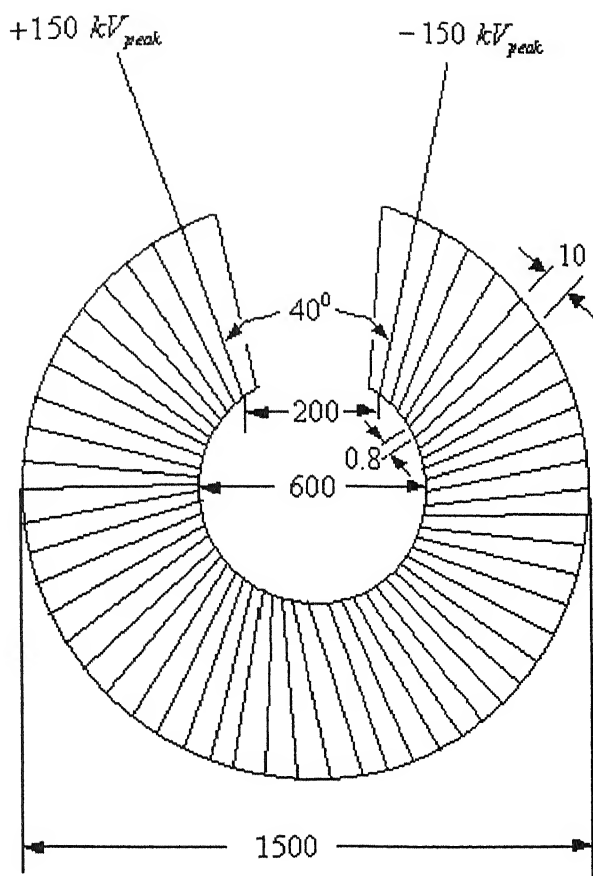
$$\Rightarrow C_o < 39.1 \text{ pF}$$

At resonance frequency 480 kHz,

$$\frac{1}{2\pi\sqrt{5 \times 10^{-3} \times C_o}} = 3 \times 480 \times 10^3$$

$$\Rightarrow C_o \cong 20 \text{ pF}$$

So we can assume that the value of overall stray capacitance C_o should be less than 20 pF to achieve self-resonance frequency greater than 360 kHz.



All dimensions are in mm

$N = 280$

▨ $5 \times 5 \text{ mm}^2$ wire cross-section
copper area 12.4 mm^2

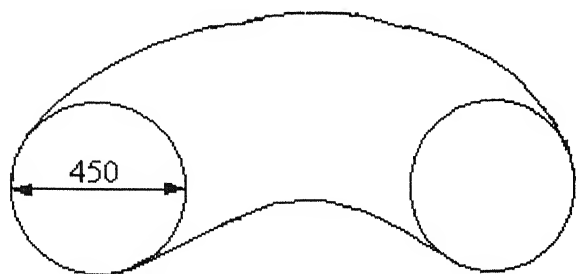
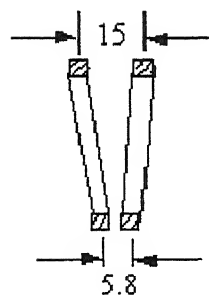


Fig. 7.7 Dimensions of toroidal shaped air-core.

7.3.1 STRAY CAPACITANCE FOR DIFFERENT EDGE FACTOR k :

Fig. 7.11 shows a value of stray capacitance for different edge factor k with all other parameters remains constant. The geometrical parameters and calculated values for the turn-to-turn capacitance (C_t), turn-to-shield capacitance, overall stray capacitances are given in table 7.1. Fig. 7.11 shows that stray capacitance increases with edge factor.

Table 7.1

Geometrical Parameters of Inductor for different edge factor (k)

For all cases: $N=280$, Insulation coating, $t=0.1$ mm of relative permittivity, $\epsilon_r = 3.0$, shield distance (h)=400 mm

Edge factor k	Coil Diameter D (mm)	Wire size a (mm)	Pitch p (mm)	Turn-to-shield capacitance C_s (pF)	Turn-to-turn capacitance C_t (pF)	Overall stray capacitance C_o (pF)
1.0	450	4.8	10.4	13.5385	16.0196	11.6628
1.2	450	4.8	10.4	13.5385	19.2235	12.3411
1.4	450	4.8	10.4	13.5385	22.4274	12.944

Table 7.2

Stray capacitance for different values of edge factor (k)

Edge Factor k	Turn-to-turn capacitance C_t (pF)	Overall stray capacitance C_o (pF)
1	16.0196	11.6628
1.2	19.2235	12.3411
1.4	22.4274	12.944

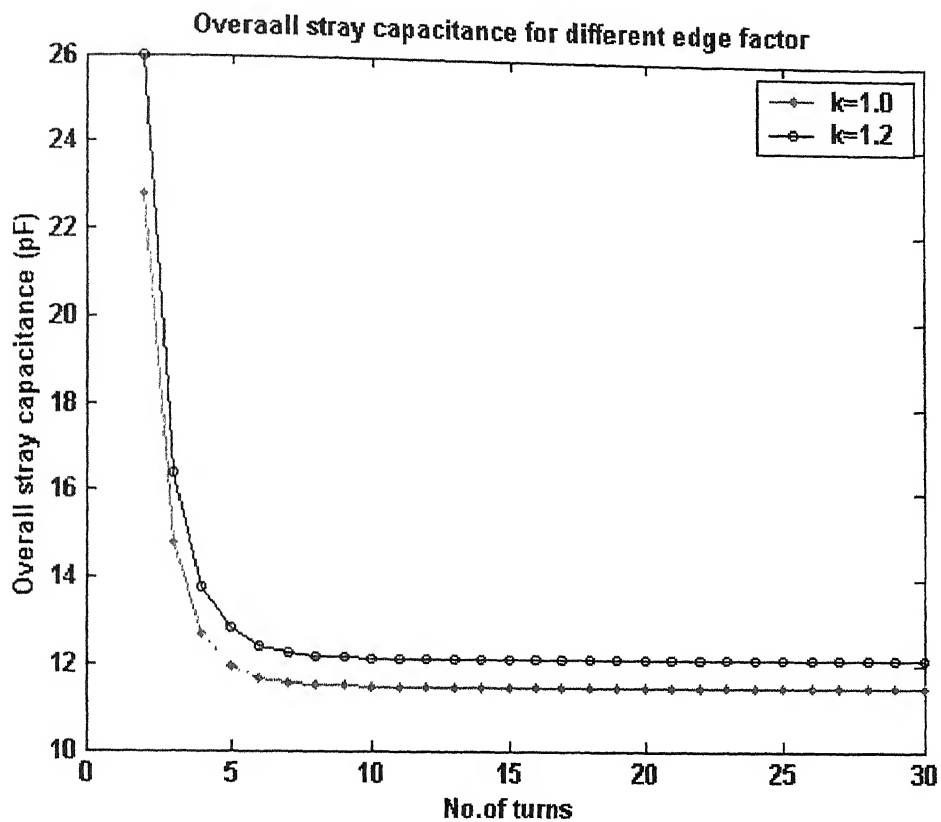


Fig 7.8. Calculated stray capacitances for different values of the winding edge factor k .

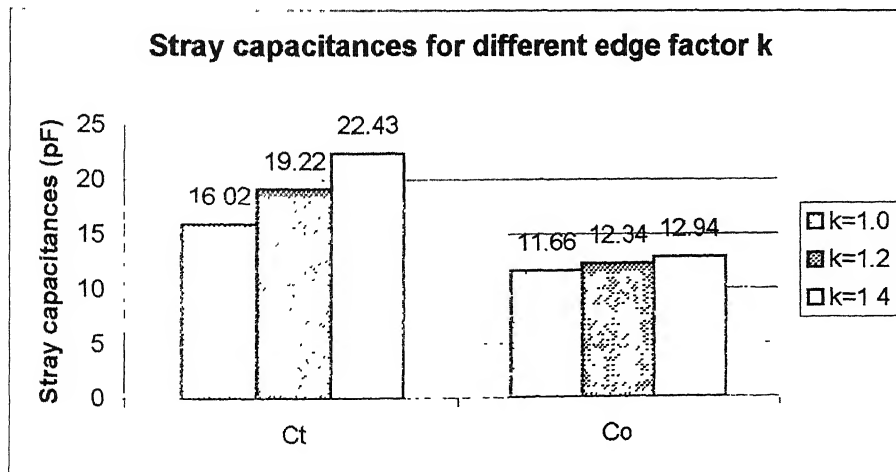


Fig. 7.9. Comparison of Stray capacitance at different winding edge factor.

7.3.2 VALUE OF STRAY CAPACITANCE WITH AND WITHOUT INSULATION COATING OVER WIRE

Table 7.3 and 7.4 shows the value of stray capacitance with and without insulation coating over Litz wire. Although, insulation thickness is 0.1 mm, there is a slight increase in capacitance due to insulation coating. Fig. 7.10 shows the variation of overall stray capacitance with a number of turns of coil with and without insulation coating.

Table 7.3

Geometrical parameters for inductor with and without insulation coating

	Edge factor k	Coil Diameter D (mm)	Wire size a (mm)	Pitch p (mm)	Shield distance h (mm)	No. of Turns N
Without insulation	1.0	450	4.8	10.4	400	280
With insulation $t = 0.1$ $\epsilon_r = 3.0$	1.0	450	4.8	10.4	400	280

Table 7.4

Stray capacitance with and without insulation coating

	Turn-to-turn capacitance C_t (pF)	Turn-to-shield capacitance C_s (pF)	Overall stray capacitance C_o (pF)
Without Insulation	15.1702	13.5385	11.4834
With insulation $t = 0.1$ $\epsilon_r = 3.0$	16.0196	13.5385	11.6628

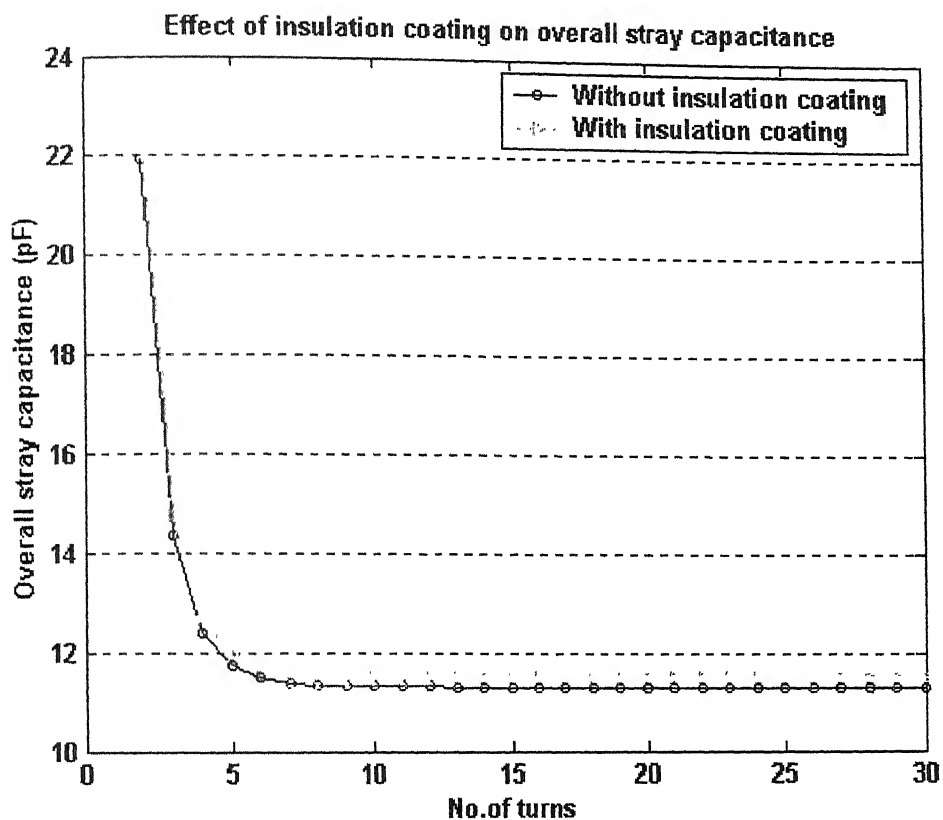


Fig. 7.10. Measured capacitances with and without insulation coating.

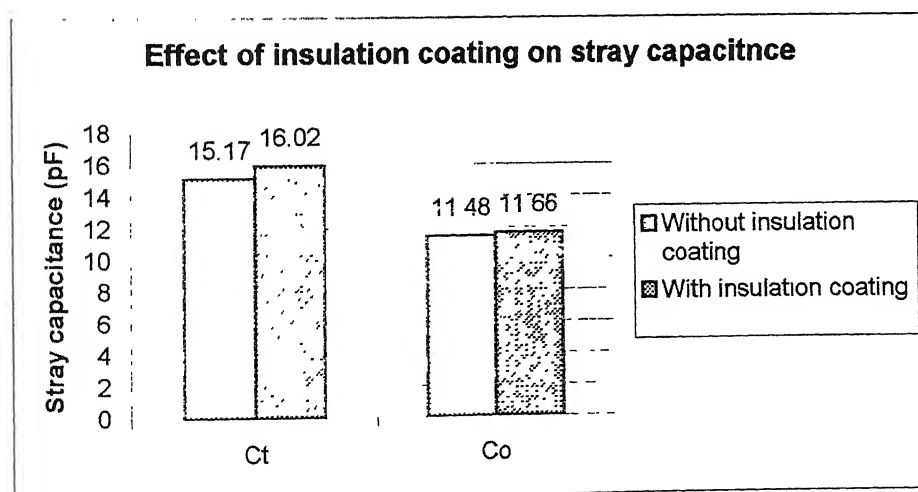


Fig.7.11 Comparison of stray capacitances with and without insulation coating.

7.3.3 VALUES OF STRAY CAPACITANCE FOR DIFFERENT VALUES OF THE WINDING PITCH

Minimum value of pitch is limited by the size of the wire, which is equal to 5 mm.

Designed pitches are:

$$\text{Inner pitch} = 5.8 \text{ mm}$$

$$\text{Outer pitch} = 15 \text{ mm}$$

So, average of this becomes 10.4 mm.

Maximum opening at the outer periphery of toroid is 500 mm, so

$$\text{Maximum value of pitch} \Rightarrow 279 \times p_{\max} = \pi \times 1500 - 500 \Rightarrow p = 15 \text{ mm}$$

Value of stray capacitances and geometrical parameters for different winding pitch is tabulated in Table 7.5 and 7.6. Fig 7.12 and 7.13 shows the variation of turn-to-turn capacitance and overall stray capacitance with number of turns for a different winding pitch. Fig 7.14 reveals that turn-to-turn capacitance and overall stray capacitance decreases with increasing winding pitch. At designed pitch ($p=10.4 \text{ mm}$) overall stray capacitance is 11.6628 pF which is less than 20 pF. Also, inductance value for pitch ($p=10.4 \text{ mm}$) is 5 mH, which we require.

Table 7.5

Geometrical parameters of inductor for different winding pitch

With insulation of $t = 0.1 \text{ mm}$, $\epsilon_r = 3.0$ over Litz wire

Edge factor k	Coil Diameter $D \text{ (mm)}$	Wire size $a \text{ (mm)}$	Pitch $p \text{ (mm)}$	Shield distance $h \text{ (mm)}$	No. of Turns N
1.0	450	4.8	10.4	400	280
1.0	450	4.8	12.0	400	280
1.0	450	4.8	13.0	400	280
1.0	450	4.8	15.0	400	280

Table 7.6

Values of stray capacitances for different values of winding pitch

Average pitch P (mm)	Turn-to-turn capacitance C_t (pF)	Turn-to-shield capacitance C_s (pF)	Overall stray capacitance C_o (pF)
10.4	16.0196	13.5385	11.6628
12.0	13.2245	13.5385	11.0564
13.0	11.9745	13.5385	10.7688
15.0	10.1325	13.5385	10.3227

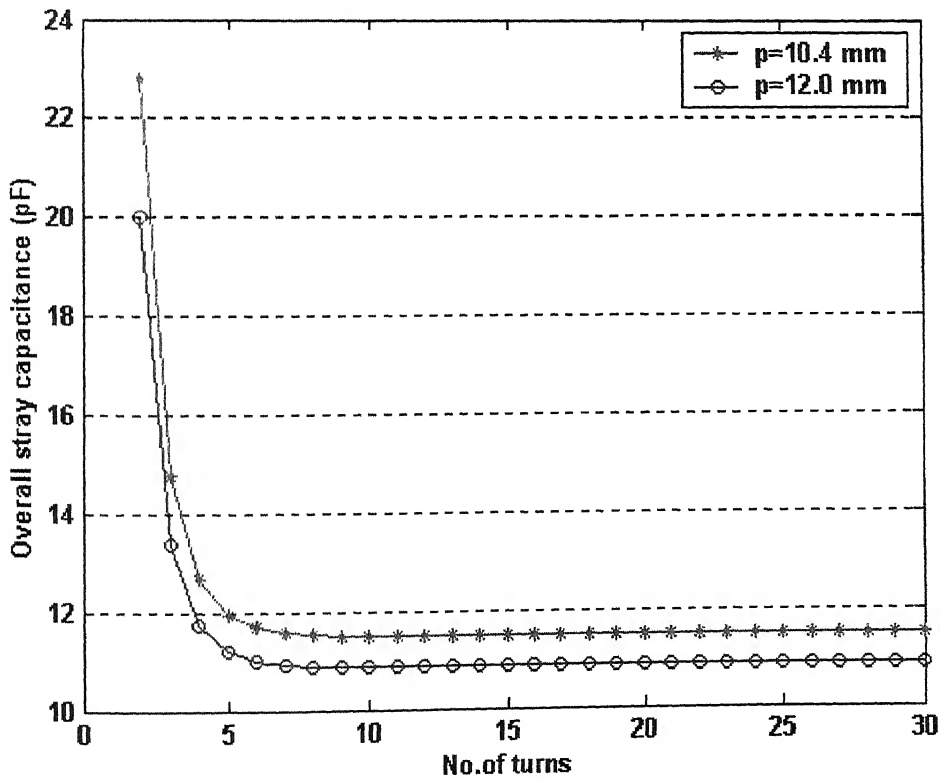


Fig. 7.12. Calculated Stray capacitance for different values of the winding pitch.

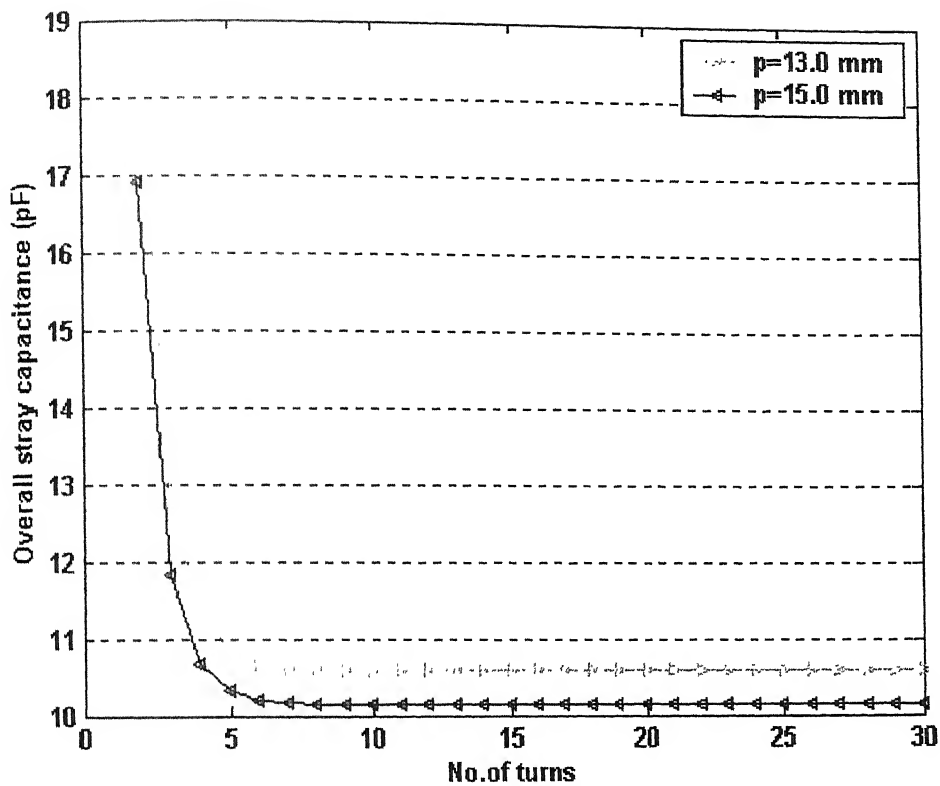


Fig. 7.13 Calculated Stray capacitance for different values of the winding pitch.

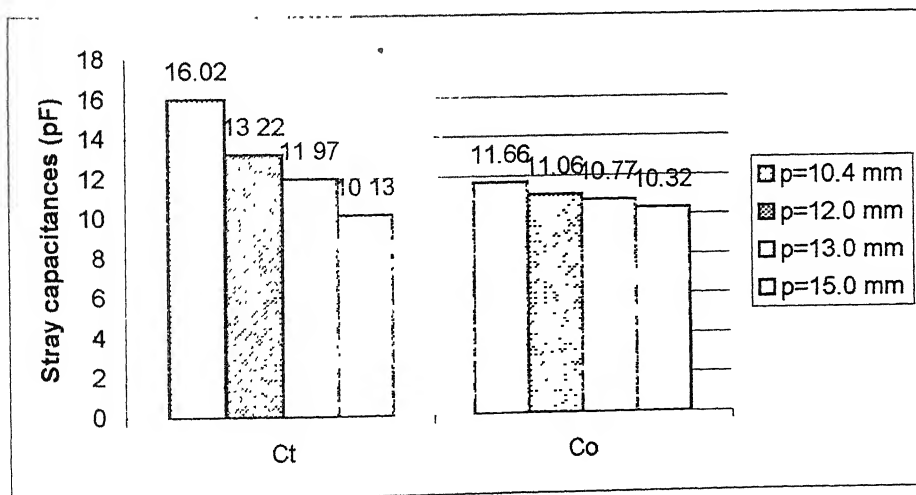


Fig. 7.14 Comparison of stray capacitances for different values of the winding pitch.

7.3.4 VALUES OF STRAY CAPACITANCE FOR DIFFERENT VALUES OF THE SHIELD DISTANCE

Shield distance means ‘ average distance from each turn to shield’. Designed value of average shield distance is 400 mm. It is clear from Fig. 7. 15, Fig. 7.16 and Fig.7.17 that turn-to-shield and overall stray capacitances decreases with increase in shield distance. Without shield overall stray capacitance is $C_t/N-1$. Introducing shield causes an increase in overall stray capacitance. Without shield overall stray capacitance decreases with increase in number of turns. On the other hand, with shield, it remains constant after a certain number of turns.

Table 7.7

Geometrical parameters of inductor for different shield distance

With insulation of $t = 0.1\text{mm}$, $\epsilon_r = 3.0$ over litz wire

Edge factor k	Coil Diameter D (mm)	Wire size a (mm)	Pitch p (mm)	Shield distance h (mm)	No. of Turns N
1.0	450	4.8	10.4	300	280
1.0	450	4.8	10.4	350	280
1.0	450	4.8	10.4	400	280
1.0	450	4.8	10.4	450	280

Table 7.8

Values of stray capacitances for different values of winding pitch

Shield Distance h (mm)	Turn-to-turn capacitance C_t (pF)	Turn-to-shield capacitance C_s (pF)	Overall stray capacitance C_o (pF)
300	16.0196	14.2439	12.0853
350	16.0196	13.857	11.854
400	16.0196	13.5385	11.6628
450	16.0196	12.2694	11.5007

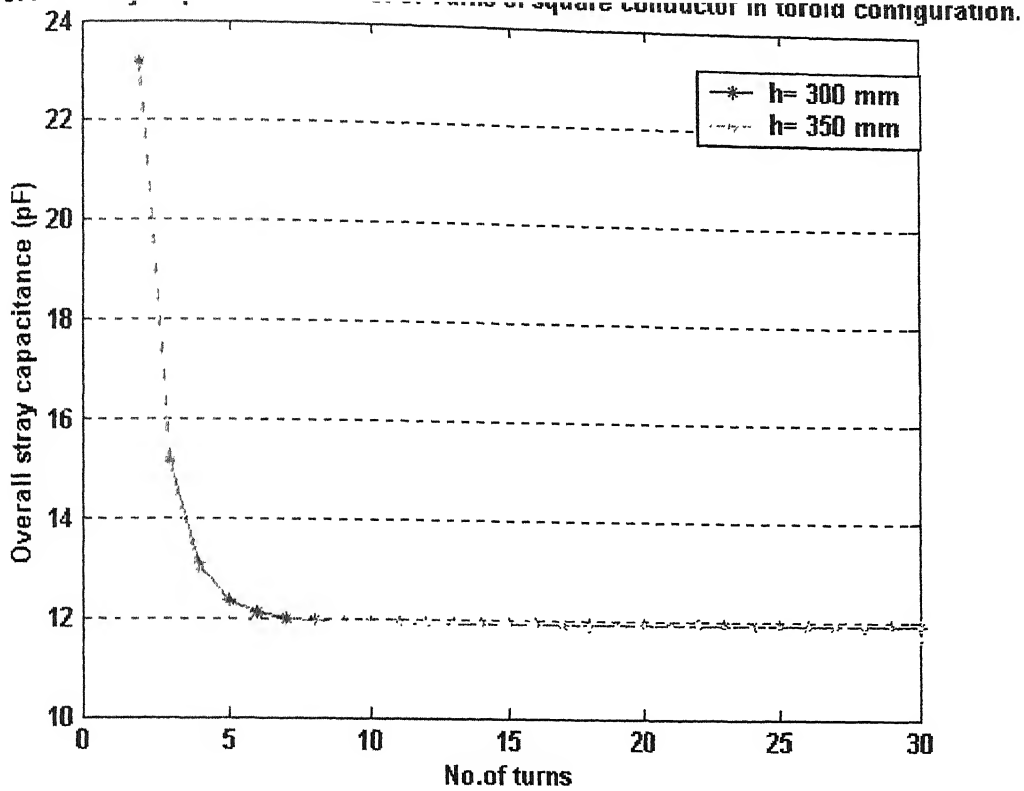


Fig. 7.15. Calculated stray capacitances for different values of the shield distance.

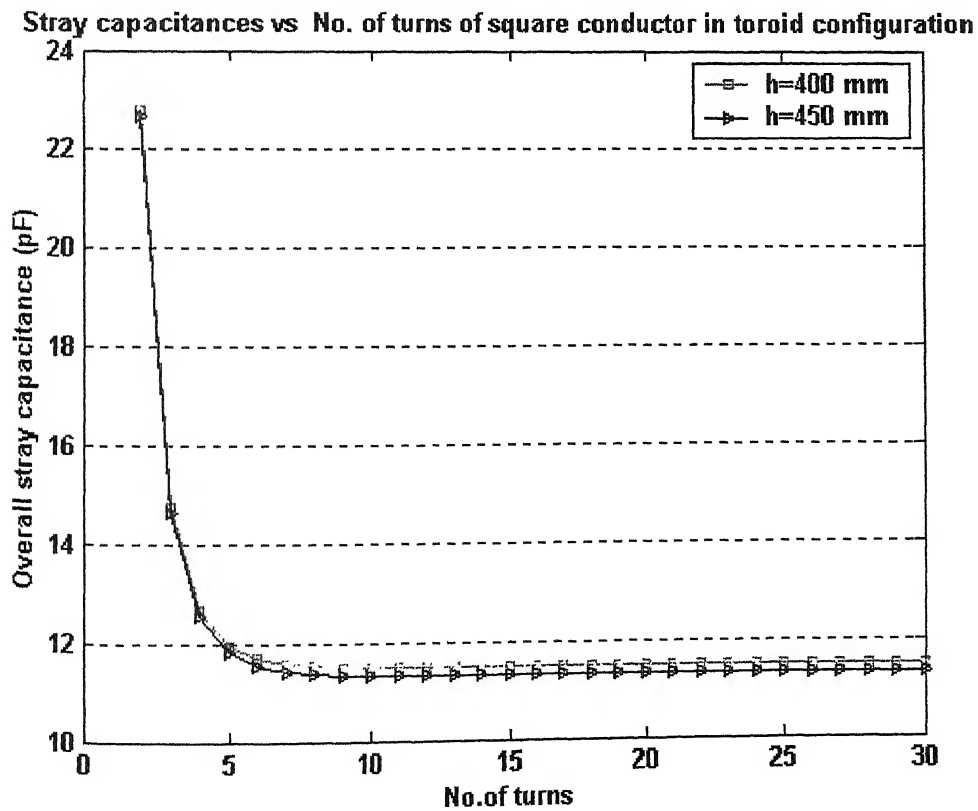


Fig. 7.16 Calculated stray capacitances for different values of the shield distance.

Stray capacitances for different shield distance

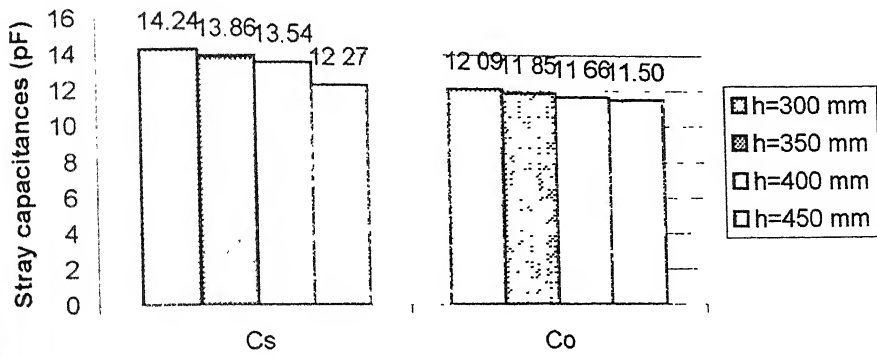


Fig. 7.17 Comparison of stray capacitances for different values of the shield distance.

EXPERIMENTAL INVESTIGATIONS

8.1 INTRODUCTION

Following experiments were performed in this work;

1. High frequency response of inductor with toroidal core.
 - (a) High frequency response of prototype air-core toroidal inductor
 - (b) High frequency response of ferrite core toroidal inductor
2. High frequency response of 2464/AWG 40 Litz wire of 1 m length
 - (a) Determination of Loss tangent of Litz wire conductor with variable frequency
 - (b) Determination of dielectric loss tangent of litz wire insulation with variable frequency
3. Breakdown tests on square litz-wire just over the polyester yarn cover.

8.2 HIGH FREQUENCY RESPONSE OF TOROIDAL SHAPED INDUCTOR

To perform this experiment a prototype Air-core toroidal inductor (rectangular cross section) and ferrite core toroidal inductor (rectangular cross-section) were built. Inductance and quality factor of each model were measured using “HP 4284A Precision LCR meter”. Measured value is tabulated in table 8.1 and 8.2. High frequency response i.e. inductance Vs frequency and quality factor Vs frequency are shown in tables and Fig. 8.1 to 8.3. It is clear from these figures, that air-core toroid inductor has better frequency response than ferrite core. Since we require an inductor (secondary winding of RF transformer) of about 5 mH. Also we need inductor having very high Q-factor for a better attenuation. Therefore, Tables and Fig. 8.1-8.3 reveal that air-core toroidal inductor is the best choice for this purpose.

Table 8.1

Measured data for prototype **air-core toroidal inductor** (rectangular cross section)

$N = 220$ turns, SWG ≈ 17 , single wire, single layer spaced, Outer diameter of toroid = 1515 mm, Inner diameter of toroid = 455 mm, Axial height = 510 mm

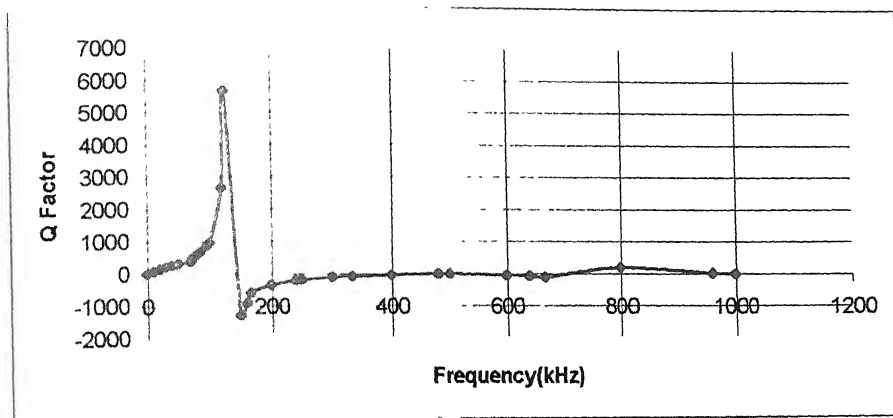
Frequency f (kHz)	Inductance L (mH)	Quality factor Q
1	7.0306	8.68
10	6.934	83
20	6.925	151.8
30	6.912	210.9
40	6.894	261.8
50	6.874	312.5
70	6.843	371.4
71.42	6.811	454.8
80	6.78	605
85.714	6.76	686
96	6.716	890
100	6.7	962
120	6.594	2665
125	6.553	5675
150	6.402	-1265
160	6.327	-900
166.6	6.233	-590
200	5.912	-352
240	5.448	-204.5
250	5.304	-184
300	4.465	-105
333.3	3.797	-74
400	2.278	-36.5
480	0.503	-8.13
500	0.137	-1.92
600	-1.208	-38.9
640	-1.422	-66.5
666.6	-1.48	-93.1
800	-1.049	201
960	0.487	25.5
1000	0.003	1

Table 8.2

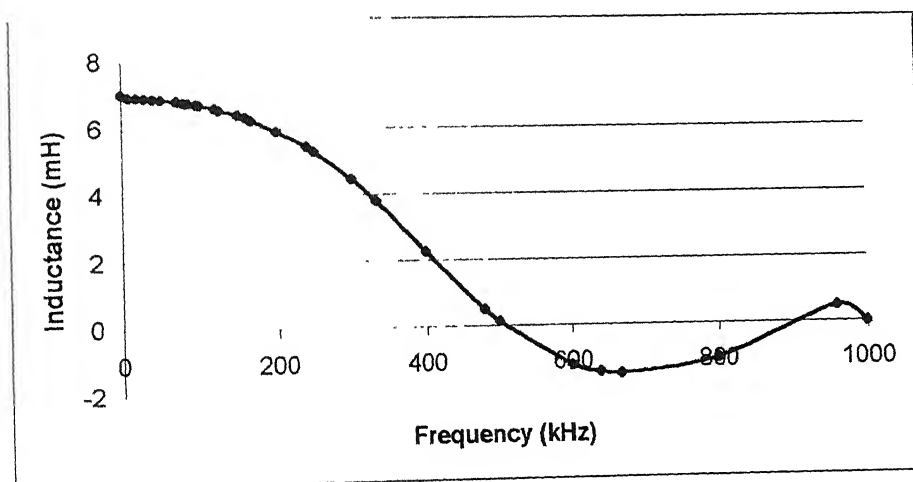
Measured data for **ferrite core toroidal inductor** (circular cross section)

N=136 turns, SWG-17, single layer single wire spaced, Outer diameter of toroid=145 mm, Inner diameter of toroid=83 mm

Frequency f (kHz)	Inductance L (mH)	Quality factor Q
1	4.52	50
1.2	4.79	48.38
5	12.3	34.87
10	20.3	31.46
20	26.3	29.6
30	28.5	29.11
50	29.9	28.78
60	25.8	30.49
80	22.9	32.23
85.714	21.2	33.541
96	19.6	34.31
100	19.3	34.81
120	14.5	40.67
150	8.2	57.33
200	0.62	550
250	4.2	-55.39
300	7.38	-23.02
400	10.8	-9.377
500	12.5	-5.5296
600	13.6	-3.4434
800	14.8	-1.7764
960	14.9	1.16
1000	1	0.00322



(a)



(b)

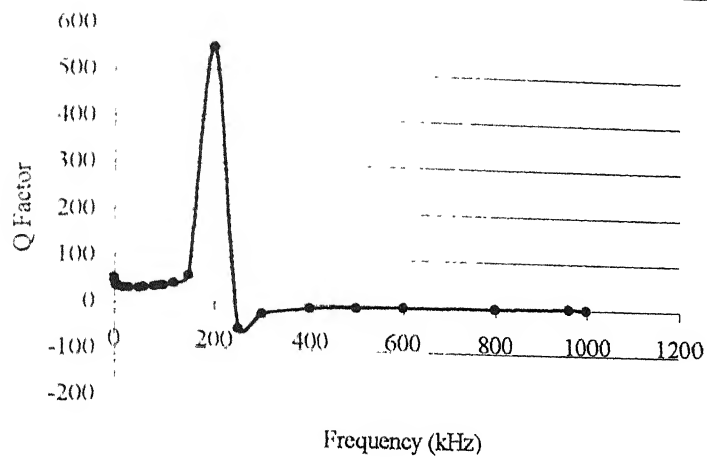
Fig.8.1 (a) Q-curve and (b) Inductance curve, for prototype air-core toroidal inductor (rectangular cross section) of following specifications:

Number of turns, $N=220$, Outer diameter of toroid (OD)=1515 mm

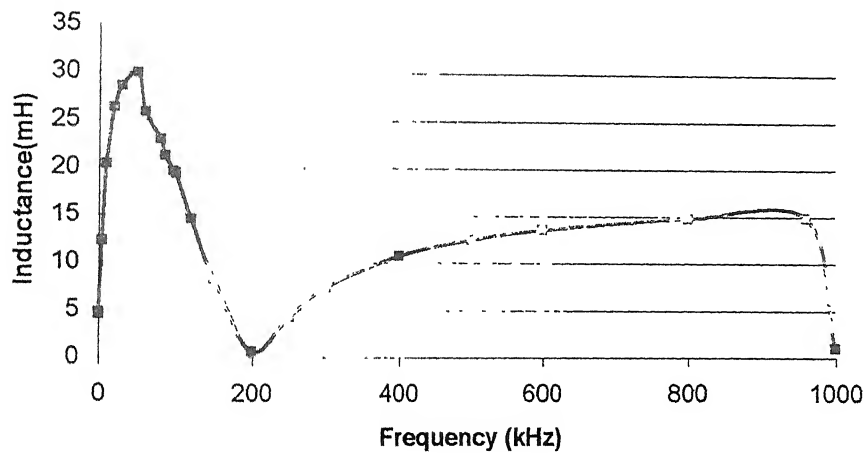
Inner diameter of toroid (ID)=455 mm, Axial height of toroid =510 mm

Winding: SWG 17 single wire single layer spaced.

Original data measured using "HP 4284A precision LCR meter".



(a)



(b)

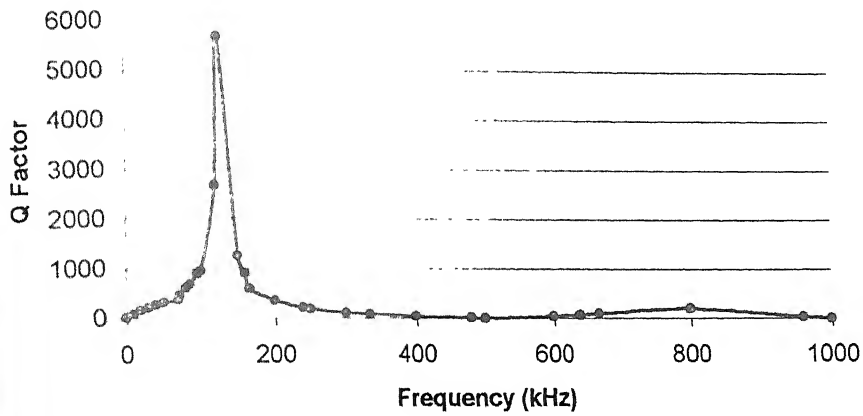
Fig.8.2 (a) Q-curve and (b) Inductance curve, for ferrite core toroidal inductor (circular cross section) of following specifications:

Number of turns, $N=136$, Outer diameter of toroid (OD)=145 mm

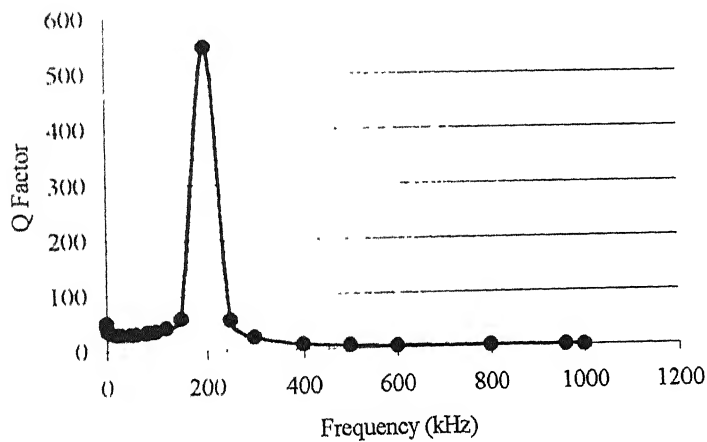
Inner diameter of toroid (ID)=83 mm

Winding: SWG 17 single wire single layer spaced.

Original data measured using "HP 4284A precision LCR meter".



(a)



(b)

Fig. 8.3 Q (magnitude) curves for (a) prototype air-core toroidal inductor, (b) Ferrite core toroidal inductor.

8.3 HIGH FREQUENCY RESPONSE OF 2464/AWG40 LITZ WIRE OF ONE METER LENGTH

This test was performed on Litz wire conductor and Litz wire insulation. Litz wire insulation comprises enamel insulation and polyester fiber (Tergel). Therefore, frequency response of 2464/AWG 40 Litz wire insulation is the frequency response of composite insulation (Enamel and polyester fiber).

8.3.1 DETERMINATION OF LOSS TANGENT OF LITZ-WIRE CONDUCTOR WITH INCREASING FREQUENCY

This test was conducted across Litz-wire terminals. Loss tangent was measured using impedance analyzer at different frequencies. This loss tangent includes dc resistance loss tangent, skin effect loss tangent and proximity effect loss as described in chapter 4. Measured values are tabulated in table 8.3. Fig. 8.5 shows the loss tangent due to contribution of dc resistance and eddy current loss (skin effect and proximity effect). It reveals that for frequency range 1 kHz-2 MHz total loss tangent due to dc resistance and eddy current losses decrease. Beyond this it increases very rapidly with frequency. For lower frequency (1 kHz-2 MHz) skin effect and proximity effect are negligible. Beyond 2 MHz proximity effect is dominated. Thus for high frequency inductors, e.g. operating at frequencies of about 5 MHz or higher it may be advantageous to use solid wire unless very finely stranded conductors are available.

Table 8.3

Measured values of loss tangent for 1m length Litz wire conductor of 2464/AWG40

Frequency
 f (kHz)

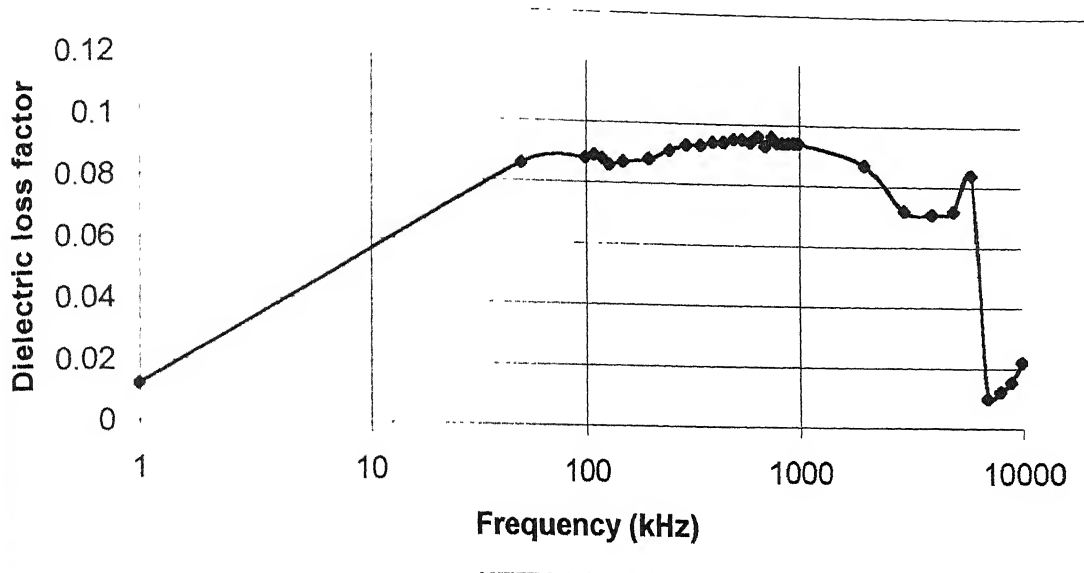
Loss tangent due to dc resistance and eddy current losses
 $\tan \delta$

100	0.046
110	0.0424
120	0.039
130	0.038
150	0.036
170	0.036
200	0.033
220	0.0311
240	0.0301
260	0.029
300	0.027
360	0.024
400	0.0234
450	0.021
500	0.019
600	0.019
650	0.0191
700	0.017
750	0.016
800	0.016
850	0.017
900	0.016
950	0.015
1000	0.014
2000	0.0131
3000	0.0121
4000	0.088
5000	0.083

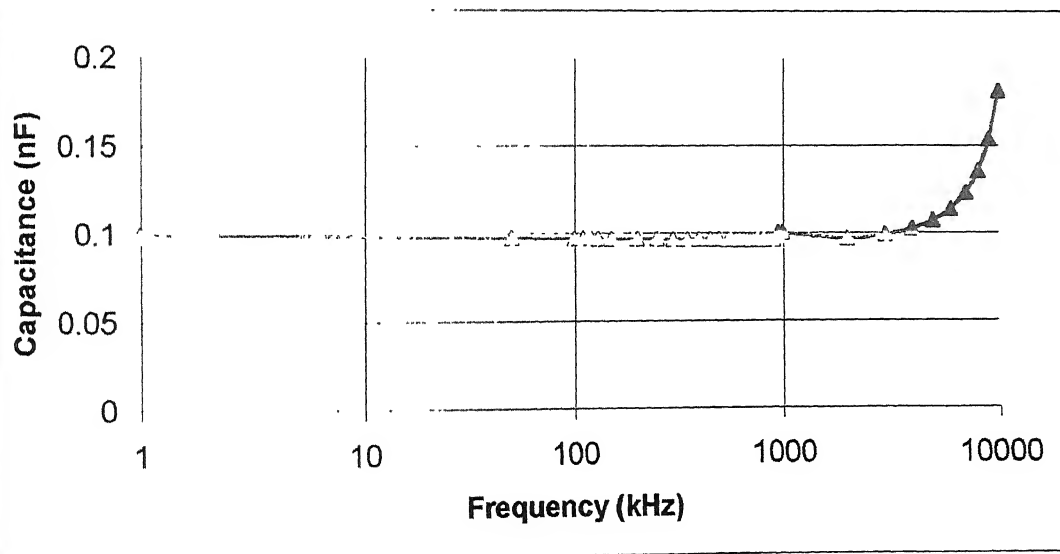
Table 8.4

Measured data for Insulation characteristics for 1 m length Litz wire of 2464/AWG 40

Frequency f (kHz)	Dielectric loss factor $\tan \delta$	Capacitance C (nF)
1	0.0123	0.0997
50	0.086	0.0975
100	0.088	0.09699
110	0.089	0.09699
120	0.088	0.09694
130	0.086	0.09686
150	0.087	0.09679
200	0.088	0.09666
250	0.091	0.0966
300	0.093	0.0965
350	0.093	0.0963
400	0.094	0.0962
450	0.094	0.0962
500	0.095	0.0962
550	0.095	0.0961
600	0.094	0.0961
650	0.096	0.096
700	0.093	0.096
750	0.096	0.09603
800	0.094	0.09595
850	0.094	0.09596
900	0.094	0.09596
950	0.094	0.09996
1000	0.094	0.09999
2000	0.087	0.09684
3000	0.072	0.099
4000	0.071	0.1023
5000	0.072	0.1071
6000	0.084	0.1136
7000	0.01	0.12276
8000	0.0122	0.13524
9000	0.0155	0.15349
10000	0.022	0.181



(a)



(b)

Fig. 8.6 (a) Dielectric loss factor and (b) capacitance as a function of frequency for one meter length litz wire having following specifications:

Number of strands=2464 of AWG40 ,each are insulated with each other by enamel. Litz wire outer insulation is polyester fiber (Tergel). Size of Litz wire: 5mm×5mm square cross section with no sharp edge.

8.4 BREAKDOWN TEST ON SQUARE LITZ POLYESTER YARN

INSULATED WIRE

To perform this test, A thin soldering wire (lead) was wrapped tightly over polyester yarn of Litz wire (1m length). Table 8.5 shows measured results for different specimens of Litz wire. It is concluded from Fig 8.7 that a breakdown characteristic of Litz wire insulation depends upon the extent of moisture contamination, impurities in the dielectric and environment. Also it is concluded that overlapping a Nomex paper over the polyester yarn cover causes an increase in breakdown strength of the composite dielectric (polyester yarn and Nomex paper).

Table 8.5

Measured results for breakdown characteristics for one meter length Litz wire insulation

S.No.	Litz wire specimen conditions	Breakdown voltage
1	New fresh untouched wire	1300 V dc
2	New fresh untouched with 2 mil thick Nomex paper of 50% overlapping	3200 V dc
3	Contaminated with moisture, dirt and environment	600 V- 800 v dc

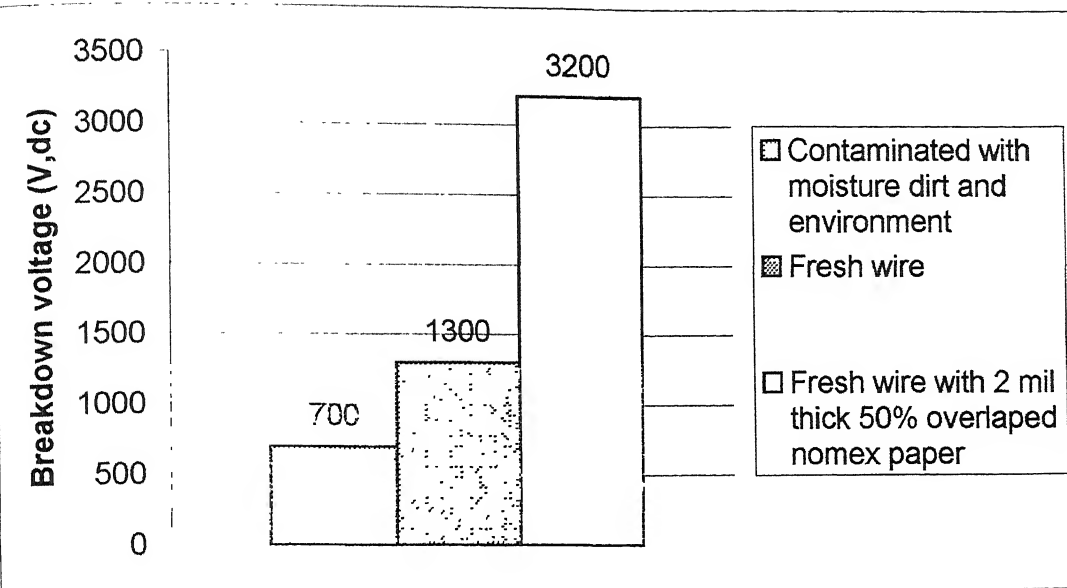


Fig. 8.7 Breakdown characteristics for one meter length Litz wire having following specifications:

Number of strands=2464 of AWG40 , insulated with each other by enamel coating. Litz wire outer insulation is polyester fiber (Tergel). Size of Litz wire: 5mm×5mm square cross section with no sharp edge. Thickness of polyester fiber over Litz wire conductor, $t=0.1$ mm, relative permittivity of polyester fiber, $\epsilon_r=3.0$.

FINITE ELEMENT ANALYSIS OF ELCTRIC FIELD INTENSITY

9.1 INTRODUCTOIN

Finite Element Method (FEM) is a numerical method for the estimation of electric field intensity in a given electrode system. Although the history of application of numerical methods can be traced back to the time of Gauss (1777-1855) and Boltzmann (1844-1906), it was in the 1940s that this method received more attention in USA, for solving general linear and even nonlinear partial differential equations. This method has since received attention not only for solving electric and magnetic fields but is also applied in civil engineering. In this chapter, the fundamentals of the finite element are introduced for the analysis of electric field intensity for simple electrode configurations. Main focus of this chapter is to analyze electric field intensity for circular and square shaped electrodes.

9.2 FINITE ELEMENT METHOD (FEM)

In this method the field between the electrodes is divided into discrete elements. The shape of these discrete elements is chosen to be triangular for two dimensional representation and tetrahedron (a structure with four surfaces) for three dimensional field representation, Fig. 9.1 and 9.2. The shape and size of each triangle or tetrahedron is chosen suitably of finite dimensions and these are irregularly distributed within the field.

At those locations where a higher electric stress is expected, triangles of smaller vertices should be chosen, as shown in Fig. 9.1. In fact, the locations at higher stresses would need to cover with triangles of smaller dimensions. This method, unlike Finite Difference Method, does not involve a direct solution of Laplace equation. Instead, the approach in FEM is concerned with the factual characteristics of an electrostatic field that the total energy enclosed in the whole field region acquires a minimum value. In other words, the potential Φ under given conditions of electrode surface should make the enclosed energy function to be a minimum for a given dielectric volume 'V', therefore,

$$\int_V \frac{1}{2} \epsilon (grad \Phi)^2 dV \rightarrow \text{minimum} \quad (9.1)$$

which is obtained by solving the basic potential Equation , $\vec{E} = - \text{grad } \Phi$. W is the electrical energy stored in the volume of dielectric considered.

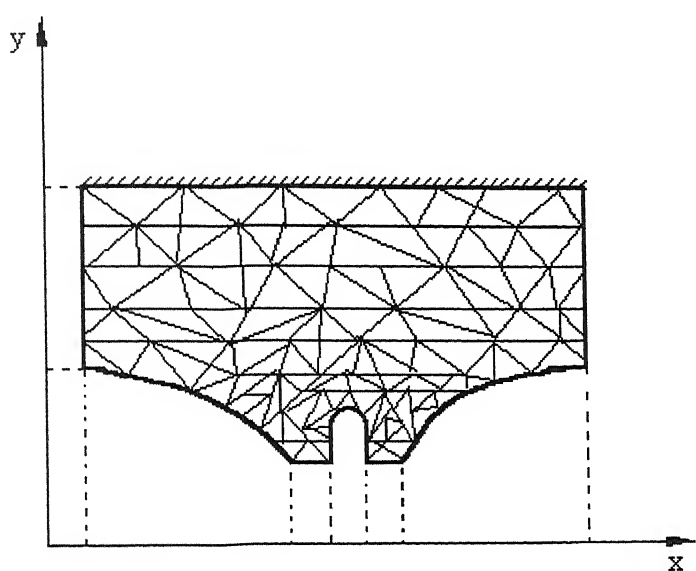


Fig. 9.1 Finite Element Mesh using Triangles.

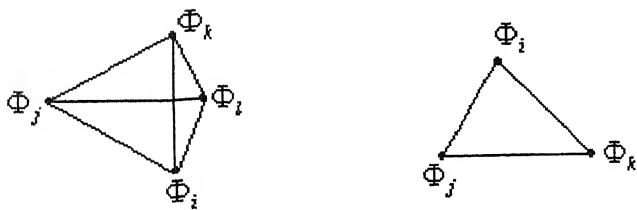


Fig.9.2 A Tetrahedron and a triangular finite element.

Let us consider an electrostatic field without any space charge in a single isotropic dielectric between two electrodes. Then the potential Φ would be determined by the boundaries, that is, the metal electrode surfaces. The above equation 9.1 for electrical energy W , stored within the whole region of such a Laplacian field is given in cartesian coordinates as follows:

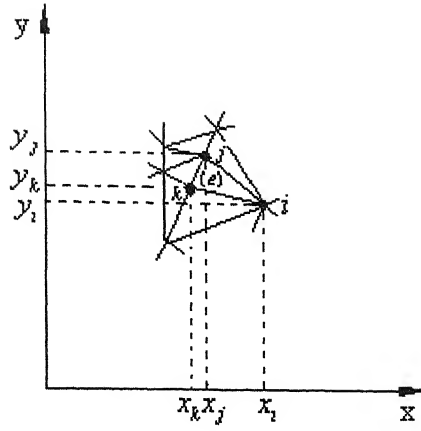


Fig. 9.3 Part of two-dimensional field subdivided into irregular triangular elements on x- y plane.

Equation 9.4 implies that the potentials within the element are linearly distributed and the field intensity is constant. For the element (e) under consideration. The unknown potentials at respective nodes i, j, and k are given by the equations,

$$\begin{aligned}\Phi_i &= a_1 + a_2x_i + a_3y_i \\ \Phi_j &= a_1 + a_2x_j + a_3y_j \\ \Phi_k &= a_1 + a_2x_k + a_3y_k\end{aligned}\tag{9.5}$$

and the coefficients a_1 , a_2 , and a_3 may be determined by applying Cramer's rule,

$$\begin{aligned}a_1 &= \frac{1}{2\Delta_e}(\alpha_i\Phi_i + \alpha_j\Phi_j + \alpha_k\Phi_k) \\ a_2 &= \frac{1}{2\Delta_e}(\beta_i\Phi_i + \beta_j\Phi_j + \beta_k\Phi_k) \\ a_3 &= \frac{1}{2\Delta_e}(\gamma_i\Phi_i + \gamma_j\Phi_j + \gamma_k\Phi_k)\end{aligned}\tag{9.6}$$

where

$$\begin{aligned}\alpha_i &= x_jy_k - x_ky_j & \beta_i &= y_j - y_k \\ \alpha_j &= x_ky_i - x_iy_k & \beta_j &= y_k - y_i \\ \alpha_k &= x_iy_j - x_jy_i & \beta_k &= y_i - y_j\end{aligned}$$

$$\gamma_i = x_k - x_j$$

$$\gamma_j = x_i - x_k$$

$$\gamma_k = x_j - x_i$$

$$\begin{aligned} 2 \Delta_e &= \alpha_i + \alpha_j + \alpha_k \\ &= \beta_i \gamma_j - \beta_j \gamma_i \end{aligned}$$

The symbol Δ_e represents area of the triangular element i, j, k under consideration.

From equation 9.4, the partial derivatives of Φ are,

$$\frac{\partial \Phi}{\partial x} = a_2 = f(\Phi_i, \Phi_j, \Phi_k) \frac{\partial \Phi}{\partial x} = a_2 = f(\Phi_i, \Phi_j, \Phi_k)$$

and

(9.7)

$$\frac{\partial \Phi}{\partial y} = a_3 = f(\Phi_i, \Phi_j, \Phi_k)$$

In order to minimise the energy within the whole system, only derivatives of the energies with respect to the potential distribution in each element are of interest here. For the element (e) under consideration, if W_e is the energy enclosed in this element, then the energy per unit length in the z direction W_e / z , denoted by W_{Δ_e} can be given by equation 9.3 as follows:

$$W_{\Delta_e} = \frac{W_e}{z} = \frac{1}{2} \Delta_e \varepsilon \left[\left(\frac{\partial \Phi}{\partial x} \right)^2 + \left(\frac{\partial \Phi}{\partial y} \right)^2 \right] \quad (9.8)$$

since $\iint_A dx dy$ provides the area Δ_e of the element described.

To minimise the energy in this specific element (e), the expression can be derived by differentiating equation 9.7 partially with respect to Φ_i , Φ_j and Φ_k . Thus, taking into account equations 9.6 and 9.7, the differentiation with respect to Φ_i results in,

$$\begin{aligned} \frac{\partial W_{\Delta_e}}{\partial \Phi_i} &= \frac{1}{2} \varepsilon \Delta_e \left(2a_2 \frac{\partial a_2}{\partial \Phi_i} + \frac{\partial a_3}{\partial \Phi_i} \right) \\ &= \frac{1}{2} \varepsilon (a_2 \beta_i + a_3 \gamma_i) \\ &= \frac{\varepsilon}{4 \Delta_e} \left[(\beta_i^2 + \gamma_i^2) \Phi_i + (\beta_i \beta_j + \gamma_i \gamma_j) \Phi_j + (\beta_i \beta_k + \gamma_i \gamma_k) \Phi_k \right] \end{aligned}$$

The set of all three equations with respect to Φ_i , Φ_j and Φ_k can be expressed in matrix form,

$$\begin{aligned} \frac{\partial W_{\Delta_e}}{\partial \Phi_e} &= \frac{\varepsilon}{4\Delta_e} \begin{pmatrix} (\beta_i^2 + \gamma_i^2) & (\beta_i\beta_j + \gamma_i\gamma_j) & (\beta_i\beta_k + \gamma_i\gamma_k) \\ (\beta_j\beta_i + \gamma_j\gamma_i) & (\beta_j^2 + \gamma_j^2) & (\beta_j\beta_k + \gamma_j\gamma_k) \\ (\beta_k\beta_i + \gamma_k\gamma_i) & (\beta_k\beta_j + \gamma_k\gamma_j) & (\beta_k^2 + \gamma_k^2) \end{pmatrix} \begin{pmatrix} \Phi_i \\ \Phi_j \\ \Phi_k \end{pmatrix} \\ &= \begin{pmatrix} (h_{ii})_e & (h_{ij})_e & (h_{ik})_e \\ (h_{ji})_e & (h_{jj})_e & (h_{jk})_e \\ (h_{ki})_e & (h_{kj})_e & (h_{kk})_e \end{pmatrix} \begin{pmatrix} \Phi_i \\ \Phi_j \\ \Phi_k \end{pmatrix} \\ &= (h)_e (\Phi)_e \end{aligned} \quad (9.9)$$

The matrix $(h)_e$ is known as the “stiffness matrix” for the individual element (e), geometrically locating and containing functional sensitivity with respect to the potentials. It also contains the permittivity of the dielectric material.

The energy in the individual element W_{Δ_e} is dependent upon the node potentials of the element (Φ_i, Φ_j, Φ_k) . If we denote the total energy in the whole system of given elements by W_Λ , the relation for minimising the energy within the complete system can be given as,

$$\frac{\partial W_\Lambda}{\partial \Phi} = 0 \quad (9.10)$$

where (Φ) is the potential vector for all the nodes within a given system.

Considerations to account for the potentials of the triangular element (e) yet remain to be applied. Figure 9.3 shows the triangular element (e) being surrounded by other triangular elements. Any node potential within such a system depends upon the potentials of the surrounding nodes. The number of surrounding nodes to a node is dependent upon the network and may vary from node to node within a network. However, it is always a small number of nodes.

Let us consider node k of the element given the number 5 as shown in Fig. 9.4. Four triangular elements (1) to (4) meet at this node. The nodes adjacent to node 5 are

numbered 1 to 4. For this set of elements, following relation is obtained on applying equation 9.10,

$$\frac{\partial W_{\Lambda}}{\partial \Phi_5} = 0$$

where W_{Λ} is the total energy of the system with four elements and Φ_1 to Φ_5 are the potentials of nodes 1 to 5.

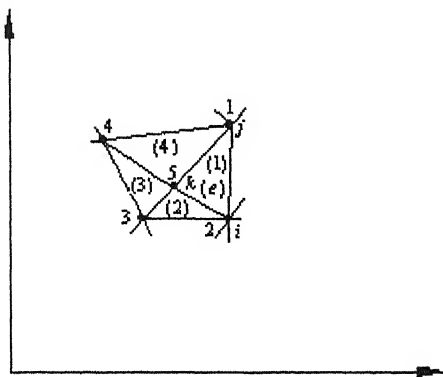


Fig. 9.4 Node k of element (e), shown as node No. 5 connected to four triangular elements (1) to (4).

Applying equation 9.9 to each of these four elements, that is, replacing the index e by individual numbers as given in Fig 9.4, the above equation works out by adding the contribution from each elements as follows:

$$\begin{aligned} \left(\frac{\partial W_{\Lambda}}{\partial \Phi_5} = 0 \right) &= \left[(h_{kk})_1 \Phi_5 + (h_{kk})_2 \Phi_5 + (h_{kk})_3 \Phi_5 + (h_{kk})_4 \Phi_5 \right] \\ &+ \left[(h_{ik})_1 \Phi_2 + (h_{ik})_2 \Phi_3 + (h_{ik})_3 \Phi_4 + (h_{ik})_4 \Phi_1 \right] \\ &+ \left[(h_{jk})_1 \Phi_1 + (h_{jk})_2 \Phi_2 + (h_{jk})_3 \Phi_3 + (h_{jk})_4 \Phi_4 \right] \\ &= \left[(h_{jk})_1 + (h_{ik})_4 \right] \Phi_1 + \left[(h_{ik})_1 + (h_{jk})_2 \right] \Phi_2 \end{aligned}$$

$$\begin{aligned}
& + \left[(h_{jk})_2 + (h_{ik})_2 \right] \Phi_3 + \left[(h_{ik})_3 + (h_{jk})_4 \right] \Phi_4 \\
& + \left[(h_{kk})_1 + (h_{kk})_2 + (h_{kk})_3 + (h_{kk})_4 \right] \Phi_5
\end{aligned}$$

this equation can also be written in the form

$$H_{15}\Phi_1 + H_{25}\Phi_2 + H_{35}\Phi_3 + H_{45}\Phi_4 + H_{55}\Phi_5 = 0$$

The potential Φ_5 can be calculated if the potentials Φ_1 to Φ_4 are known, which depend upon the larger network. Therefore, for every unknown potential, a corresponding equation has to be set up. For a system in which Laplace equation is applicable, that is, the space charge free electrostatic fields, the solution may be written as,

$$\frac{\partial W}{\partial(\Phi)} = 0 = [H] (\Phi) \quad (9.11)$$

The FEM leads to comparatively simpler techniques for estimating fields at highly curved and thin electrode surfaces with different dielectric materials. However, its suitability remains mainly for weakly nonuniform and symmetrical fields which can be easily represented by two dimensional geometries. For three dimensional field configurations, there are reservations in its application.

This work has done using software “FEMLAB, Multiphysics in MATLAB”, for a circular and square electrode configurations.

9.3 BOUNDARY CONDITIONS

To obtain a unique solution to our problem, either the unknown or its normal derivative must be specified at each point on the boundary. Further, the potential of at least one point in the problem must be specified to render the global matrix non-singular. When we specify the potential at a point, we call this a Dirichlet condition. If the potential is specified as constant along a line (the electrode boundary) this becomes an equi-potential. If the value of potential is zero, we call this the homogeneous Dirichlet condition. When specify the normal derivative of the potential we specify a Neumann condition [35].

9.4 FEMLAB SIMULATION RESULTS

FEMLAB simulation results for circular conductor and square conductor configuration are shown in Fig 9.5 to 9.11. Fig. 9.5 shows the Finite Element Mesh using triangles for (a) circular conductor configuration, (b) square conductor configuration and (c) square conductor configuration with no sharp edge.

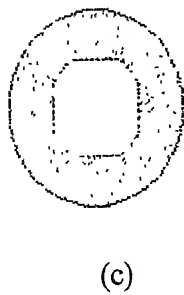
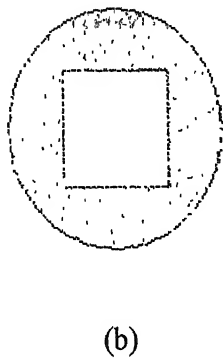
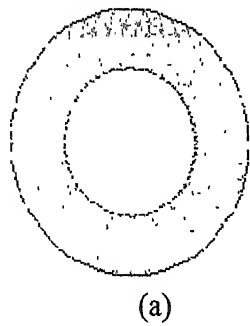
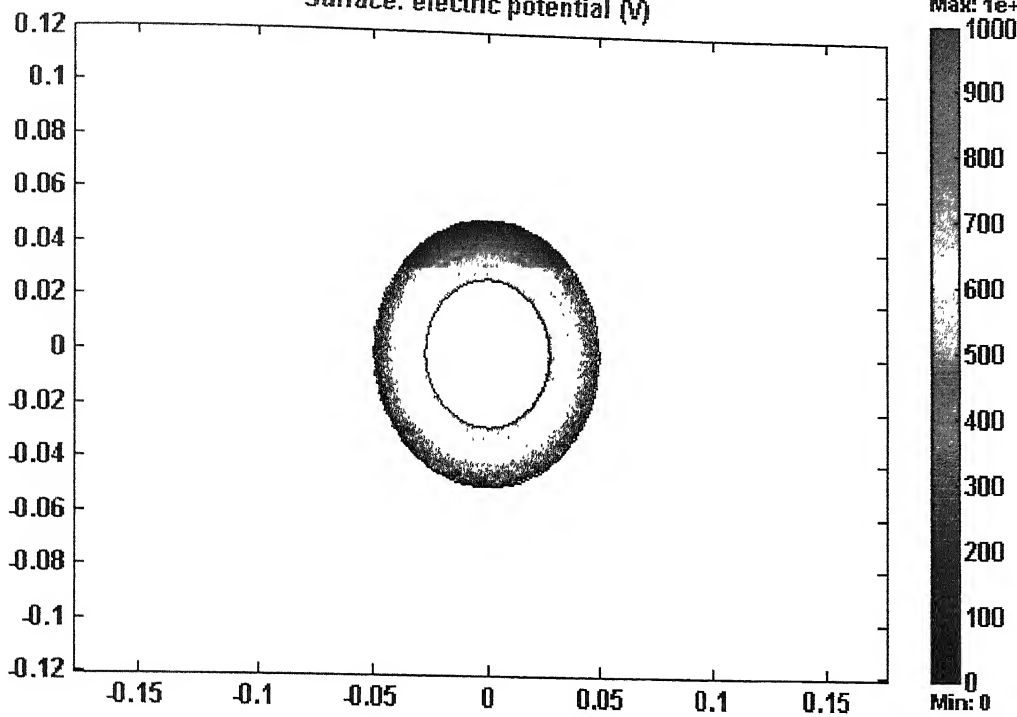
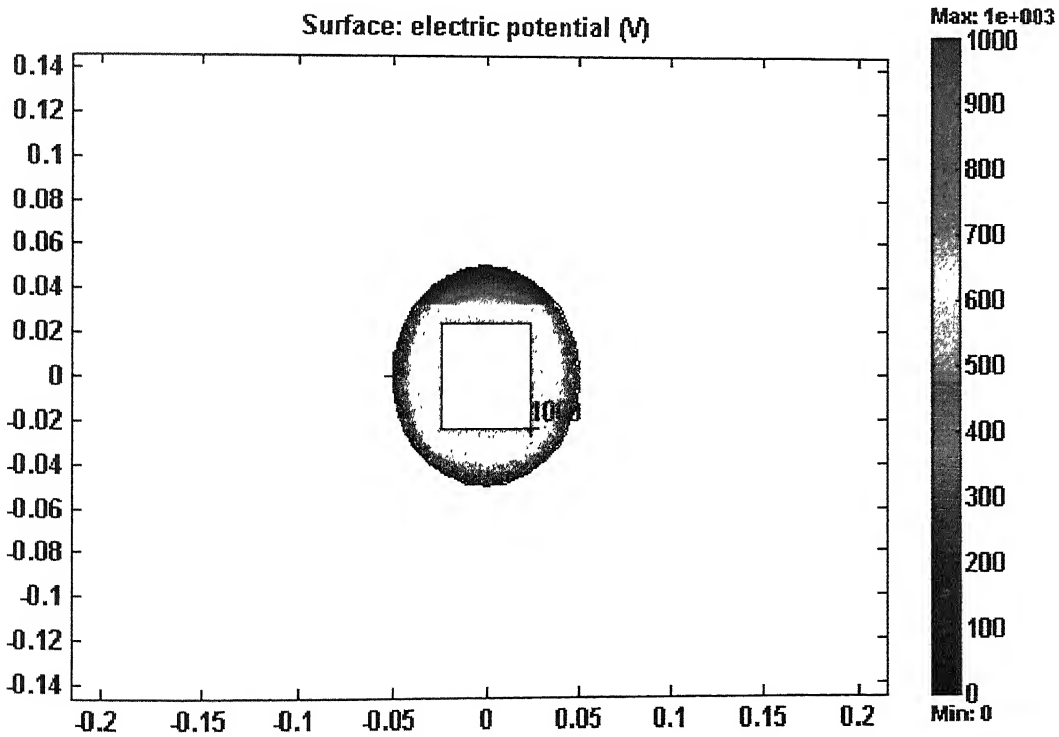


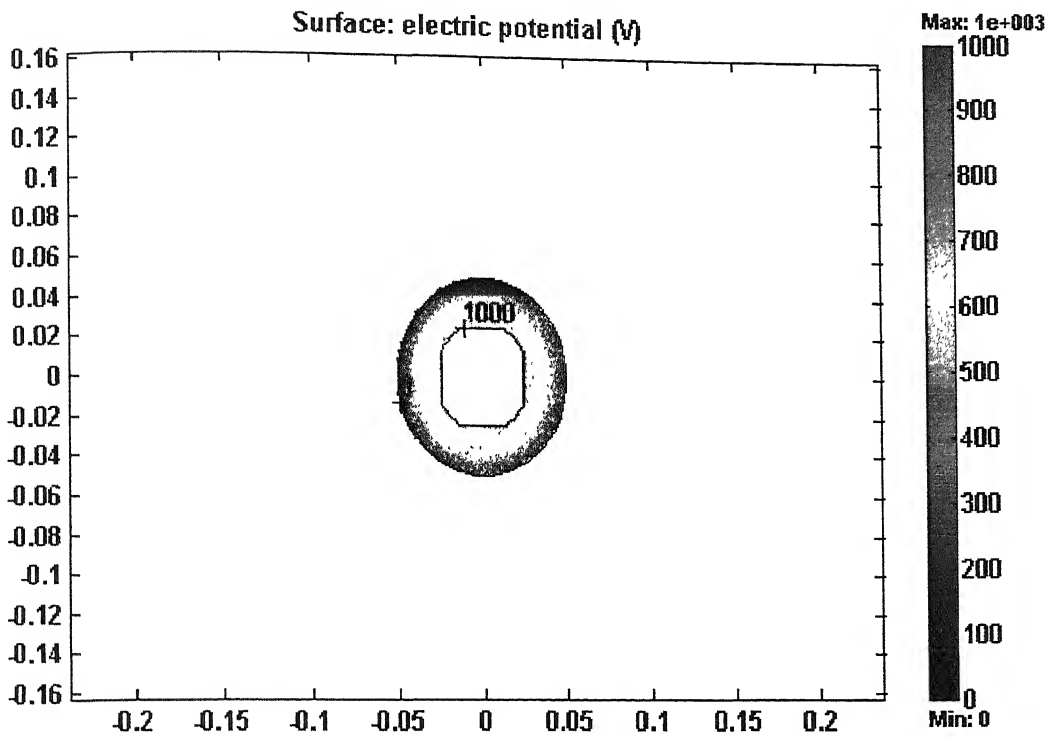
Fig. 9.5 Finite element mesh using triangles for (a) circular conductor configuration, (b) square conductor configuration and (c) square conductor configuration with no sharp edge.



(a)



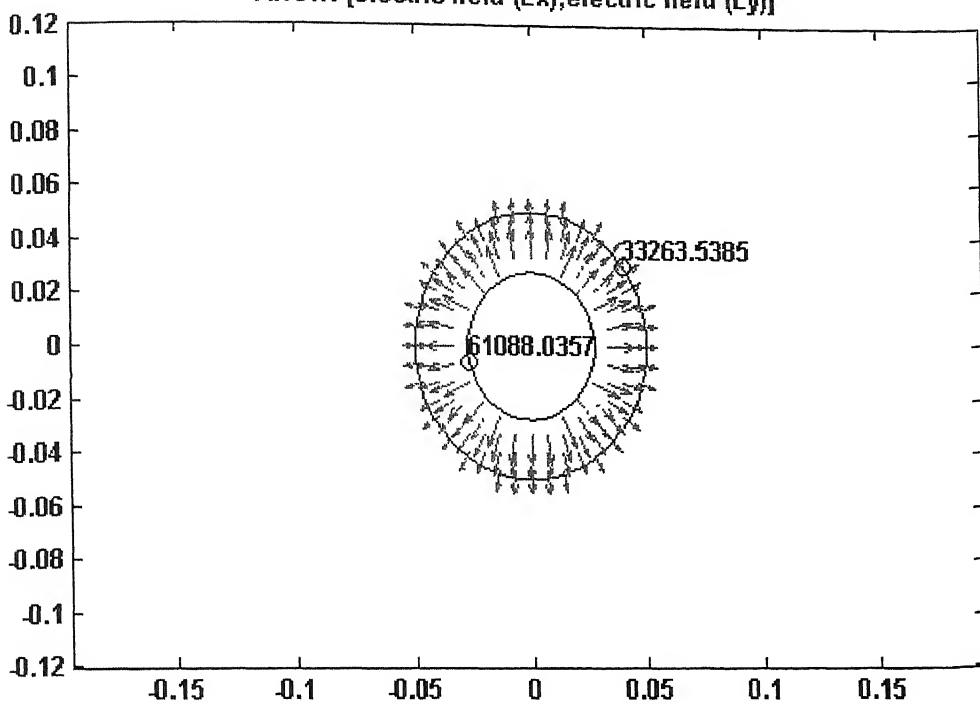
(b)



(c)

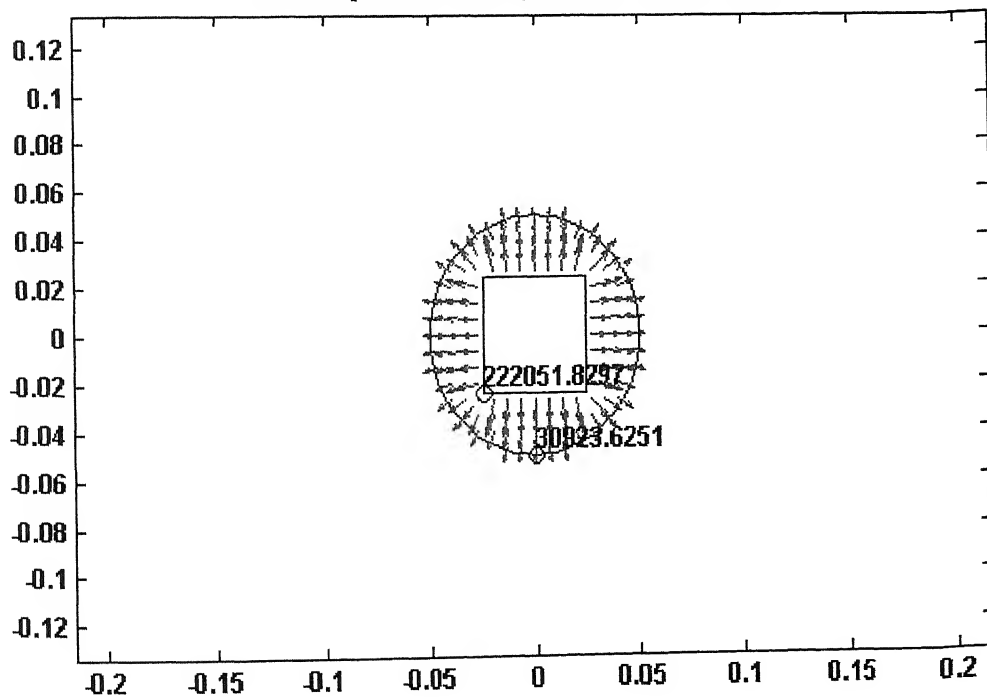
Fig. 9.6 An electric potential distribution in dielectric for (a) circular conductor configuration, (b) square conductor configuration and (c) square conductor configuration with no sharp edge.

Arrow: [electric field (Ex),electric field (Ey)]

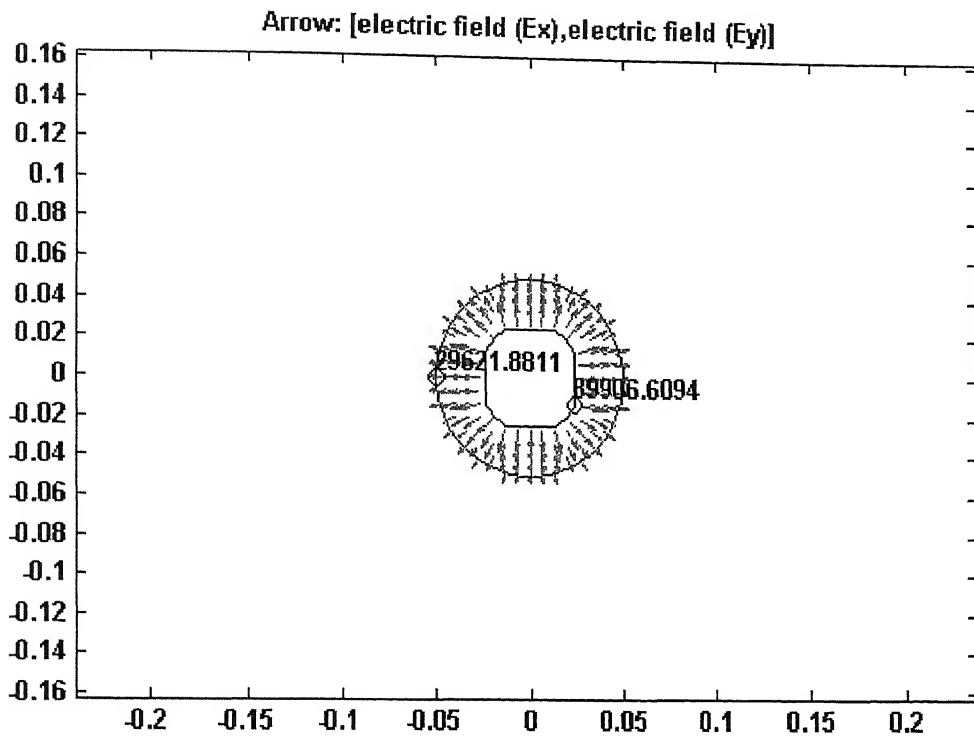


(a)

Arrow: [electric field (Ex),electric field (Ey)]



(b)



(c)

Fig.9.7 An electric field distribution in dielectric for (a) circular conductor configuration, (b) square conductor configuration and (c) square conductor configuration with no sharp edge.

It is concluded from figure 9.7 (a), (b) and (c), that electric field enhancement is more at the electrode surface for square conductor configuration than for circular conductor configuration of same cross section area. The field intensity enhancement is maximum at the square corners, the right angle edges. In case of square conductor configuration with no sharp edge, field enhancement at conductor surface is reduced considerably, as shown in table 9.1.

Table 9.1

Simulated values of electric field intensity at the conductor surface for circular, square and square with no sharp edge, conductor configurations.

	Circular conductor	Square conductor	Square conductor with no sharp edge
Relative Maximum electric field intensity	61088.04	222051.83	89906.61

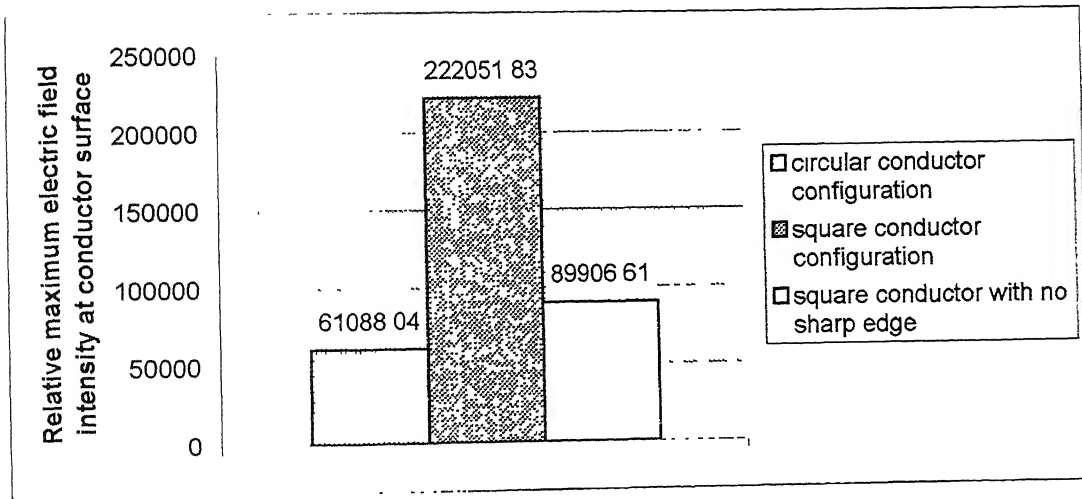
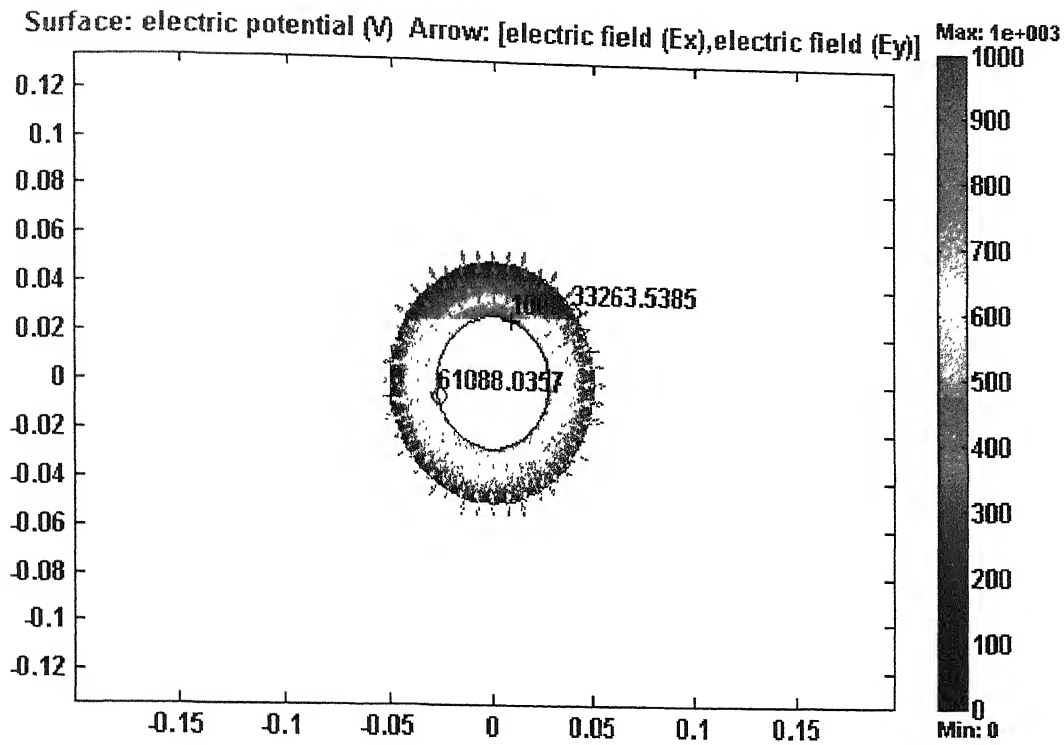
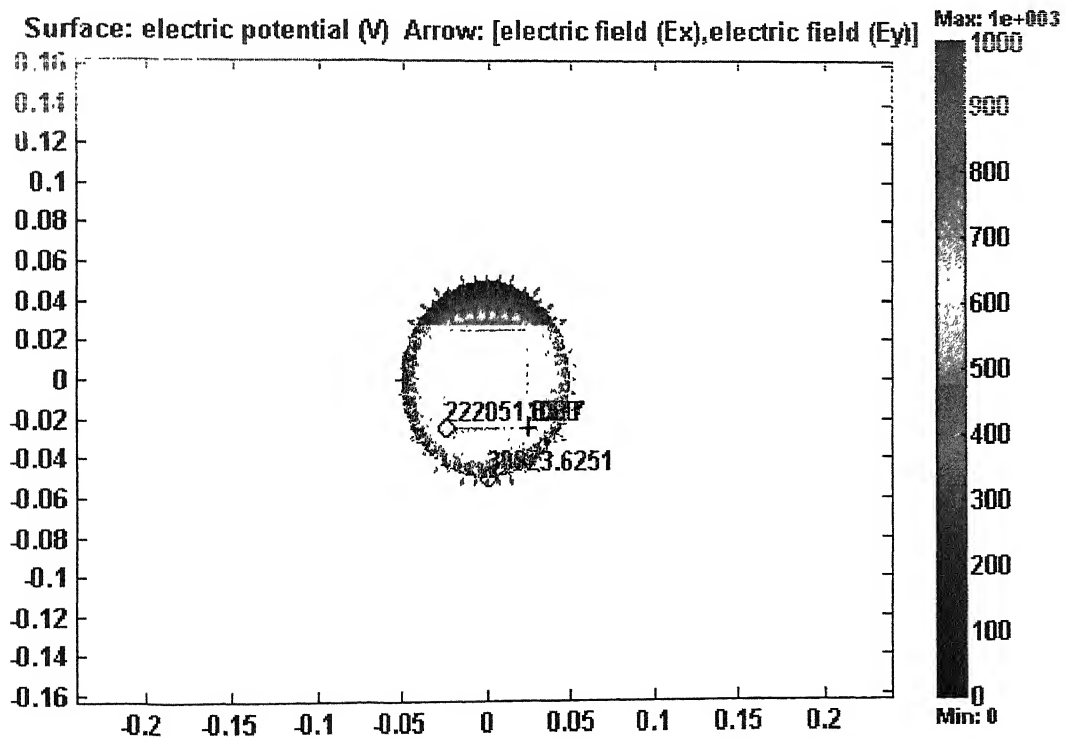


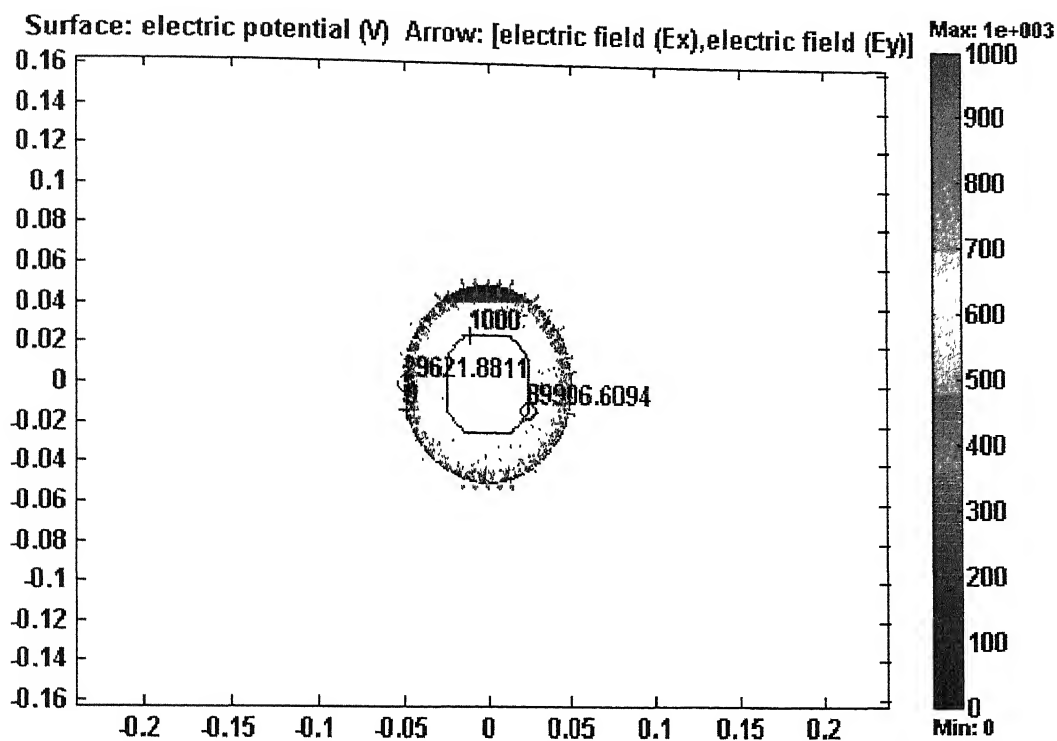
Fig. 9.8 Comparison of relative maximum electric field intensity at the conductor surface for circular, square and square with no sharp edge conductor configurations



(a)

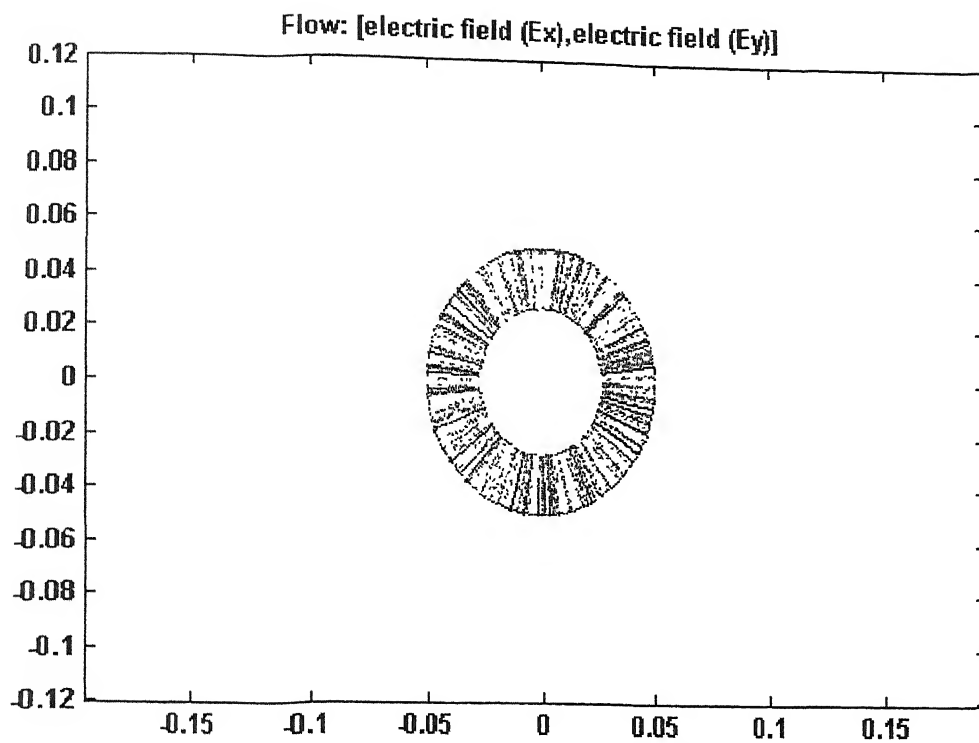


(b)

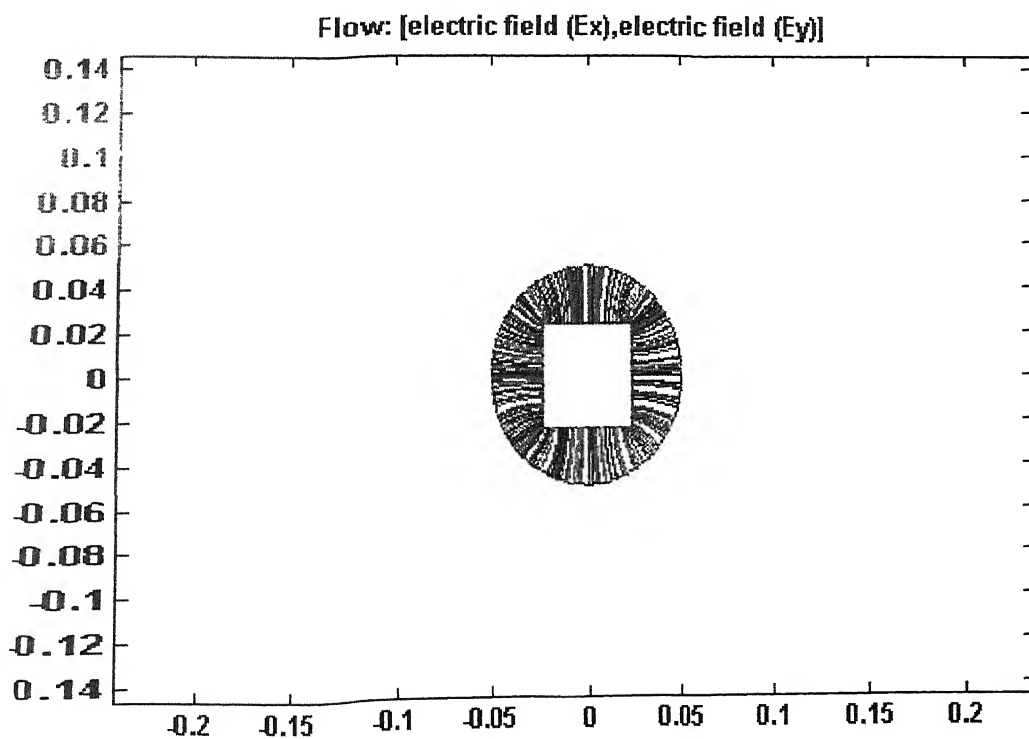


(c)

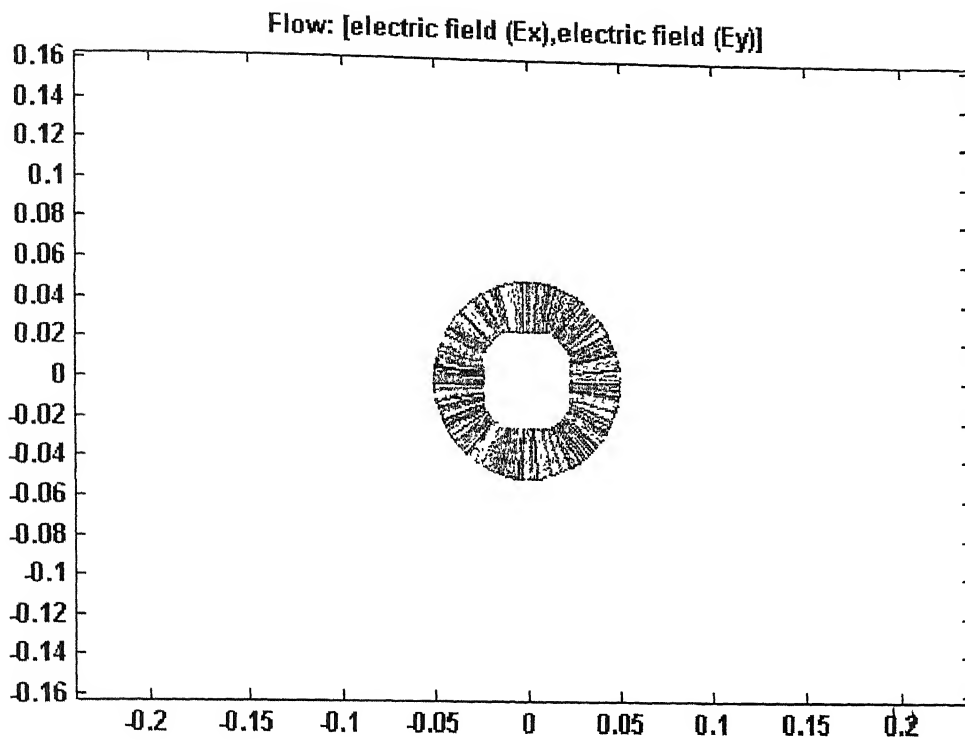
Fig. 9.9 Electric potential and electric field intensity distribution for (a) circular conductor configuration, (b) square conductor configuration and (c) square conductor configuration with no sharp edge.



(a)

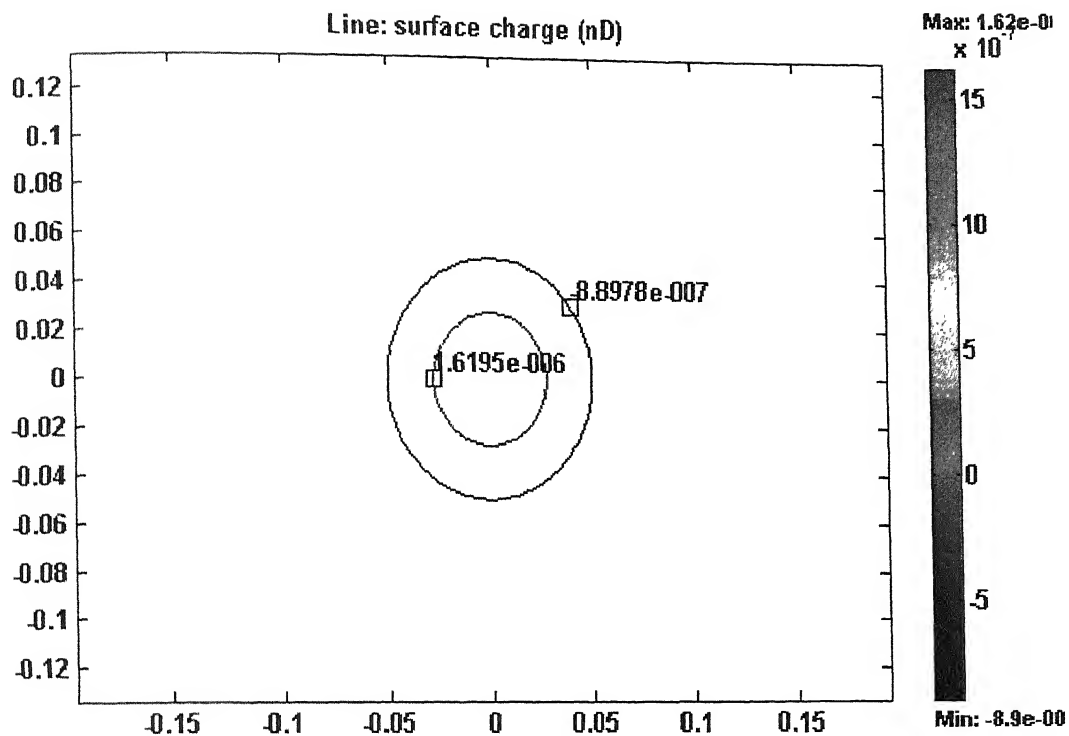


(b)

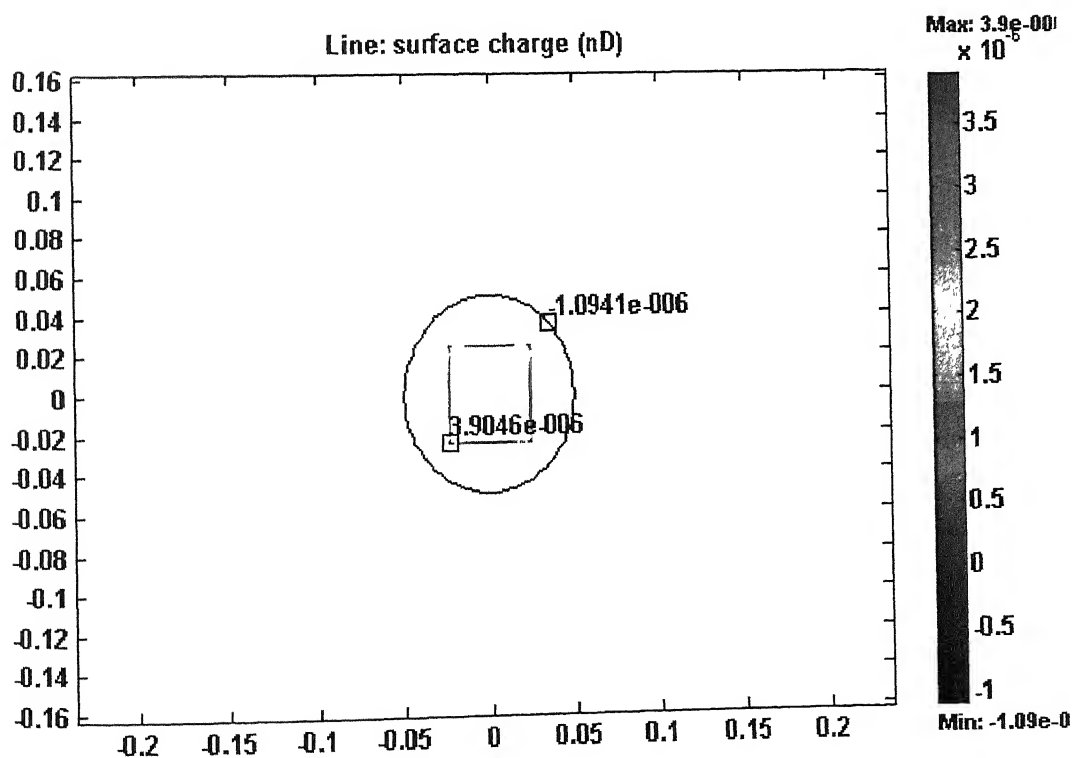


(c)

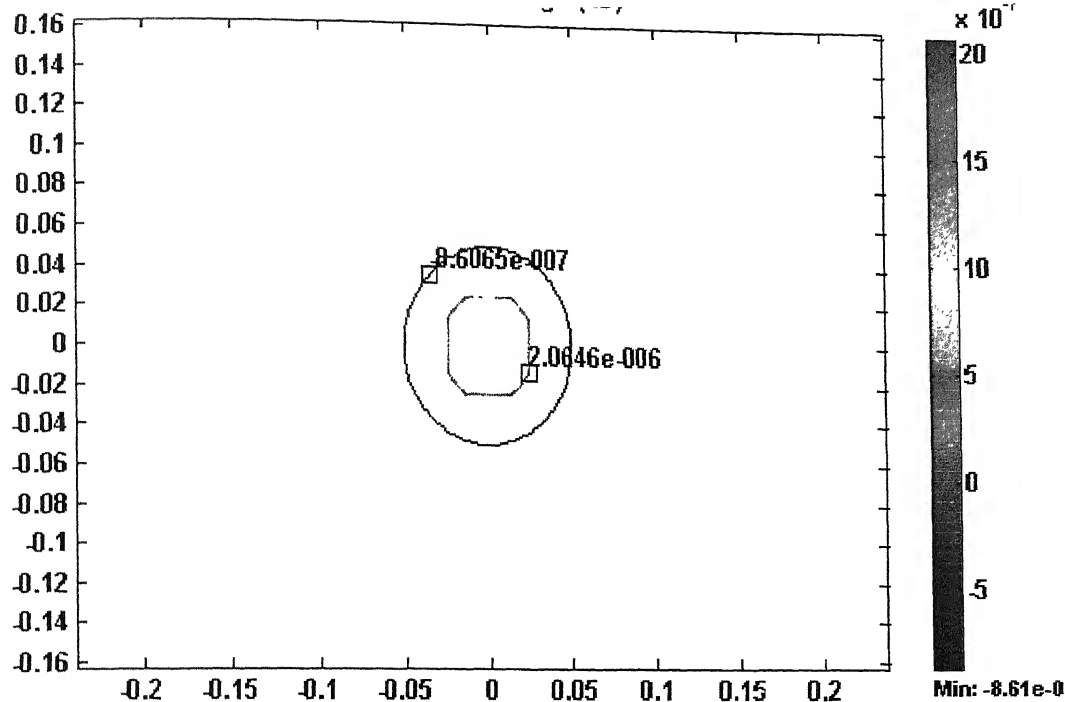
Fig. 9.10 Electric field lines through dielectric for (a) circular conductor configuration, (b) square conductor configuration, and (c) square conductor with no sharp edge configuration.



(a)



(b)



(c)

Fig. 9.11 Surface charge distribution for (a) circular conductor configuration, (b) square conductor configuration, and (c) square conductor with no sharp edge configuration.

Fig. 9.11 (a), (b) and (c) reveal that maximum surface charge resides at the sharp edges of the conductor. Although, in case of square conductor with no sharp edge configuration, maximum surface charge at conductor surface is lower than in case of square conductor configuration, but it is higher than in case of circular conductor configuration.

	Circular conductor configuration	Square conductor configuration	Square conductor with no sharp edge configuration
Maximum surface charge at conductor surface	1.6195 e-006	3.9046 e-0.006	2.0646 e-006

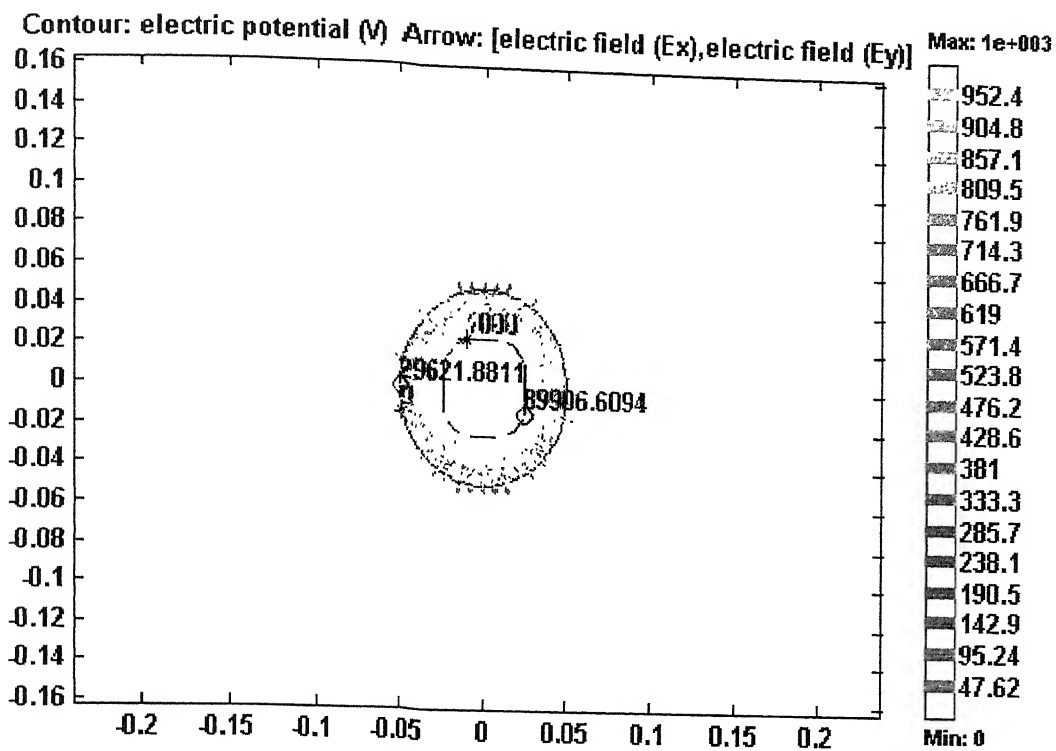


Fig. 9.12 Electric potential and electric field lines for square conductor with no sharp edge configuration.

CHAPTER 10

CONCLUSION AND SCOPE FOR FUTURE WORK

A high voltage ($300 \text{ kV}_{\text{peak to peak}}$), 120 kHz RF transformer based on the design considerations outlined in this work has been designed and constructed at APPD, BARC, Mumbai. Its electrical performance characteristics are currently being analysed. Important conclusions of this work can be made as follows:

- ❖ High Q factor can be achieved by minimising the losses due to high frequency, high voltage, and also dc.
- ❖ With air-core toroidal coil very high quality factor (> 1000) can be achieved. There are no hysteresis and residual magnetic core losses in case of air-core. On the contrary, a toroidal coil with ferrite core has poor quality factor and hysteresis and high residual core loss at high frequency (120 kHz).
- ❖ Skin and proximity effects at higher frequency can be minimised by using Litz wire with proper selection of wire gauge, enamel thickness and good scheme of transposition or bunching. Although, these effects can also be minimised by using solid wire of very large cross section (8 times larger than Litz wire diameter for 120 kHz), but it will increase the size of the transformer excessively.
- ❖ At frequencies $> 5 \text{ MHz}$, Litz wire becomes less practical. The effect of high capacitance between the strands is the reasons for this high-frequency limit.
- ❖ Single layer, single wire, spaced winding scheme provides better cooling and low stray capacitance.
- ❖ Optimal design of toroidal air-core coil depends upon the winding pitch, turn-to-shield distance, insulation coating over Litz wire and winding edge factor. MATLAB calculations show that overall stray capacitance strongly depends upon turn-to-shield distance. Without shield, overall stray capacitance decreases with increase in number of turns in a coil. On the other hand, with shield, it becomes approximately constant after a particular number of turns. Overall stray capacitance decreases with increase in shield distance.
- ❖ Overall stray capacitance also decreases with increase in winding pitch.

- ❖ Contribution of Litz wire insulation coating on overall stray capacitances can be neglected if thickness of insulation is very small compared to winding pitch.
- ❖ The optimum design of single-layer toroidal air-core inductors for 120 kHz application matches the desired value of the coil inductance (5 mH) and the first self-resonant frequency (expressed for overall stray capacitance <20 pF).
- ❖ Dielectric loss factor is high at working frequency. Therefore, efficient cooling is to be considered during design.
- ❖ FEMLAB simulation results: sharp edges at conductor surface lead to tremendous enhancement of the electric field on the dielectric. Electric field intensity on the dielectric near conductor surface is 3.5 times more in case of square conductor than in circular conductors. Square cross section Litz wire reduces the size of toroidal coil marginally but at the same time more field enhancement at sharp edge is present. Hence to reduce the field enhancement at sharp edges, square cross-section Litz wire with no sharp edge is recommended.
- ❖ The dielectric strength of SF₆ increases with higher pressure. Dielectric strength of SF₆ is greatly reduced under nonuniform field conditions.
- ❖ Any protrusion on electrode surface may give rise to partial breakdown in SF₆ gas.
- ❖ The foreign particle contaminants in SF₆ gas play an important role for its dielectric performance. These may cause the deterioration of the insulation by formation of decomposition product due to corona discharge. Hence the coil-winding work should be done in highly clean controlled environment.
- ❖ Breakdown strength of Litz wire insulation strongly depends upon the presence of contaminated environment moisture and dust etc. Therefore, proper care must be taken in handling it and during the winding finish.

SCOPE FOR FUTURE WORK

- ❖ Optimization of shape and dimensions of the winding, Litz wire, is required in order to achieve a Quality factor of about 2000 at 120 kHz.
- ❖ Investigation on the dielectric properties of SF₆ at 120 kHz, 300 kV_{peak to peak} should be made.

APPENDIX A

COMPARASION OF LITZ WIRE WITH SOLID WIRE

A-1 PROPERTIES OF THE FINE ENAMELLED COPPER WIRE- AWG 40

Properties	Nominal	Maximum	Minimum
Bare copper diameter, mm	0.0798	0.08204	0.07747
Enameled copper diameter, mm	-----	0.09398	0.08509
Increase in diameter due to insulation, mm	-----	-----	0.00762
Copper area, mm ²	4.996×10^{-3}	5.286×10^{-3}	4.714×10^{-3}
Resistance per unit length, $\Omega/\mu\text{m}$ (Conductivity of copper , $\sigma = 58 \times 10^6$ $\Omega^{-1}\text{m}^{-1}$) Ω^{-1}	3.451	3.262	3.657

A-2 2464/ AWG 40 LITZ WIRE DIMENSIONS

Overall Litz wire cross section : $5 \times 5 \text{ mm}^2$ square cross section with no sharp edge,
diagonal length (measured) = 5.8 mm

Equivalent copper area : 12.5 mm^2

Thickness of insulation coating over entire Litz wire conductor : 0.1 mm

A-3 OVERALL DIAMETER OF 2464 STRANDS EACH AWG 40 LITZ WIRE

Total no. of strands = $1 + 3n(1 + n)$

Where n is no. of layers in stranded conductor.

So,

$$2464 = 1 + 3n(1 + n)$$

solving this equation, we have

$$n = 29$$

Overall circular diameter of 2464 strands each AWG 40 Litz wire is given by,

$$d_o = d_I (1 + 2n) , \text{ Where } d_I \text{ is the diameter of individual strands.}$$

Putting values of d_I from section B-1 gives

$$d_o (\text{Maximum}) = 5.54482 \text{ mm} ;$$

$$d_o (\text{Minimum}) = 5.02031 \text{ mm}$$

So average value of overall circular diameter $d_o = 5.283 \text{ mm}$

Suppose we consider a circular and square cross section conductor having same area, then following relations can be obtained,

$$a = 0.886 d_o , \text{ where } a \text{ is the breath of the square cross section}$$

conductor.

$$\Rightarrow a = 0.886 \times 5.283 = 4.68 \text{ mm}$$

so with insulation coating ,breath of square cross section Litz wire = $4.68 + 0.2 = 4.88$ mm. Measured value of a is 5.0 mm. This reveals that if we choose square cross section Litz wire, size of the toroidal coil will reduce by 11.4 % of size of toroidal coil with circular cross section Litz wire. But sharp edge at square Litz wire may be responsible for more (3 times) field enhancement at conductor surface as discussed in chapter 9, so square cross section Litz wire with no sharp edge is chosen.

A-4. RESISTANCE OF LITZ WIRE AND SOLID WIRE OF SAME COPPER CROSS SECTION AREA

Resistance per unit length of copper conductor is given by,

$$R = \frac{1}{\sigma A}$$

For 120 kHz, value of skin depth Δ is given by,

$$\Delta = \frac{1}{\sqrt{\pi f \mu \sigma}} = \frac{1}{\sqrt{\pi \times 120 \times 10^3 \times 4 \times \pi \times 10^{-7} \times 58 \times 10^6}} = 190 \mu\text{m}$$

Effective copper area for solid wire,

$$A_s = \frac{\pi}{4} \left[(3.9894)^2 - (3.9894 - 2 \times 0.190)^2 \right] = \frac{\pi}{4} \left[d^2 - (d - 2\Delta)^2 \right] \quad (\text{A-1})$$

Where d is the diameter of solid wire.

For a same cross section area 12.5 mm^2 , diameter of solid wire will be 3.9894 mm.

Putting the values of d and Δ in equation A-1 we have,

$$\begin{aligned} A_s &= \frac{\pi}{4} \left[(3.9894)^2 - (3.9894 - 2 \times 0.190)^2 \right] \\ &= 1.363937 \text{ mm}^2 \end{aligned}$$

so, Resistance ratio for solid wire to Litz wire will be

$$\begin{aligned} \frac{R_{solid}}{R_{Litz}} &= \frac{A_{Litz}}{A_{solid}} = \frac{12.5}{1.363937} \\ \Rightarrow R_{solid} &= 9.165 R_{Litz} \end{aligned}$$

A-5 EQUIVALENT DIAMETER OF SOLID WIRE HAVING RESISTANCE AS LITZ WIRE

$$\text{Equivalent copper area of solid wire} = \frac{\pi}{4} \left[d^2 - (d - 2\Delta)^2 \right]$$

$$\Rightarrow 12.5 = \frac{\pi}{4} \left[d^2 - (d - 2 \times 0.190)^2 \right]$$

$$\Rightarrow d = 39.79464 \text{ mm}$$

so, it is concluded that to have a same resistance, diameter of solid wire will be 8 times more than that of Litz wire.

APPENDIX B

THE HIGH-FREQUENCY RESISTANCE OF TOROIDAL COILS

B-1 INTRODUCTION

The characteristic property of a toroidal coil is its complete astaticism, that is to say, its magnetic field lies entirely within the coil and therefore no electromagnetic interference between the coil and neighbouring coils. The theory of the losses in inductance coils in general has been discussed in chapter 4 and 5. The results of this theory so far as they affect toroidal coils are summarised below.

The general formula^[7] for the high-frequency resistance of a coil in which the turns are not too closely packed is

$$R_{ac} = R_{dc} \left\{ 1 + F + \left(\frac{KNd}{2D} \right)^2 G \right\} \quad (\text{B-1})$$

when the coil is wound with solid wire, and

$$R_{ac} = R_{dc} \left\{ 1 + F + \left(\frac{k}{d_o^2} + \frac{1}{4} \frac{K^2 N^2}{D^2} \right) n^2 d^2 G \right\} \quad (\text{B-2})$$

when the coil is wound with stranded (Litz) wire.

In these formulae the symbols have the following interpretation:-

R_{ac} = High-frequency resistance of toroidal coil.

R_{dc} = D.C. resistance of coil.

N = Number of turns.

n = Number of strands.

d = Diameter of one strand.

d_o = Overall diameter of stranded wire.

D = Overall diameter of coil.

The factors F and G depend upon the frequency, f , and the diameter, d , of a single strand. We first calculate a quantity z from the formula $z = d\sqrt{f}/92.8$, d in this formula being in mms. and the frequency in Hz, and then read off F and G from table B-1.

The factor k entering only in the stranded wire formula depends on the number of strands and has the following values^[7]: -

n	1	3	9	27	Large
k	0	1.55	1.84	1.92	2

Table B-1

Values of the functions^[7] F and G

d = diameter of single strand in mm, f = frequency in Hz:

$$z = d\sqrt{f}/92.8$$

z	$1+F$	G
0.0	1.000	-----
0.1	1.000	-----
0.2	1.000	$z^4/64$
0.3	1.000	-----
0.4	1.000	-----
0.5	1.000	0.000097
0.6	1.001	0.00202
0.7	1.001	0.00373
0.8	1.002	0.00632
0.9	1.003	0.01006
1.0	1.005	0.01519

The factor K depends upon the type of coil. For a single toroid of circular section formula for K is given by^[7],

$$K = 2(1-x)^{\frac{1}{2}} / (1-2x)^{\frac{3}{4}} \quad (\text{B-3})$$

in which x is the ratio of the diameter D_s of the winding section of the toroid to the overall diameter D .

B-2 CALCULATION FOR HIGH FREQUENCY RESISTANCE

Specifications of toroidal coil as described in section 7.3 are

$$N = 280$$

$$D = 1500 \text{ mm}$$

$$D_s = 450 \text{ mm}$$

$$n = 2464$$

And Litz wire specifications are

$$d = 0.08742 \text{ mm}; R_{dc} = 1.7 \text{ m}\Omega/\text{m} \Rightarrow 1.7 \times 10^{-3} \times \pi \times 0.450 \times 280 = 0.673 \text{ }\Omega$$

$$d_o = 5.0 \text{ mm}$$

For operating frequency, f , at 120 kHz,

$$z = d\sqrt{f}/92.8$$

$$\Rightarrow z = 0.08742 \times \sqrt{120000}/92.8$$

$$\Rightarrow z = 0.326$$

Corresponding values of F and G obtained from table B-1 is 1.000 and 1.772×10^{-3} respectively.

Calculated value of K for $x = \frac{D_s}{D} = \frac{450}{1500} = 0.3$, using equation (B-3) is

3.327.

Putting all these values in equation (B-2), we have,

$$R_{ac} = R_{dc} \left\{ 1 + \left(\frac{2}{(5.0)^2} + \frac{1}{4} \left(\frac{3.327 \times 280}{1500} \right)^2 \right) \times (2464)^2 \times (0.08742)^2 \times 1.772 \times 10^{-3} \right\}$$

$$\Rightarrow R_{ac} = R_{dc} \times 2.45$$

$$\Rightarrow R_{ac} = 0.673 \times 2.45$$

$$\Rightarrow R_{ac} = 1.65 \text{ }\Omega$$

$$\begin{aligned} \text{So, Quality factor, } Q, \text{ of coil} &= \frac{\omega L}{R_{ac}} = \frac{2 \times \pi \times 120 \times 10^3 \times 5 \times 10^{-3}}{1.65} \\ &= 2285 \end{aligned}$$

APPENDIX C

NUMBER OF TURNS IN PRIMARY WINDING OF AIR-CORE TOROIDAL TRANSFORMER

Equivalent circuit of high voltage high-frequency air-core toroidal transformer is shown in Fig. C-1 and its specifications are

$$V_1 = 10 \text{ kV} \quad , \quad V_2 = 300 \text{ kV}_{\text{peak}}$$

$$I_1 = 5 \text{ A} \quad , \quad I_2 = 50 \text{ A}$$

$$L_T = 5 \text{ mH} \quad , \quad C_T = 350 \text{ pF}$$

$$\text{Quality factor, } Q = 200$$

$$\text{Coefficient of coupling, } k = 0.3$$

$$\text{Number of turns in secondary winding, } N_2 = 280$$

$$\text{Toroidal winding cross section area, } A = 0.159 \text{ m}^2$$

$$\text{Mean axial length of toroidal coil, } l_c = 2.95 \text{ m}$$

$$\text{Number of primary turns required, } N_1 = ?$$

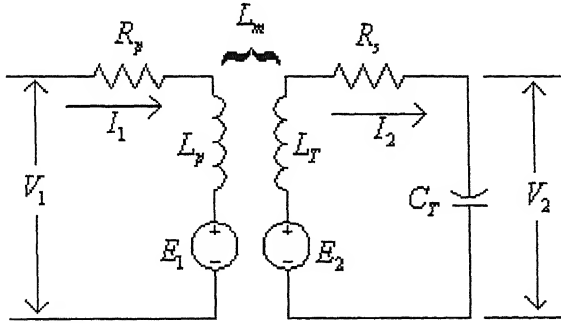


Fig.C-1 Equivalent circuit diagram of high voltage high-frequency toroidal shaped air-core transformer.

$$\text{Induced voltage in secondary winding, } E_2 = \frac{V_2}{Q} = \frac{300 \times 10^3 / \sqrt{2}}{200} = 1.061 \text{ kV}_{\text{rms}}$$

$$\text{Also, induced voltage in the secondary winding, } E_2 = \omega L_m I_1$$

$$\Rightarrow 1.061 \times 10^3 = 2 \times \pi \times 120 \times 10^3 \times L_m \times 5$$

$$\Rightarrow L_m = 0.2814 \text{ mH}$$

Coefficient of coupling, $k = \frac{L_m}{\sqrt{L_p L_T}}$

$$\Rightarrow L_p = \left(\frac{L_m}{k} \right)^2 \cdot \frac{1}{L_T}$$

Putting values of k, L_m and L_T , we get

$$L_p = 0.17596 \text{ mH}$$

Number of turns required getting inductance, $L_p = 0.17596 \text{ mH}$, will be 8-9.

So, required no. of turns for primary winding, $N_1 = 8 \text{ to } 9$.

REFERENCES

- [1] P.J.Devine, "The Requirements of a High Voltage DC Power Supply", International publication, Leicester University, 1995.
- [2] G. Liderati, "High Voltage, High Power switched Mode Power Supply for Ion Production', ENEL C.R.T N.
- [3] W.T. McLyman, "Magnetic Core Selection for Transformers and Inductors", Marcel Decker, Inc., New York, 1982, pp-235.
- [4] N.R. Grossner, "Transformers for Electronic Circuits", McGraw Hill, New York, 2nd Edition, 1983, pp-190.
- [5] Jai P. Agrawal, "Power Electronic Systems Theory and Design", Prentice Hall, Inc. New Jersey, 2001, pp-49.
- [6] Paul N. Murgatroyd, "The Optimal Form for Coreless Inductors", IEEE Transactions on magnetics, Vol. 25, No. 3, May 1989.
- [7] S. Butterworth, "The High-Frequency Resistance of Toroidal Coils", Experimental wireless and The Wireless Engineer, 1929, pp-13-16.
- [8] M.S. Naidu and V.K.Kamaraju, "High voltage engineering", Tata McGraw-Hill Publishing Company Limited, New Delhi.
- [9] E.C. Snelling, "Soft Ferrites Properties and Applications", 2nd Edition, Butterworth & Co. (Publishers) Ltd, 1988, pp-158.
- [10] NAGAOKA, H. "The inductance coefficients of solenoids", J. Coll. Sci. imp. Univ. Tokyo, 27, art 6 (1909).
- [11] GROVER, F.W. "Inductance Calculations", van Nostrand Company (1946) pp-149, pp169-170
- [12] Arora R., Mosch W., "High Voltage Insulation Engineering and Behavior of Dielectrics", New Age International, New Delhi 1995 & 1999.
- [13] Macfadyen K.A., Radley W.G., "Small Transformers and Inductors", Chapman & Hall Ltd, London, 1953, pp-152-157.
- [14] Butterworth s., "Effective Resistance of Inductance Coils at Radio Frequency", Experimental wireless, 3, 203, 1926.
- [15] Ferroxcube, "Linear Ferrite materials and components, sixth edition".

- [16] Welsby, V.A., "The theory and Design of Inductance Coils", McDonald and company, 1960.
- [17] Goad, Stephen D., "The Theory and Design of Switched Mode Power Transformers for Minimum Conductor Loss", University Microfilms International, 1986.
- [18] William Gerard Hurley, Werner Hugo Wolfle, and Jhon G. Breslin, "IEEE Transactions on Power Electronics", Vol. 13, No. 4, July 1998, pp- 651-659.
- [19] Reinhold Ludwig, Pavel Bretchko, "RF Circuit Design, Theory and Applications", Prentice-Hall, Inc, Upper Saddle River, NJ, 2000
- [20] Nathan R. Grossner, "Transformers for Electronic Circuits", McGraw-Hill Book Company, 1983.
- [21] L.F. Blume, T.C. Lennox, S. Minnesi, V.M. Montsinger, A. Boyajian, G. Camilli, "Transformer Engineering", John Willy & sons, Inc., New York 1951.
- [22] "Reference Data for radio engineers" ITT, pp 29-31.
- [23] Frank M. Clark, "Insulating Materials for Design and Engineering Practice", Jhon Willy & sons, 1962
- [24] "Material Data Sheet", The Gund Company, Inc, St. Louis, Missouri
- [25] <http://www.dupont.com/kapton/general/spelec.html>
- [26] P. Halder, "An investigation of Partial Discharge Inception Voltage in Air and SF₆ Gas", M.Tech Thesis, Deptt. Of Electrical Engg., IIT Kanpur; Dec. 2000.
- [27] P.J. Devine, P.W. Lefley, J.C.Fothergil, "A High Power high Frequency Transformer For High Voltage Applications", EPSRC/DTI PEDDS link project with Deakin Daveset Rectifiers Ltd, University of Leicester, United kingdom.
- [28] Petkov, R. "Optimum design of a high-power, high-frequency transformer", IEEE Transaction on power electronics, Vol. 11, No.1, 1996, pp 33-42.
- [29] D.P. Bertsekas, "Constrained Optimization and Lagrange Multiplier Methods", New York; Academic press, 1982.
- [30] R.Horst and H. Tuy, "Global Optimization", Berlin; Springer-Verlag, 2nd Edition, 1993.
- [31] G. Grandi, U. Reggiani, M.K. Kazimierczuk, A. Massarini, "Optimal Design of Single layer Solenoid Air-Core Inductors for High Frequency Applications", IEEE 1997, 0-7803-3694-1/97, pp358-361.

- [32] A. Zaky, and R. Hawley, "Fundamentals of electromagnetic Field Theory", Harrap e Co Ltd: London, 1974.
- [33] G. Grandi, M.K. Kazimierczuk, A. Massarini, U. Reggiani, "Stray Capacitances of Single-Layer Air-Core Inductors for High Frequency Applications", Proc. of IAS 96 Conf., San Diego, CA, Oct. 1996, pp. 1384-1388.
- [34] S. Zhang, M. M. Morcos, K.D. Srivastava, "Metallic Particle Movement and Insulation Breakdown in Compressed GIS/GITL with Dielectric Coated Enclosures", International Symposium on High Voltage Engineering (ISH), 20 – 24 August 2001, pp-425-428.
- [35] Sheppard J. Salon, "Finite Element Analysis of Electrical Machines", Kluwer Academiv Publishers, Boston, ISBN 0-7923-9594-8, 1995.
- [36] Arora R., Halder P., "Investigation of the Streamer Corona in SF₆ Gas", International Symposium on High Voltage Engineering (ISH), 20 – 24 August 2001, pp-331-334.
- [37] Reuben Lee, "Electronic Transformers and Circuits" Jhon Wiley & Sons, Inc. New York, 1955, pp-214-236.
- [38] Peter C.L. Yip, "High-Frequency Circuit Design and Measurements", Chapman and Hall, London, 1990, pp-42-70.